ABSTRACT

NETWORK LIFETIME EXTENSION, POWER CONSERVATION AND INTERFERENCE SUPPRESSION FOR NEXT GENERATION MOBILE WIRELESS NETWORKS

by
Amer Catovic

Two major focus research areas related to the design of the next generation multihop wireless networks are network lifetime extension and interference suppression. In this dissertation, these two issues are addressed.

In the area of interference suppression, a new family of projection multiuser detectors, based on a generalized, two-stage design is proposed. Projection multiuser detectors provide efficient protection against undesired interference of unknown power, while preserving simple design, with closed-form solution for error probabilities. It is shown that these detectors are linearly optimal, if the interference power is unknown.

In the area of network lifetime extension, a new approach to minimum energy routing for multihop wireless networks in Rayleigh fading channels is proposed. It is based on the concept of power combining, whereby two users transmit same signal to the destination user, emulating transmit diversity with two transmit antennas. Analytical framework for the evaluation of the benefits of power combining, in terms of the total transmit power reduction, is defined. Simulation results, which match closely the analytical results, indicate that significant improvements, in terms of transmit power reduction and network lifetime extension, are achievable. The messaging load, generated by the new scheme, is moderate, and can be further optimized.

NETWORK LIFETIME EXTENSION, POWER CONSERVATION AND INTERFERENCE SUPPRESSION FOR NEXT GENERATION MOBILE WIRELESS NETWORKS

by
Amer Catovic

A Dissertation
Submitted to the Faculty of
New Jersey Institute of Technology
in Partial Fulfillment of the Requirements for the Degree of
Doctor of Philosophy in Electrical Engineering

Department of Electrical and Computer Engineering

January 2003

APPROVAL PAGE

NETWORK LIFETIME EXTENSION, POWER CONSERVATION AND INTERFERENCE SUPPRESSION FOR NEXT GENERATION MOBILE WIRELESS NETWORKS

Amer Catovic

Dr. Sirin Tekinay, Dissertation Adviser — Date
Assistant Professor, Department of Electrical and Computer Engineering, NJIT

Dr. Ali N. Akansu, Committee Member — Date
Professor, Department of Electrical and Computer Engineering, NJIT

Dr. Nirwan Ansari, Committee Member — Date
Professor, Department of Electrical and Computer Engineering, NJIT

Dr. Alexander M. Haimovich, Committee Member — Date
Professor, Department of Electrical and Computer Engineering, NJIT

Dr. Symeon Papavassiliou, Committee Member — Date
Assistant Professor, Department of Electrical and Computer Engineering, NJIT

Dr. Jack Winters, Committee Member — Date
Jack Winters Communications, LLC

BIOGRAPHICAL SKETCH

Author: Amer Catovic

Degree: Doctor of Philosophy

Date: January 2003

Undergraduate and Graduate Education:

- Doctor of Philosophy in Electrical Engineering,
  New Jersey Institute of Technology, Newark, NJ, 2003
- Master of Science in Electrical Engineering,
  Bosphorus University, Istanbul, Turkey, 1998
- Bachelor of Science in Electronics Engineering,
  Université des Sciences et de la Technologie d'Oran, Oran, Algeria, 1996

Major: Electrical Engineering

Selected Publications:

A. Catovic, S. Tekinay, "Reducing transmit power and extending network lifetime via user cooperation in next generation multihop wireless networks", Journal of Communications and Networks, Vol. 4, No. 4, December 2002, pp.351-362.

A. Catovic, S. Tekinay, "Selective multiuser detection for cellular CDMA systems", International Journal of Wireless Information Networks, Vol. 9, No. 4, October 2002, pp. 259-273

A. Catovic, S. Tekinay, "Multiuser detection techniques for hierarchical cell structures in cellular CDMA systems", International Journal on Wireless Information Networks, Kluwer Academic Publishers, Vol. 9, No. 1, January 2002, pp. 24-35

A. Catovic, S. Oktug, G. Dundar, "Hierarchical neuro-fuzzy call admission controller for ATM networks", Computer Communications Journal, Elsevier, Vol. 24, Issue 11, June 2001, pp. 1031-1044

A. Catovic, S. Tekinay "Geolocation updating schemes for location aware services in wireless networks", IEEE Military Communications Conference, MILCOM 2001, October 2001, Washington D.C.

This dissertation is dedicated to
my parents,
Besim&Mensura Catovic

ACKNOWLEDGEMENT

The author wishes to express his sincere gratitude to his supervisor, Professor Sirin Tekinay, for her continuous support, guidance, and friendship during his Ph.D. studies. He sincerely hopes that our long-lasting friendship will remain as one more original contribution of this research.

Special thanks to Professors Ali Akansu, Nirwan Ansari, Alexander Haimovich and Symeon Papavassiliou for serving as the members of the Committee. The author owes gratitude to Dr. Jack Winters for reserving his time and efforts to serve as an external member of the committee.

The author would like to thank to NTTDoCoMo Wireless Communications Laboratory of NTTDoCoMo Japan at Yokosuka Research Park for their funding of the research, their active involvement in following its progress and for the extraordinary opportunity to visit NTTDoCoMo Japan headquarters and present our research results there. Special thanks to Dr. Toru Otsu, the Director of the NTTDoCoMo Wireless Communications Lab.

Finally, thanks to all my family members and friends for their continuous support and interest in my research. In particular, thanks to all my friends from Bosnia, Algeria, Turkey and USA. The words of their support and encouragement are interweaved with every single line of this dissertation.

TABLE OF CONTENTS

TABLE OF CONTENTS
(Continued)

Chapter **Page**

TABLE OF CONTENTS
(Continued)

Chapter **Page**

TABLE OF CONTENTS
(Continued)

Chapter **Page**

LIST OF TABLES

Table **Page**

LIST OF FIGURES

LIST OF FIGURES
(Continued)

Figure **Page**

LIST OF FIGURES
(Continued)

Figure **Page**

CHAPTER 1

INTRODUCTION

1.1 Preliminaries

It seems that third generation (3G) wireless networks will not be able to entirely satisfy the spirit of "anytime, anywhere" service in terms of increased desired data rates for wireless access. Large-scale wireless networks continue to struggle with capacity limitations brought about by the very nature of the cellular architecture. As a consequence, many variations of broadband wireless access technologies have been deployed, or are on the drawing boards. They have been placed under the generic umbrella of the *next generation wireless networks*, or *fourth generation (4G) wireless networks*. There is no unique definition of these two terms. They rather encompass all the efforts in going beyond the 3G concepts.

The motivations behind these efforts are diverse. One subset of these technologies have hinged on the compromise of mobility for higher data rates. Higher data rates over the air have been available in the form of wireless local area networks (WLANs), which have been in use for quite a long time, and which, by definition, are restricted in geographic scope. A family of proximity-based communication systems has been developed for next generation systems, including infostations, rooftop systems, mesh systems and personal area networks. Another subset of next generation wireless technologies has been driven by direct demands of military and commercial applications. The most illustrative example of these are *mobile ad hoc networks* (MANET). They have been driven by the demands presented by the military for self-organizing networks of wireless mobile terminals (MT) able to operate in the battlefield conditions, including the

absence of fixed network and power supply infrastructure. Emergency rescue operations share the same requirements with respect to the lack of infrastructure, while several other markets are interested in on-the-fly self-organizing networks of MTs, such as automotive industry, consumer electronics etc.

In this work, several aspects of practical implementation of MANETs are studied, namely their energy efficiency and battery life, and interference suppression of the existing overlaying networks or other MANETs operating in the same area. In this work, CDMA technology is assumed as the technology for multiple access, but most of the work is applicable to wideband signals in general.

1.2 Contributions and Organization of the Dissertation

1.2.1 Main Contributions of the Dissertation

The contributions of this dissertation can be grouped into two main areas. In the first one, the focus is on the energy efficiency and battery life optimization of MANETs. The widely used assumption of distance-based deterministic channel in MANETs is removed and a new approach to the minimum energy routing (MER) for MANETs in channels with Rayleigh fading and shadowing is defined. This new approach exploits inherent potential of MANETs for transmit diversity to combat fading, reduces the transmit power and extends network battery life without increasing the complexity of MTs. The theoretical fundamentals for the use of transmit diversity in MANETs are provided, and a new MER algorithm for MANETs in Rayleigh fading channels is defined. The results show that the new approach offers significant gains in terms of energy consumption and network battery life compared to the results obtained by using the existing MER schemes based on the simplistic channel model. The proposed technique provides 20-100%

increase in the network lifetime and 15-150% decrease in the average consumed power per route, depending on the desired received signal quality, at the cost of a moderate signaling overhead.

In the second area, the focus was on the methods for suppression of the interference of the existing overlaying wireless networks and/or other MANETs operating in the same area. The problem is placed in the context of hierarchical cell structures in 3G systems and apply near-far resistant multiuser detection techniques to suppress the overlay interference. This new class of multiuser detectors is computationally simple and provides efficient protection against the undesired interference. The protection is in fact optimal if the amplitudes (powers) of the interferers are not known. The new approach is directly applicable to augmented cellular structures, described in the subsequent sections.

1.2.2 Organization of the Dissertation

In the subsequent sections, the motivation and the main theoretical background behind this work is presented, along with a critical review of prior work in the area and the preliminary results. In Chapter 2, the contribution in the area of overlay interference suppression for overlaid MANETs is presented. In Chapter 3, the theoretical fundamentals for the use of transmit diversity in MANET are given, including the definitions, feasibility and power gain analyses. A new MER algorithm for MANETs in Rayleigh fading channels is proposed. In Chapter 4, the system model for a MANET is defined and the simulation tool, developed for performance analysis of the algorithm, is presented. In Chapter 5, the results are presented, along with the discussion.

1.3 Mobile Ad Hoc Networks

The recent interest in mobile ad hoc networks (MANET) stems from the commercial value of their applications. Besides military applications, a vast variety of applications are anticipated emerge in the coming years. They include emergency rescue operations, navigation and tracking services for automotive industry, home networking, sensor networks, location-aware services, on-the-fly LANs etc. However, there is no widely accepted definition of the concept of MANET. Hence, the only way of defining a MANET is through the set of features it posseses, which have been universally accepted in the literature.

Lack of fixed infrastructure is the most widely recognized feature of MANET, which is mandated by the nature of the current and envisioned commercial applications, such as military applications and emergency rescue operations. In contrast to cellular wireless networks relying on base stations (BS) (Figure 1.1.a) and fixed networks relying on routers to provide the universal communication gateway for all users, in MANET mobile terminals (MT) communicate with each other directly by creating a network on the fly (Figure 1.1.b).

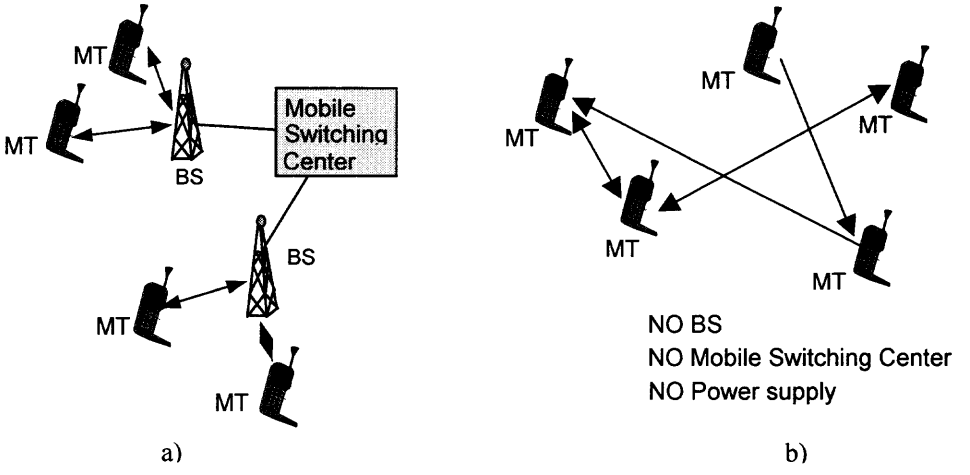

Figure 1.1 Wireless cellular network (a) and MANET (b).

This is reflected in the fact that MANET has no central control entity, such as BS in cellular networks, performing vital network functions, such as routing and power control. Therefore, network protocols for MANET must be distributed. Another feature of MANET is the lack of pre-determined topology, which is associated with the mobility of MTs. In MANET, messages may not be transmitted directly from the source MT to the destination MT, but rather relayed by the intermediate MTs. Due to this feature, MANETs are usually referred to as multihop networks.

1.3.1 Augmented Cellular Architectures

In the recent years, network architectures that take advantage of the high bandwidth available in close proximity, low power communications have been receiving serious consideration for larger scale operation, despite sacrificing continuous coverage. On the other hand, each type of network is accessible only by specialized mobile terminals. The current trend in mobile transceiver technologies points towards providing access to a multiplicity of networks, enabling a new network design philosophy, namely, adaptive network architectures. This new philosophy introduces the capability of optimally reconfiguring network hierarchy on a per-session basis, based on the capacity and performance requirements of the network and the session, respectively. With adaptive hierarchy reconfiguration, peer-to-peer communication augments the infrastructure. In some recently published works, new ideas for networks with combined cellular and MANET features have been presented. A network with combined features of a cellular wireless network and MANET was proposed by Tekinay in [1], termed "Cellular Ad Hoc Augmented Network, (CAHAN)" (Figure 1.2). In this basically cellular system, ad hoc

networking is turned on by command from a BS, in order to increase the coverage and/or reduce the transmit power.

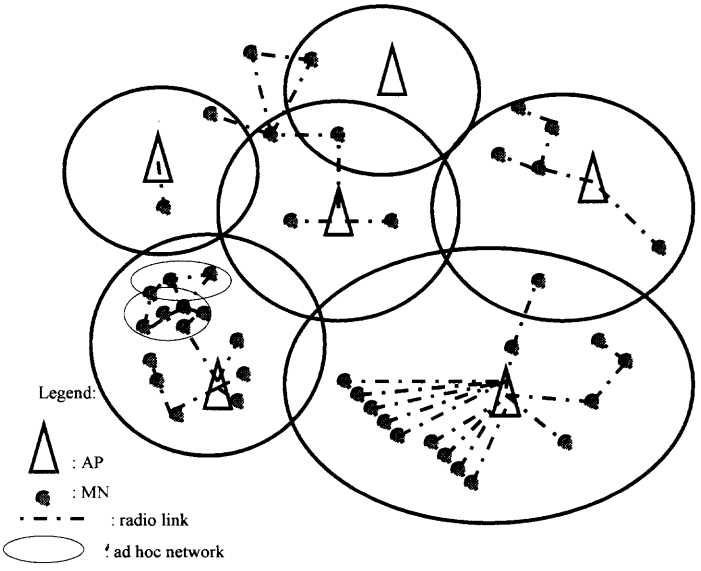

Figure 1.2 CAHAN Architecture.

In this system, BS can represent a node or a cluster head in ad hoc network. Significant benefits have been reported, especially in multicast type services. A similar idea was pursued in [2], only named "Integrated Cellular and Ad Hoc Relaying System, (iCAR)". Here, the major concern is to address the congestion problem due to unbalanced traffic in the cellular system and provide interoperability for heterogeneous networks, by using ad hoc relaying stations to relay traffic from one cell to another dynamically. Improvements in terms of system capacity, transmit power and system coverage with respect to cellular systems have been reported.

1.4 Power-aware Routing Schemes for MANET

1.4.1 Classification of Power-aware Routing Schemes for MANET

Starting with the earliest research results on MANETs, it has been perceived that the routing schemes for MANETs have to be in one way or another power-aware, or energy-aware. This stems from the nature of the most salient applications of MANETs, which are very often associated with unavailability of energy to re-charge the batteries in MTs. Most illustrative applications that fall into this category are digital battlefield, emergency rescue operations, and other applications where MANETs are used to provide a replacement for a destroyed, damaged or temporarily unavailable fixed network infrastructure. The unavailability of fixed network infrastructure is often associated with the unavailability of power supply infrastructure. In addition, even when power supply infrastructure is available, the rate of energy consumption of MTs is very often much higher then the rate at which users have access to it or are willing to dedicate the time for battery re-charging. In any case, it is essential to keep the network operational as long as possible.

Besides the efforts towards designing long life batteries, power-aware routing has emerged as a complementary research area aiming to reduce the consumed power of mobile stations and extend the battery life of MTs and the network lifetime. In the relevant literature, two different definitions of network lifetime have been introduced. According to the first definition, the network lifetime is the time until the network is partitioned into two disconnected sub-networks, i.e. the time to the first network partition. In the second definition, the network lifetime is the time until the first node runs out of energy. The first definition is more general, but the second definition seems to have found wider usage. Here, the network lifetime is defined in the latter sense.

Another class of applications has also played important role in the motivation for a very extensive research in energy-aware routing schemes for MANETs. Namely, some applications will require MANETs to be deployed within the coverage area of an existing wireless network infrastructure. These applications include augmented cellular networks, discussed in Section 1.3.1, as well as on-the-fly LANs, automotive applications, home networking and others. Due to the overlapping of the coverage areas of the MANETs and the existing wireless networks, there will exist mutual interference between them. From that perspective, it is desirable to reduce the total transmit power of MANETs, in order to reduce the interference. In addition to this, MANETs are expected to be operating in the unlicensed spectrum. Thus, the interference between MANETs is also a serious concern. Because of all the above, it is clear that reducing the transmit power in MANETs is a major issue.

There have been several different approaches to the power-aware routing in the literature in the past several years. They can be roughly grouped into three categories:

- Minimum energy routing (MER)
- Maximum battery life routing (MBLR)
- Power-aware protocol design

MER approach minimizes the average energy consumed to route a packet from the source node to the destination node. Therefore, using MER, the average power consumption of the entire network is minimized. This is suitable for scenarios in which the interference generated to the surrounding environment needs to be minimized. One serious drawback of this approach reported in the literature is that some nodes will carry more traffic than others, depending on their position and mobility pattern within the

network, and will therefore run out of battery energy sooner than others. Thus, minimization of average power consumption does not tackle the problem of maximizing network lifetime. MBLR directly addresses the goal of maximizing network lifetime.

There are two major sub-approaches in MBLR: one consists in adjusting the link metrics so to reflect some measure of the "affinity" of a node to route the traffic, which is generally an increasing function of the residual battery energy the node has; the other consists in load-balancing techniques to maximize time to network partition. Despite directly addressing the problem of network lifetime maximization, MBLR does not minimize the average power consumed by the network, and can therefore generate higher interference to the environment. Also, the information about remaining battery power levels of all MTs in the network required for route computation presents a serious drawback with respect to the amount of signaling required to provide this information.

Power-aware protocols aim to maximize battery life of MTs by designing power-aware multiple access protocols and signaling schemes. Several modes are defined for MTs, such as *sleeping*, *idle*, *transmitting* and *receiving*. Each of these modes has its associated power consumption. The next problem is to decide on the appropriate times for the transition between the modes. This generally requires signaling between the MTs to allert each other about incoming packets, which is the cost of the scheme. In addition, inter-mode transitions consume additional power and generate delay. The issue is then to optimize the MTs' sojourn times in each of the modes with respect to the tradeoff between the signaling and delay on one hand and the total consumed power on the other hand.

1.4.2 Minimum Energy Routing for MANET

As discussed in the previous section, the objective of MER is to minimize the energy consumed to route the packets from the source to the destination. This can be achieved by defining the power required to provide successful transmission as the cost metric. Let P_{mn} denote the transmit power required to provide successful transmission between nodes m and n. The total transmit power for route l, P_l, is then:

$$P_l = \sum_{i,j} P_{ij} \tag{1.1}$$

where the summation is performed over all pairs of successive nodes along the route. The desired route, k, can be obtained from:

$$P_k = \min_{l \in A} P_l \tag{1.2}$$

where A is the set of all possible routes. The best possible route, k, can be found using standard shortest path algorithms, such as Dijkstra or Belman-Ford. In most applications routes with less hops are more desirable, because of the delay and also because of the fact that the power used when receiving data is not negligible. In fact, the receiver power is in the same order of magnitude as the transmit power [3], [4]. To accommodate this, the cost matrix can be modified to account for receiver power:

$$C_{ij} = P_{ij}^t + P_j^r \tag{1.3}$$

where P_{ij}^t and P_j^r represent the transmit power between nodes i and j and the receiver power of node j, respectively. This leads to the following cost for route l:

$$C_l = \sum_{i,j} C_{ij} \tag{1.4}$$

where, like before, the summation is performed over all pairs of successive nodes along the route. The criterion for the selection of the best route k now is

$$k = \arg\min_{l \in A} C_l \tag{1.5}$$

It is evident that the selection of routes using the criterion given by (1.1) and (1.2) minimizes the total transmit power of the network. Although the introduction of the receiver power term into the cost matrix in (1.3) minimizes the total *consumed* power of the network and therefore it does not guarantee that the total transmit power of the network is minimized. When route selection criterion given by (1.4) and (1.5) is used, it is clear that the total transmit power of the network will be minimal. This means that the network will generate minimum interference to its surroundings, which is an important aspect of MER.

On the other hand, the explicit objective of MER is not to maximize the network lifetime. Here, the second definition of the network lifetime given in Section 1.4.1 is adopted; i.e., the network lifetime is the time until the first node runs out of battery energy. In order to illustrate this, consider the network in Figure 1.3.

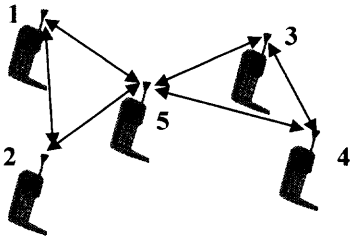

Figure 1.3 Illustration of the slave node problem.

Without loss of generality, non-distance-dependent attenuation components in all links are assumed equal. In this network, node 5 will take part in all routes going from

nodes 1 and 2 to nodes 3 and 4 and vice-versa, as well as the routes starting from or ending at node 5. As a result, node 5 will most likely drain out its battery resources at a faster rate than the other nodes in the network and will be the first to die. This is clearly the consequence of the position of the node 5 with respect to the other nodes in the network. Note that if the non-distance-dependent channel attenuation components are not equal, then some of the other nodes may take the role of node 5. In this case the number of routes in which a node participates will not be the function of the position, but rather on the channel conditions in the network. The result, however, will be the same; namely, some nodes will take part in more routes than others, and will expend their battery power at much faster rate than others. These nodes are called *slave nodes*. This problem has been identified by some authors as 'serious drawback' [4] and 'critical disadvantage' [5] of the MER approach.

One can argue that although the network lifetime maximization is not the explicit objective of MER, the problem of slave nodes is overstated. This is because the problem arises only in static networks, i.e. network with static nodes. On the other hand, if the nodes are moving, the channel conditions constantly change. This results in changing route costs, which means that the status of the slave node is not permanent. Effectively, after sufficiently long time, which is comparable to the channel coherence time [6], the channel conditions will change into a new, independent value. The channel coherence time depends on the node's mobility and ranges from seconds to minutes. Thus, during the lifetime of the battery, the channel conditions will change many times throughout the network, putting the nodes in and out of the slave node position. Therefore, the problem of slave nodes is only present with static networks. Many applications assume moving

nodes, thus the relevance of the problem diminishes. Figure 1.4 shows the simulation results for the average network lifetime for networks with and without mobility, as a function of the number of nodes in the network, for two different values of the desired error probability (i.e. SNR) at the receiver. In the static case, MTs have fixed positions, uniformly distributed within the network coverage area. In the dynamic case, MTs are moving uniformly with random speeds between 0 and 22 mph in random direction, reflecting off the coverage area boundaries back into the coverage area. Network and MT parameters, such as the coverage area size, channel characteristics, transceiver power, detection power thresholds and initial battery capacity*, are kept identical for both cases. In both cases, the routing metrics given by (1.3) is used.

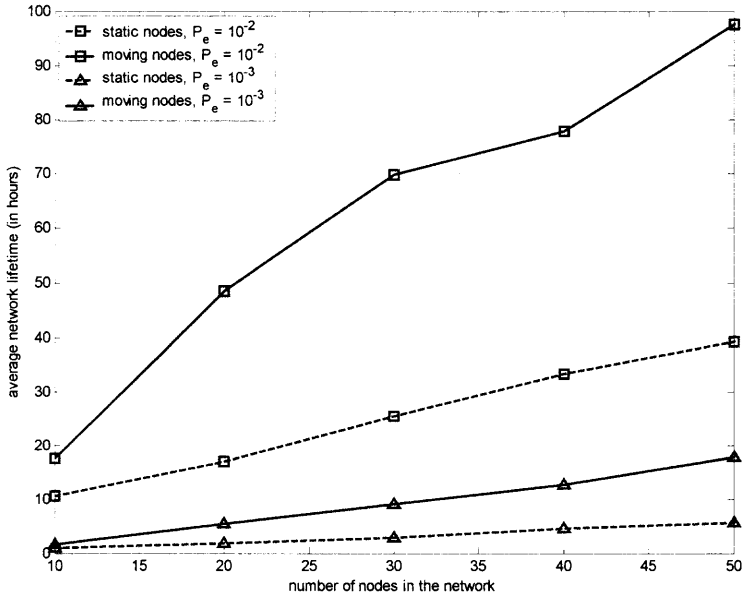

Figure 1.4 Average network lifetime for network with static and moving nodes.

* They are equal to the parameters of the network used in the simulation in Chapter 4, page 98. They were omitted since they are not of paramount importance for the results presented here.

As can be seen clearly from the graph, mobility helps to increase the network lifetime by helping the nodes to escape from the slave node position. Figure 1.5.a shows the histogram of the average residual battery energy in the MTs after the first MT dies, normalized to the initial battery energy, for a static network with 20, 30 and 40 MTs. Figure 1.5.b shows the same result for a network with moving MTs. As can be seen in a dynamic network, the energy consumption is more evenly distributed among MTs. This is reflected in the fact that more nodes get to exhaust their batteries before the first node dies. Note that in the network with static nodes, most of the nodes have their batteries at high energy level when the first node dies.

Figure 1.6 shows the standard deviation of the network lifetime normalized to the mean network lifetime, computed using 10 instances of the simulation each using different seed for the random number generator. One can observe that mobility does not only extend the network lifetime but also reduces its variability, i.e. makes it more predictable. These observations represent strong arguments against the statement that MER does not improve network lifetime. On the other hand, they emphasize the advantages of MER, namely interference reduction and ease of implementation.
The discussion above justifies the selection of MER as the technique of choice for energy-aware routing protocol for MANETs. Moreover, MER allows for easy implementation of channel-aware techniques for routing in MANETs, which take advantage of the inherent diversity of MANETs. In particular, the transmit diversity is used to reduce the transmission cost and exploit the multitude of diversity branches available in MANETs. The subsequent sections will further elaborate on this new approach to channel-aware MER for MANETs.

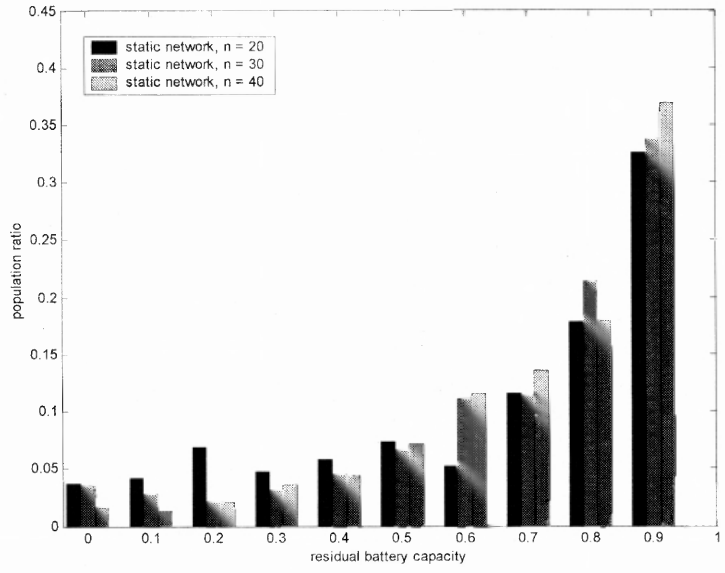

a)

Figure 1.5.a Histogram of the residual battery capacity in a network with static nodes.

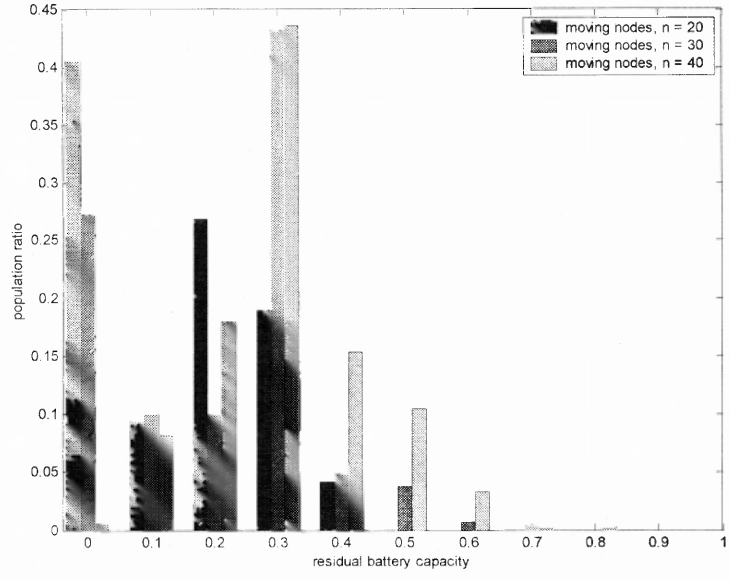

b)

Figure 1.5.b Histogram of the residual battery capacity in a network with dynamic nodes.

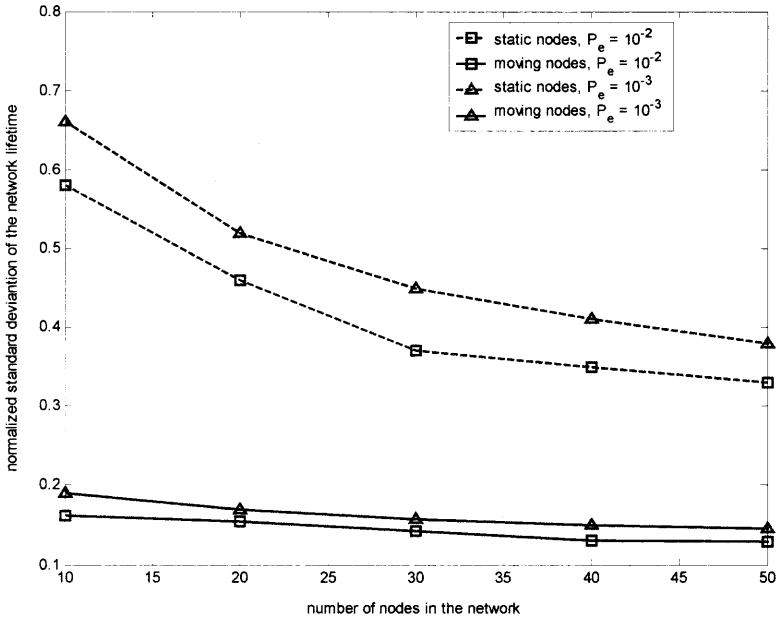

Figure 1.6 Normalized standard deviation of the network lifetime for a network with static and moving nodes.

1.4.3 Literature Survey of Power-aware Routing Schemes for MANETs

The best review of the research in all three categories listed above is given in [4], in which authors present different approaches, discuss their merits and propose their own power-aware multiple access protocol. Another thorough survey is given in [10].

MER has been discussed in [7], [8] and [9]. While all three papers investigate MER and its effect on the network lifetime, [7] also proposes the distributed algorithm for maintaining network connectivity with minimum required energy. The approach is based on each node computing a set of its *neighbors* in a distributed fashion. The authors show that if the neighbors are selected appropriately, the graph consisting of the nodes and their links with their neighbors is a connected graph containing all minimum energy routes in the network. This graph is called the *enclosure graph*. Only the links belonging

to the enclosure graph need to be established in the network. This considerably reduces the power that MTs need to consume in order to maintain connectivity with the rest of the network. The significant drawback of this paper, as well as the vast majority of papers treating the subject, is the simplistic channel model. The authors assume that the channel model is only distance-based, thus converting the problem greatly dependent on the nature of the wireless propagation channel into one dependent only on the geometry of the network. The authors assume no shadowing or fading, and thus, their algorithm would not perform optimally in realistic conditions. Nevertheless, their approach to minimizing the energy the network consumes for maintaining connectivity can be extended to include realistic channel models, which is the one of the contributions of this work.

MBLR based on a metrics reflecting the affinity of a node to route a packet, which is in turn a function of the residual battery energy of the node is discussed in [5]. The author proposes a hybrid cost metric, which leans toward MER when all nodes have significant remaining battery energy, and switches to affinity-based metrics, i.e. MBL routing, when the battery energy of nodes is low. The question, then, becomes when to switch from MER to MBL routing, and this depends on the network topology. MBL routing schemes based on load-balancing techniques are considered in [11], [12], [13], [14], [15]. It has been observed that maximizing the time to the first network partition is a NP-complete problem in the case of unequal packet sizes. The authors of [11] propose a set of heuristics to circumvent the computational complexity associated with the optimal solution. They first discuss the flow augmentation algorithm in which the flow is augmented on the shortest path by an incremental amount, whereas the cost metrics is dependent on the residual battery energy of the nodes. After the flow augmentation, the

shortest cost paths are re-calculated. The result of the algorithm is the flow that will be used at each node to properly split the traffic. Next, the authors propose the flow redirection algorithm based on the metrics of the minimum lifeitime of the route, defined as the minimum of the lifetimes of the nodes along the route. They redirect a portion of each flow at every node in a way that the minimum lifetime of every route with positive flow will increase or at least will stay the same. These algorithms are distributed.

The major drawback of these algorithms and the approach in general is that performance is strongly dependent on the network topology, in addition to the interference the network may generate to the surroundings. They also require that information about battery energy levels of all MTs in the network is available for route computation.

A survey on the power-aware schemes in the MAC layer is given in [10]. In this paper, authors review the power-aware aspects of the network layers, and focus on the MAC layer. In [16], the authors propose the algorithm to change the mode of the MT based on the application-level information. In [17], an energy-consumption model of a MT in a MANET is derived based on the actual parameters of WLAN cards, to be used in designing optimal switching from one mode to another.

The common shortcoming of all power-aware routing schemes in the literature is the over-simplification of wireless channel models. Vast majority of papers simply neglect the fact that the wireless channel models are in fact subject to impairments, such as fading. They are only restricted to distance-based channel model. This results in two types of oversights. First, algorithms that achieve their goal for simplified channel models may not do so for realistic channel models. For example, a minimum energy route with

simple distance-based channel model may not be the minimum energy route if it is severely affected by fading. Second, neglecting the channel impairments hides the potential ways to mitigate these impairments using channel-aware minimum energy routing schemes.

Recently, the potential of channel-aware routing schemes to combat channel impairments has started to gain recognition in the literature. The diversity has been singled out as a particularly suitable approach to mitigate channel impairments through routing. This is due to the fact that MANETs inherently provide spatial diversity, and consequently route diversity. The fact that each node is a transmitter and a receiver yields a perfect scenario for transmit/receive diversity. Boyer at al. study the use of transmit diversity in very simplified network scenarios [18], investigating if the relaying should be done by just amplifying the received signal or decoding it and re-transmitting. Souryal et al. investigate the route diversity as a way of mitigating fading [19]. However, their approach is rather complicated, as it requires the information on the fast-varying channel condition along the entire route.

The power-aware routing schemes described above provide a variety of approaches to minimization of power consumption and maximization of network lifetime. The main focus of this work is the MER approach. Its appeal stems from its ability to combine the network lifetime extension with interference minimization, which is the combination suitable for many applications, as discussed above. As explained in the introduction and as will be elaborated in the subsequent sections, the idea pursued here is to remove the simplistic channel modeling and investigate the potential of routing schemes to cope with channel impairments in MANETs.

1.5 Fundamentals of Transmit Diversity

1.5.1 Introduction

Diversity techniques in general exploit the idea of generating multiple independent replicas of the transmitted signal at the receiver. Although the replicas are obtained by multiple transmissions of the same signals, if they are affected by independent channel attenuations, the probability that all replicas are severely degraded by the channel decreases rapidly with the number of independent signal replicas. The receiver can thus properly combine the received replicas in order to extract the transmitted signal correctly. Diversity is usually used to combat fading, in which case the fading affecting the signal replicas must be independent from each other.

There are several ways in which one can provide the receiver with independently fading replicas of the same signal. They include frequency diversity, time diversity and antenna diversity. In frequency diversity the same signal is transmitted on several carriers, where the separation between successive carriers required for providing independent carrier fading equals or exceeds the coherence bandwidth of the channel. Time diversity consists in transmitting the signal in different times, whose separation equals or exceeds the coherence time of the channel. Antenna diversity employs multiple transmit and/or receive antennas. Receive diversity (Figure 1.7.a) uses multiple antennas at the receiver and performs combining in order to improve the quality of the received signal. The independence condition will be fulfilled if the receive antennas are separated by few wavelengths. In transmit diversity (Figure 1.7.b), multiple transmit antennas are used to transmit the signal, whose multiple replicas are then received combined at

receiver. The independence condition here stipulates that the transmit antennas must be separated by several wavelengths.

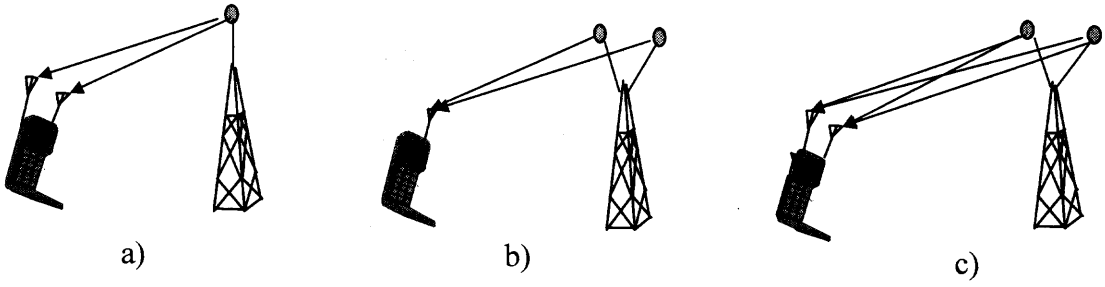

Figure 1.7 Diversity techniques: receive diversity (a), transmit diversity (b) and transmit/receive diversity (c).

Transmit and receive diversity is also possible (Figure 1.7.c), using multiple transmit and multiple receive antennas. The resulting channel is known as multiple-input-multiple-output (MIMO) channel.

Among antenna diversity techniques, receive diversity provides the best performance for the same total transmit power. The major problem with receive diversity approach is the cost, size and power of the remote units. The use of multiple antennas and combining circuits makes the remote units larger and more expensive. As a result, receive diversity techniques have almost exclusively been used at the base stations. At the current state of technology, receive diversity is not considered for implementation.

Recently, transmit diversity schemes have drawn significant attention in the research community [20], [21]. The independence condition is achieved either by adequate space-time or space-frequency encoding of the signal at the transmitter [22]. Performance-wise, transmit diversity is inferior to receive diversity. As a rule of thumb,

transmit diversity with two transmit antennas achieves a 3 dB inferior performance to receive diversity with two receive antennas [22].

Another, more sophisticated, method for obtaining diversity is based on the idea of exploiting the multipath components of the fading signal [23]. It has been generally accepted that fading statistics of multipath components are independent. One can exploit these multipath components by use of a signal having a bandwidth much greater than the coherence bandwidth of the channel. A signal with bandwidth W will resolve multipath components separated in time by at least $1/W$. Consequently, with a multipath spread of T_m, there are T_mW resolvable signal replicas. The optimal receiver for processing a wideband signal in multipath fading is called a RAKE receiver or a RAKE matched filter [Viterbi]. In the following section, the most important characteristics of the RAKE receiver will be summarized, in particular the expressions for the detection error probability, at the extent that they relate to this work

1.5.2 Error Probability of RAKE Receiver

The RAKE receiver is the maximum likelihood (ML) detector for a signal transmitted over the generalized fading channel, which is characterized by L independent paths, each of which is a slowly varying fading channel with Gaussian noise. Thus, the received signal is a set of noisy delayed replicas of the transmitted signal, whereby each replica is affected by independent fading. The RAKE receiver essentially implements the maximum-ratio combining (MRC) form of diversity [24]. For coherent detection and known path delays and BPSK modulation, the error probability of the RAKE receiver can be easily derived. Two different cases can be considered; first, one can assume that the

mean square values of the fading attenuation on all paths are equal, which amounts to assuming equal signal-to-noise ratios (SNR) on all paths:

$$\bar{\gamma}_i = \frac{E}{N_0} E(\alpha_i^2) = \frac{E}{N_0} E(\alpha^2) = \bar{\gamma} \tag{1.6}$$

where α_i is the fading attenuation on the i^{th} path, E is the energy-per-bit of the transmitted signal and N_0 is the noise power. The second important case is the one where the mean square values of the channel attenuation on different paths (i.e. SNRs) are not equal. This case is more common, as it accommodates channel delay profiles reported by the field measurements [25]. The closed-form solution for the error probability of the RAKE receiver for coherent detection, BPSK modulation, known path delays and equal SNRs on all L paths was derived in [23]:

$$P_e = [0.5(1-\mu)]^L \sum_{k=0}^{L-1} \binom{L-1+k}{k} [0.5(1+\mu)]^k \tag{1.7}$$

where by definition:

$$\mu = \sqrt{\frac{\bar{\gamma}}{1+\bar{\gamma}}} \tag{1.8}$$

The closed-form also solution exists for the error probability of the RAKE receiver for coherent detection, BPSK modulation, known path delays and non-equal SNRs on all L paths [23]:

$$P_e = \frac{1}{2} \sum_{k=1}^{L} \pi_k \left[1 - \sqrt{\frac{\bar{\gamma}_k}{1+\bar{\gamma}_k}} \right] \tag{1.9}$$

where π_k is defined as

$$\pi_k = \prod_{\substack{i=1 \\ i \neq k}}^{L} \frac{\bar{\gamma}_k}{\bar{\gamma}_k - \bar{\gamma}_i} \tag{1.10}$$

Important approximation of (4) is available for $\bar{\gamma}_k >> 1, k = 1...L$:

$$P_e \approx \binom{2L-1}{L} \prod_{k=1}^{L} \frac{1}{4\bar{\gamma}_k} \tag{1.11}$$

In the derivation of the error probabilities (1.2) and (1.4) perfect estimates of the channel tap weights are assumed. In practice, relatively good estimates can be obtained if the channel fading is sufficiently slow, e.g. if the ratio of the channel coherence time to the symbol duration is not less than 100 [23].

1.6 New Approach to Minimum Energy Routing in Rayleigh-fading Channels

Based on the discussion in Sections 1.4.1 and 1.4.2, the main characteristics of the MER approach to energy-aware routing in MANETS are

- minimization of the total transmit power, hence the minimization of the interference generated to the surroundings
- maximization of the network lifetime

The combination of the above two benefits makes MER a promising approach to the design of energy efficient MANETs. The shortcoming of the approaches previous to MER in MANET consist in the oversimplification of the channel models used to compute the link cost metrics, as discussed in Section 1.4.3. In this work, the assumption of distance-based channel models is removed and a much more realistic channel model, composed of path loss, shadowing and Rayleigh fading, is considered instead. With these additional channel impairments taken into account, the routing schemes based on only the distance-based channel models would perform unsatisfactorily.

The fundamental phenomenon that makes reliable wireless transmission difficult is time-varying multipath fading. Theoretically, the most effective technique to mitigate

multipath fading is transmitter power control. Perfect power control is the assumption widely used in the literature to justify omitting the fading from the channel model [7], [8], [11].

Alamouti cites two major problems with the assumption of power control [22]: the first is the required transmitter dynamic range to overcome fading; the second is the feedback information regarding channel conditions that needs to be made available by the receiver to the transmitter, which results in throughput degradation and considerable added complexity to both transmitter and the receiver. Increased complexity of MTs is a serious drawback for MANETs. One could add two more problems raised by the assumption of perfect power control. First, power control is never perfect. As reported in [Viterbi], the error in power control is a lognormal random variable with the standard deviation of 3 dB. Second, the experience in the implementation of power control mechanisms is available only from cellular systems, whereby power control has only been implemented in the downlink, with the base station performing required measurements of the received signal and feeding back the power control commands to MTs. Significant research efforts that have focused on the convergence and the optimality of different power control schemes were restricted to this particular centralized, BS-oriented scenario [26], [27],[28], [29]. In the context of MANETs the feasibility of a successful implementation of power control mechanism, in which a centralized entity performing power control of all transmitters is not in the picture, has not yet been studied. In the case where different receiving MTs, are sending power-control commands independently of each other to their respective transmitting MTs, whether and under what conditions would a power control scheme converge and be

efficient has not been thoroughly analyzed. Therefore, the assumption of fast-rate power control in combating the fading needs to be removed.

Shadowing can also seriously hamper the reliability of communications in the wireless medium. Fortunately, the correlation distance of shadowing attenuation is significantly larger than the correlation distance of fading, and is comparable to the correlation distance of the path loss attenuation. In addition, the coherence bandwidth of fading is very large, which results in identical shadowing attenuation in both directions. Thus, efficient open-loop slow-rate power control is sufficient to cope with shadowing*. One can thus assume that MTs perform open-loop power control that efficiently copes with shadowing. However, *shadowing is not neglected*, as is the case in most of the literature, it is just assumed that the shadowing attenuations *are known*. In fact, open-loop power control makes up for the composite path loss plus shadowing attenuation, i.e. one can assume that this composite attenuation is known. From this point of view, there is no interest in observing path loss and shadowing separately.

In the absence of the fast-rate power control, the idea is to combat Rayleigh fading using diversity. In MANETs, each MT serves as a transmitter and/or a receiver and MTs are usually scattered in a uniform fashion round a coverage area. Thus, MANETs possess inherent potential to exploit diversity techniques. There are two levels of diversity in MANETs, namely route diversity and transmit/receive diversity.

Route diversity is created by the multiplicity in the available routes between a given source and a destination. One way to exploit the route diversity consists in splitting the flow of packets between a given source and a destination into two or more flows, using

---

* Open-loop power control [49] adjusts the power level of the transmitted signal according to the power level of the received signal, i.e. no feedback from the receiver is required

weighting which reflects the current channel conditions along the routes. This is in fact load balancing with load splitting. However, this approach is essentially in contrast with the distributed nature of MANETs; namely, the channel conditions on all routes must be known at the source in order to select the best route. Given the high rate of change of channel conditions, this seems to be unfeasible, even if the issue of high signaling load generated by the exchange of channel information among nodes is neglected. Another, similar approach, consists in splitting the traffic over two routes in order to be able to provide the transmit diversity in the final hop of the route. Unfortunately, this approach also relies on the information about the fading along the routes, and it only exploits diversity in the final hop of the route.

In this work, transmit/receive diversity is used to combat fading, reduce the network's total consumed power and extend network lifetime. In particular, the fourth form of transmit/receive diversity is used, as discussed in Section 1.5.1, based on the use of wideband signal to exploit the multipath nature of the fading channel. One can thus assume that the signal is a wideband signal, such as CDMA signal. The approach is hence directly applicable to CDMA-based systems.

As discussed in Section 1.5.1, the multipath nature of the fading signal is exploitable only if the delay spread of the multipath components is larger than the pulse duration of the wideband signal in CDMA this is the chip duration). This is the case in cellular systems, where the distance between the BS and MTs allow for large delays between the multipath components. On the other hand, in indoor environments, the delay spread is not large enough to allow the resolvability of the multipath components; thus, for indoor systems, the Rayleigh fading is generally considered to be single-path. Table

1.1 and Table 1.2 show the delay profile for a typical outdoor [25] and indoor environment [30], respectively.

Table 1.1 Delay Profile of a Typical Outdoor Environment

Delay (in μs)	**0**	**0.2**	**0.5**	**1.6**	**2.3**	**5.0**
Fractional power (in dB)	-3.02	0	-2	-6	-7.93	-10.10

Source: G.L. Stuber, Principles of mobile Communication, Kluwer Academic Publishers, Norwell, MA, 1997, p. 84

Table 1.2 Delay Profile of a Typical Indoor Environment

Delay (in ns)	**0**	**8**	**20**	**30**	**50**	**80**
Fractional power (in dB)	-20	0	-16	-9	-12	-14

Source: Institute for Telecommunication Sciences 2000 Technical Progress Report, http://www.its.bldroc.gov/tpr/2000/its_t/wireless/wireless_fig1.gif

The average distance between MTs in MANET application is much closer to the distance range of indoor systems than to that of cellular systems. Therefore, single-path Rayleigh fading is assumed. In order to exploit the multipath diversity, *it is created artificially*. Namely, artificial delay profile is created by transmitting the same signal from two MTs-transmitters to the same MT-receiver, as illustrated in Figure 1.8.

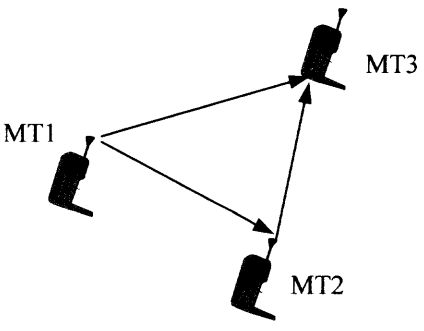

Figure 1.8 Artificial creation of delay profile.

In Figure 1-2, MT 1 has a packet to transmit to MT 3. It transmits it on channel 1. It then transmits it to MT 2 on channel 2, which then transmits it to MT 3 on channel 1 after some delay T_1. The reception and processing of the packet by MT 2 generates additional delay of T_p. The total delay between the signals received by MT 3 from MT 1 and MT 2 is thus

$$T_d = T_1 + T_p \tag{1.12}$$

By changing T_1, the delay T_d can be controlled. MT 3 uses the RAKE receiver and may not be aware that the transmission is being performed using multiple transmitters. From its perspective, the received signal is the multipath fading signal with delay spread T_d.

This mechanism can be used for each hop along the route. The issues of the transmit power gain achieved by the transmit diversity, the optimal power allocation on the diversity branches and the effect on the network lifetime will be extensively studied in the subsequent chapters. The use of transmit diversity will significantly affect the link costs and the way the routes are being established. Theoretically, the number of MTs involved in the transmission of a signal between a given source and a destination using diversity may be twice larger than the number involved in the transmission without diversity. Thus, the signaling between MTs required to exchange the information related to diversity transmission, such as power levels on the diversity branches and link costs, will be accordingly affected.

Clearly, this approach allows to exploit diversity *in each hop along the route*. It is fully distributed, meaning that only the information involving the MTs participating in the transmission/reception is required for the initiation of the diversity transmission. Thus, the difficulties of the route-diversity-based approaches are avoided. The intent is to

produce a routing algorithm that uses diversity transmission at each hop, detects the best MTs to participate in the diversity transmission and provides MTs with information required to initiate diversity transmission. The algorithm ought to be distributed and self-organizing. Since it is based on the MER approach, it should minimize the total consumed power of the network and maximize network lifetime.

CHAPTER 2

OVERLAY INTERFERENCE SUPPRESSION FOR NEXT GENERATION WIRELESS NETWORKS

2.1 Introduction

In this chapter, a new approach to the suppression of the interference in next generation CDMA networks is presented. The discussion starts by establishing the relation with the problem of the suppression of inter-tier interference in the hierarchical macrocell/microcell structures in cellular systems, as shown in Figure 2.1 below.

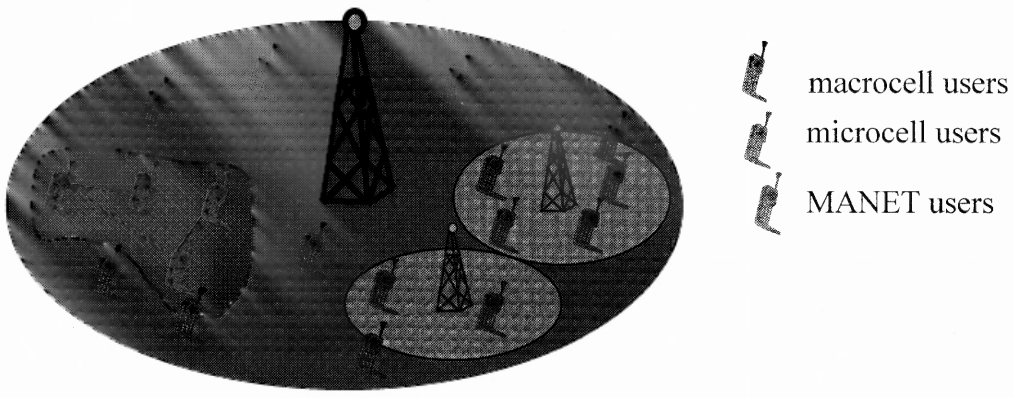

Figure 2.1 Inter-tier interference in next generation wireless networks.

The problem of interference suppression in next generation wireless networks is thus equivalent to the problem of the suppression of macrocell interference in microcells in hierarchical cell structures for cellular systems. The latter, more general formulation of the problem, will be addressed here. The results are straightforwardly extendable to the original problem of interference suppression in MANET. The material presented in this chapter was published in [50] and [51].

Hierarchical cellular microcell/macrocell architectures have been introduced into cellular wireless systems with the intent to minimize the signaling and processing power required for tracking and handoff management of high-mobility users. In addition, hierarchical systems can augment the total capacity by creating new microcells in hot traffic spots, and preserve the investment cost by preserving current macrocell deployment while adding new microcells. Significant improvements in terms of teletraffic performance [31], hot-spot traffic relief [32], [33] and overall capacity [34] have been reported. Hierarchical microcell/macrocell structures have been widely implemented in wireless networks, especially in indoor and urban downtown-like environments. Different multiple-access schemes opened the way for different hierarchical system designs, such as FDMA-only, TDMA-only and hybrid TDMA/FDMA and TDMA/CDMA [35]. On the other hand, CDMA-only microcell/macrocell systems have been traditionally considered as impracticable. This impression was due to inherent characteristics of CDMA, which counteract the performance of microcell/macrocell systems.

The major problem was perceived in the sensitivity of CDMA to the near-far problem. Due to significantly larger macrocell radius, high-mobility macrocell users located near to the macrocell boundary would transmit at much higher power than microcell users, generating strong interference to the surrounding microcells. In fact, the microcells on the macrocell boundary are disabled by these macrocell users. Similar considerations are also valid for the forward link, whereby the presence of the strong signal of the macrocell BS greatly reduces the forward link capacity of microcells, and vice-versa. These considerations have resulted in designs of CDMA-based networks

without hierarchical capabilities, or in designs that have left the near-far problem in the boundary microcells unsolved [35].

The UMTS/IMT-2000 Wideband CDMA standard provides Hierarchical Cell Structure (HCS) capability through Interfrequency Handover [36]. This mechanism circumvents the near-far problem by establishing macrocell and microcell tiers operating in disjoint frequency spectrums, each occupying 5 MHz of bandwidth. In this system, Mobile Stations (MSs) perform regular inter-frequency pilot measurements to decide on switching from macrocell to microcell tier and vice-versa. However, double bandwidth requirements may be two high a price to pay for many wireless. network operators. In addition to this, in the Interfrequency Handover, inter-frequency pilot measurements are time-multiplexed with packet transmissions/receptions, which may hamper the capability of MSs to promptly switch between microcell and macrocell tiers in the case when delay-sensitive traffic is being transmitted/received.

Due to recent advances in MUD theory [37],[38],[39], the view of the near-far problem as an inherent feature of CDMA systems has been abandoned. Consequently, the existence of macrocell and microcell tiers occupying the same frequency spectrum became feasible. Unlike conventional single user detectors, multiuser detectors can successfully detect signals received at different power levels. This feature can be exploited to eliminate high-mobility user interference at the microcells' BSs and low-mobility user interference at the macrocells' BSs, and thus provide the features of hierarchical cellular structures at no additional cost in terms of radio transmission resources.

2.2 Problem Statement

In this section, the difficulties encountered by single user detection in hierarchical cellular systems are analyzed. The discussion is based on a simplified scenario of a circular microcell/macrocell system, comprising of one microcell placed at the boundary of the overlaying macrocell (Fig. 2.2).

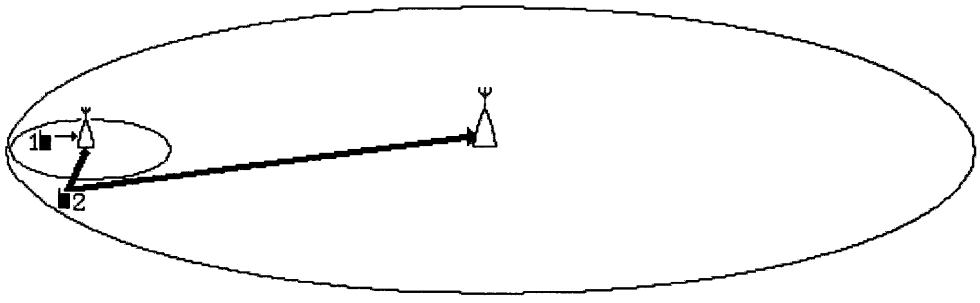

Figure 2.2 Simplified macrocell/microcell system.

The results obtained thereof can straightforwardly be extended to multi-cell systems. Assume that K_μ users are controlled by the microcell base station (BS) and K_M users are controlled by the macrocell BS, which are denoted as 'microcell users' and 'macrocell users', respectively. Assume also that the system is synchronous, as its simplicity allows for comparative analysis of different MUD techniques considered here. In addition, the performance of each technique is an indicator of the performance of its asynchronous counterpart. Short signature sequences are considered, which is realistic, since third-generation W-CDMA standard provisions the option to use short sequences in the reverse link. In order to simplify the analysis, the other-cell microcell interference is neglected. Although its approximation by Gaussian random variable strongly holds, the

correlations between other-cell interference components, as seen by different microcell users attached to the same BS, would make the analysis more complex.

Consider the basic CDMA multiuser channel model, consisting of the sum of antipodally modulated, normalized, short synchronous signature waveforms in additive white Gaussian noise. The output of a single user detector for the *k*-th user at the microcell BS, consisting of the filter matched to the signature sequence of the *k*-th microcell user is:

$$y_k = A_k^{(\mu)} b_k + \sum_{\substack{j=1 \\ j \neq k}}^{K_\mu} A_j^{(\mu)} b_j \rho_{jk} + \sum_{j=K_\mu+1}^{K_\mu+K_M} A_j^{(\mu)} b_j \rho_{jk} + n_k(t), \quad k = 1..K_\mu \tag{2.1}$$

where b_i is the bit transmitted by user i, $\rho_{ij} = \int_0^T s_i(t) s_j(t) dt$ is the correlation between signature waveforms of users j and k, $A_i^{(\mu)}$ is the amplitude of user i received at the microcell BS, and $n_k(t)$ is a zero-mean Gaussian noise with variance σ^2. The first term in (2.1) is the desired user's signal, the second term is the interference from other microcell users, or *in-cell* interference, the third term is the interference from the macrocell users, and the forth term is the noise. For the sake of simplicity, the other-cell interference is neglected. Traditionally, in order to compute the probability of the detection error, interference has been modeled as Gaussian random variable [40],[41]. This is justified by the fact that power control insures nearly equal received amplitudes, and for large number of users and low signal-to-noise ratios, the Gaussian model strongly holds. In equation (2.1), however, Gaussian approximation would not hold, as the third term is the sum of components having wide range of amplitudes. Indeed, depending on their channel gain with respect to the macrocell BS that controls them, and their channel gain with respect to the microcell BS, macrocell users can be received by the microcell BS at wide range of

amplitudes. The macrocell interference will therefore be dominated by macrocell users located near to the microcell BS. This leads us to consider a simplified scenario, with only one microcell user and one macrocell user, denoted as user 1 and user 2, respectively. Equation (2.1) now becomes

$$y_1^{(\mu)}(t) = A_1^{(\mu)} b_1 + A_2^{(\mu)} b_2 \rho_{12} + n_1^{(\mu)}(t) \tag{2.2}$$

The probability of error is

$$\begin{aligned} P_1^e &= P[y_1^{(\mu)} > 0 | b_1 = -1] = 0.5P[n_1 > A_1^{(\mu)} - A_2^{(\mu)}\rho_{12}] + 0.5P[n_1 > A_1^{(\mu)} + A_2^{(\mu)}\rho_{12}] \\ &= 0.5Q\left(\frac{A_1^{(\mu)} - A_2^{(\mu)}|\rho_{12}|}{\sigma}\right) + 0.5Q\left(\frac{A_1^{(\mu)} + A_2^{(\mu)}|\rho_{12}|}{\sigma}\right) \le Q\left(\frac{A_1^{(\mu)} - A_2^{(\mu)}|\rho_{12}|}{\sigma}\right) \end{aligned} \tag{2.3}$$

The last expression is the upper bound on the error probability, which is very tight for strong interferer amplitude. It can be seen that if $A_1^{(\mu)} - A_2^{(\mu)}|\rho_{12}| < 0$, i.e.

$$\frac{A_2^{(\mu)}}{A_1^{(\mu)}} > \frac{1}{|\rho_{12}|} \tag{2.4}$$

the single user detector is no better than guessing. In order to evaluate the ratio $A_2^{(\mu)}/A_1^{(\mu)}$, assume that both macrocell and microcell BSs perform perfect power control in the way to maintain equal received amplitude, say A, for all users. The average power transmitted by the macrocell user is then $P_{tr}^{(M)} = A^2 r_M^{\beta}$, and the macrocell user power received by the microcell BS is $P_r^{(\mu)} = P_{tr}^{(M)} r_\mu^{-\beta}$, where r_M and r_μ are the distances of the macrocell user to the macrocell and microcell BS, respectively, and β is the propagation exponent. The amplitude of the macrocell user received at the microcell BS is $A_2^{(\mu)} = \left(P_r^{(\mu)}\right)^{1/2} = A(r_M / r_\mu)^{\beta/2}$. Using the propagation exponent beta of four, and noting that the amplitude of the microcell user is $A_1^{(\mu)} = A$, (2.4) becomes:

$$(r_\mu / r_M)^2 > |\rho_{12}| \tag{2.5}$$

Last expression defines the area inside which the presence of a *single active macrocell user* renders detection of a *single microcell user's* signal impossible. This area is shown in Figure 2.3, for the two outer tiers of microcells. The ratio of macrocell radius to the microcell radius is five and ρ_{12} is 0.0625. For more realistic situations, including in-cell interference, other-cell interference and more realistic error probabilities, this area covers virtually the entire macrocell, with the exception of small area around the macrocell BS.

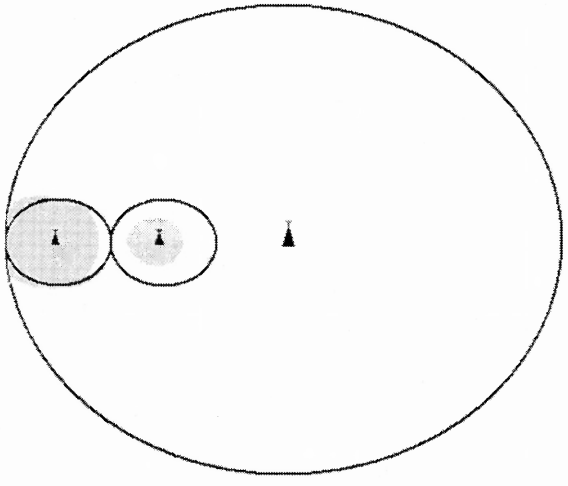

Figure 2.3 Area where one macrocell user disables the detection of microcell users.

Multiuser detection approach allows transforming this inherent CDMA problem into the one of the tradeoff between computational cost and system capacity. In terms of the MUD theory, the problem can be defined as a simultaneous detection of microcell users attached to the same microcell BS, in the following conditions:

i) Large number of in-cell interferers with equal, known amplitudes of 0 dB (under perfect power control assumption)

ii) Small number of macrocell interferers with unknown, high amplitudes (exceeding 25 dB for macrocell interferers located near to the macrocell boundary). Macrocell interferers can be attached to the overlaying macrocell, or a neighboring macrocell.

iii) Large number of other-cell microcell interferers, with low or very low, unknown amplitudes [42].

In the following section, the application of the decorrelating detector to the problem defined above is examined. In Section 2.4, the two-stage MPDs will be introduced.

2.3 Decorrelating Detector

The decorrelating detector detects the bits of interfering macrocell users along with the bits of desired microcell users. The output of the bank of K_μ filters matched to microcell users' signature sequences and K_M filters matched to macrocell users' signature sequence can be represented by a vector:

$$\underline{y} = RA_\mu \underline{b} + \underline{n} \tag{2.6}$$

where $\underline{y} = [y_1, \ldots, y_{K_\mu + K_M}]^T$, $R = \{\rho_{ij}\}$ is a $(K_\mu + K_M) \times (K_\mu + K_M)$ crosscorrelation matrix, A_μ is the diagonal matrix of users' amplitudes receieved at the microcell BS, $\underline{b} = [b_1, \ldots, b_{K_\mu + K_M}]^T$ is the vector of transmitted data bits and $\underline{n} = [n_1, \ldots, n_{K_\mu + K_M}]^T$ is the vector of zero-mean Gaussian noises with covariance matrix $\sigma^2 R$.

The decorrelating detector, or decorrelator [43], is the linear transformation

$$\hat{\underline{b}} = \text{sgn}(R^{-1} \underline{y}) \tag{2.7}$$

The decorrelating detector has several properties that make it suitable for use in the problem defined in Section 2.2. As is evident from (2.7), the decorrelator requires no

estimate of amplitudes. As the amplitude of macrocell users, which are controlled by the macrocell BS, are not known to the microcell BSs, this property is indeed crucial. Another important property of the decorrelator is that it is the optimal linear detector when amplitudes are not known [44]. This insures linear optimality in macrocell interference suppression. Furthermore, the decorrelator has minimum near-far resistance of all multiuser detectors. On the other hand, microcell BSs have good estimate of the amplitudes of their own users, and that information is not used by the decorrelator. This entails sub-optimality in the detection of microcell users. However, the sub-optimality is indeed minimal in the presence of macrocell interference, as there is little or no improvement in going from the decorrelating to the linear optimum detector for weak signals with high interferers [45]. In addition, the optimal linear detector achieves optimality only for one user at a time for a given amplitude – crosscorrelation configuration.

The error probability of the decorrelator for a microcell user k is given by:

$$P_e^k = Q\left(\frac{a_k}{\sigma\sqrt{R^+_{kk}}}\right) = Q\left(\frac{a}{\sigma\sqrt{R^+_{kk}}}\right) = Q\left(\sqrt{\frac{\eta}{R^+_{kk}}}\right), \quad k = 1 \ldots K_\mu \tag{2.8}$$

where $R_{kk}^{+} = (R^{-1})_{kk}$, $a_k = (A_\mu)_{kk} = a$ is the amplitude of microcell users, and $\eta = a^2/\sigma^2$ is the signal-to-noise ratio* maintained by the power control mechanism of the microcell BS. The computation of the inverse of the crosscorelation matrix R, which includes cross-correlations of signature sequences of microcell users and macrocell interferers, is the crucial step in the implementation of the decorrelator. The computation needs to be performed every time a new user or an interferer is present or when an existing user or an

* Not to be confused with signal-to-interference ratio (SIR), which is in fact the direct target of the power control. However, once the SIR is fixed, η is also fixed and equal for all users.

interferer becomes inactive or fades away. Therefore, recursive formulas for computations of matrix inverse can greatly reduce the computational complexity. A useful approximate expression for error probability follows from simplifying the structure of R by assuming $\rho_{ij} = \rho$ for $i \neq j$ and $\rho_{ii} = 1$.

Proposition 2.1 If $\rho_{ij} = \rho$ for $i \neq j$ and $\rho_{jj} = 1$, then:

$$P_e^k = Q\left(\sqrt{\eta \frac{[1+(K-1)\rho](1-\rho)}{1+(K-2)\rho}}\right) \tag{2.9}$$

where K is the size of R.

Equation (2.9) indicates that for sufficiently large η, augmenting the number of strong interferers barely affects the error probability of the decorrelator. Consequently, for large η, the computational complexity is the only limit to the system capacity. This is totally opposite to conventional detectors, which have negligible complexity but are substantially affected by the interference. It can also be shown that (2.9) is the decreasing function of ρ. It follows that the lower bound and upper bound on (2.8) can be obtained from (2.9) by putting $\rho = \min_{i \neq j}\{|\rho_{ij}|\}$ and $\rho = \max_{i \neq j}\{|\rho_{ij}|\}$, respectively.

The size of the cross-correlation matrix R and the necessity of re-computing R^{-1} every time the set of active interferers changes presents a major limitation to practical implementations of the decorrelator. Also, the computations are performed at the microcell BSs, generating uneven distribution of computational burden between macrocell and microcell tiers. In the following section, MPDs having significantly lower computational complexity and better processing power management between tiers are presented.

2.4 Multiuser Projection Detectors

Multiuser projection detector consists of two stages. In the first stage, called projection stage, the macrocell interference is eliminated by projection of the received signal onto the space orthogonal to the subspace spanned by macrocell users' signals. In the second stage, called detection stage, conventional MUD techniques are applied to the output of the projection stage. This gives birth to different MPDs, depending on the MUD technique used in the second stage.

2.4.1 Projection Stage

The structure of the projecton stage is described first. For the sake of geometrical interpretation, it is convenient to represent all signals as vectors in the N-dimensional space spanned by the set of N orthonormal functions, which are the shifted versions of the chip pulse. This is in fact equivalent to sampling at the chip rate. The signature sequence of user i can thus be represented as a vector $\underline{s_i} = [s_{1i}, \ldots, s_{Ni}]^T$, where $s_{ij} \in \{-1,1\}$. The received signal $\underline{r} = [r_1, \ldots, r_N]^T$, then becomes:

$$\underline{r} = SA\underline{b} + \underline{m} \tag{2.10}$$

where $\underline{m}$ is the N-dimensional noise vector, and $S = [\underline{s_1}\ \underline{s_2}\ \ldots\ \underline{s_K}]$ is an NxK matrix of users' signature sequences. Matrix S can be partitioned as $S = [S_\mu\ S_M]$, where $S_\mu = [\underline{s}_1^\mu\ \underline{s}_2^\mu\ \ldots\ \underline{s}_{K_\mu}^\mu]$ and $S_M = [\underline{s}_1^M\ \underline{s}_2^M\ \ldots\ \underline{s}_{K_M}^M]$ are NxK_μ and NxK_M matrices of signature sequences of microcell and macrocell users, respectively, where $K = K_\mu + K_M$. One can now write (2.10) as:

$$\underline{r} = S_\mu A_\mu \underline{b_\mu} + S_M A_M \underline{b_M} + \underline{m} \tag{2.11}$$

where A_μ and A_M are K_μxK_μ and K_MxK_M diagonal amplitude matrices, respectively; $\underline{b}_\mu$ and $\underline{b}_M$ are the vectors of transmitted bits of microcell and macrocell users, respectively; $\underline{m}$ is the N-dimensional Gaussian noise vector with covariance $\sigma^2 I$. Provided that each signature sequence is not spanned by other signature sequences, S_μ and S_M span disjoint subspaces, denoted as *microcell subspace*, M_μ, and *macrocell subspace*, M_M, respectively. The second term in (2.11) represents the undesired interference vector, lying in M_M. It can be eliminated by projecting the received signal onto the subspace orthogonal to M_M, denoted as *orthogonal macrocell subspace*, O_M. The projection onto O_M is achieved by multiplying by projection matrix[†] $P = (I - S_M S_M^+)$, where S_M^+ is the Moore-Penrose generalized inverse of S_M[‡]. So, the projected received signal, $r^{(p)}$, is:

$$\underline{r}^{(p)} = P\underline{r} = (I - S_M S_M^+)[S_\mu A_\mu \underline{b}_\mu + S_M A_M \underline{b}_M + \underline{m}] = S_\mu^{(p)} A_\mu \underline{b}_\mu + P\underline{m} \tag{2.12}$$

where the macrocell interference vector vanishes, and $S_\mu^{(p)} = P\ S_\mu$ is the matrix of microcell users' signature sequences projected O_M.

The final step in the projection stage is the bank of K_μ filters matched to microcell users' signature sequences. The microcell user signal vector at the output of the projection stage is then:

$$\begin{aligned} \underline{y}^{(p)} &= S_\mu^T \underline{r}^{(p)} = S_\mu^T (S_\mu^{(p)} A_\mu \underline{b}_\mu + P\underline{m}) = S_\mu^T P S_\mu A_\mu \underline{b}_\mu + S_\mu^T P\underline{m} \\ &= (PS_\mu)^T PS_\mu A_\mu \underline{b}_\mu + (PS_\mu)^T \underline{m} = S_\mu^{(p)T} S_\mu^{(p)} A_\mu \underline{b}_\mu + S_\mu^{(p)T} \underline{m} \\ &= R_\mu^{(p)} A_\mu \underline{b}_\mu + \underline{n}^{(p)} \end{aligned} \tag{2.13}$$

where $R_\mu^{(p)}$ is the crosscorrelation matrix of projected microcell signature sequences and $n^{(p)}$ is the zero-mean projected Gaussian noise, with covariance matrix $\sigma^2 R_\mu^{(p)}$. Hence,

---

[†] Projection matrices are symmetric and idempotent (i.e. P^2=P)

[‡] $S_M^+ = (S_M^T S_M)^{-1} S_M^T$

the output of the projection stage preserves the structure of the output of the conventional matched filter bank detector, wherein the effect of the macrocell interference projection is reflected through the cross-correlation matrix of the projected microcell signature sequences and covariance matrix of the noise. However, matrix $R_\mu^{(p)}$ is not normalized, i.e. $(R_\mu^{(p)})_{ii} = \rho_{ii}^{(p)} \neq 1$, although it is symmetric. In order to be able to use the existing expressions for error probabilities for MUD techniques applied to the output of the matched filter bank, a normalized cross-correlation matrix at the output of the projection stage is required. The normalization can be achieved by the following transformation:

$$R_\mu^{(p,n)} = DR_\mu^{(p)}D \tag{2.14}$$

where

$$D = \begin{bmatrix} \frac{1}{\sqrt{\rho_{11}^{(p)}}} & 0 & \cdots & 0 \\ 0 & \frac{1}{\sqrt{\rho_{22}^{(p)}}} & & \\ \vdots & & \ddots & \\ 0 & & & \frac{1}{\sqrt{\rho_{K_\mu K_\mu}^{(p)}}} \end{bmatrix} \tag{2.15}$$

It is easy to check that

$$\rho_{ij}^{(p,n)} = \frac{\rho_{ij}^{(p)}}{\sqrt{\rho_{ii}^{(p)}}\sqrt{\rho_{jj}^{(p)}}} \tag{2.16}$$

and therefore $\rho_{ii}^{(p,n)} = 1$. Obviously, since $R_\mu^{(p)}$ is symmetric, so is $R_\mu^{(p,n)}$.

The following proposition suggests the transformation of the projected signal producing a normalized cross-correlation matrix.

Proposition 2.2 Let

$$\underline{y}^{(p,n)} = D\underline{y}^{(p)} \tag{2.17}$$

Then:

$$\underline{y}^{(p,n)} = R_{\mu}^{(p,n)} A_{\mu}^{(p,n)} \underline{b}_{\mu} + \underline{n}^{(n,p)} \tag{2.18}$$

where

$$A_{\mu}^{(p,n)} = D^{-1} A_{\mu} \tag{2.19}$$

is the projected normalized amplitude matrix, and $\underline{n}^{(n,p)}$ is the Gaussian noise with covariance matrix $R_{\mu}^{(p,n)}$. Transformation (2.17) does not affect the power of the output signal $\underline{y}^{(p)}$, as it is easy to show that

$$A_{\mu} R_{\mu}^{(p)} A_{\mu} = A_{\mu}^{(p,n)} R_{\mu}^{(p,n)} A_{\mu}^{(p,n)} \tag{2.20}$$

Based on Proposition 2.2, the final form of the projection stage and MPD is shown in Figure 2.4. From equation (2.19) it is clear that the projection stage entails amplitude distortion. The amplitude of the i^{th} desired user at the output of the projection stage, $a_i^{(p,n)}$, is proportional to the degree of alignment of the user's signature sequence with O_M subspace. After the projection, users attached to the own-cell BS will no longer be received with the same amplitude, even if perfect power control is assumed (Figure 2.5).

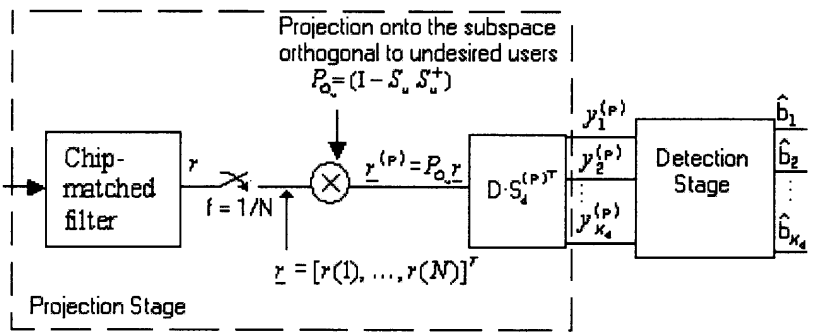

Figure 2.4 Multiuser projection detector.

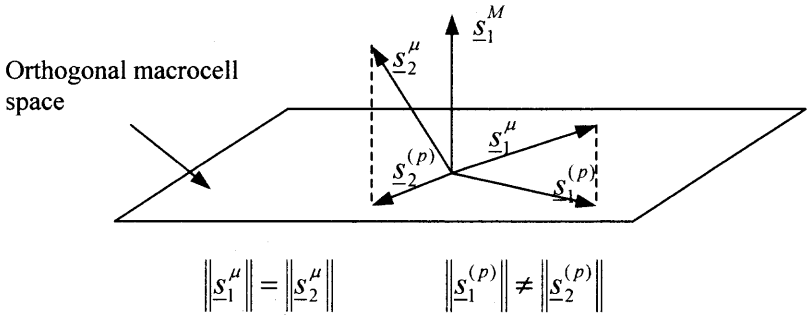

Figure 2.5 Projection onto orthogonal macrocell space.

Another important feature of the projection stage is that the amplitudes of macrocell users do not affect its output, and thus the final output of MPD. In fact, it can be shown that the projection stage provides optimal protection against macrocell interferers if their amplitudes are not known [33]. In addition, the projection stage allows better distribution of computational burden between the macrocell and microcell tiers. Namely, the computations involving macrocell users are reduced to the multiplication by the projection matrix P, which can be computed and made available by the macrocell BS.

2.4.2 Detection Stage

In this section, conventional MUD techniques are applied to the output of the projection stage, yielding different forms of MPDs. Conventional multiuser detectors have been extensively studied in the literature, so the details will not be given here. The error probabilities will be computed by modifying the corresponding expressions for error probabilities of conventional multiuser detectors in order to account for amplitude distortion and projected normalized cross-correlation matrix.

2.4.3 Single User Projection Detector (SUPD)

The simplest MPD, single user projection detector, is obtained by thresholding the output of the projection stage, resulting in (Figure 2.6)

$$\hat{b}_k = \mathrm{sgn}((\underline{y}^{(p)})_k) = \mathrm{sgn}(a_k^{(p,n)} b_k + \sum_{\substack{i=1 \\ i \neq k}}^{K_\mu} a_i^{(p,n)} \rho_{ik}^{(p,n)} b_k + n_k^{(p,n)}) \tag{2.21}$$

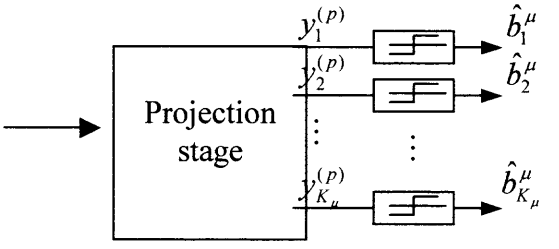

Figure 2.6 Single user projection detector (SUPD).

The second term in (2.21) is the projected in-cell interference. If the number of interfering users is large, the approximation by a zero-mean Gaussian variable with power

$$\sigma_I^2 = \sum_{\substack{i=1 \\ i \neq k}}^{K_\mu} (a_i^{(p,n)})^2 (\rho_{ik}^{(p,n)})^2 \tag{2.22}$$

strongly holds. The error probability for a microcell user is given by:

$$P_e^k = Q\left(\frac{a_k^{(p,n)}}{\sqrt{\sigma^2 + \sum_{\substack{i=1 \\ i \neq k}}^{K_\mu} (a_i^{(p,n)})^2 (\rho_{ik}^{(p,n)})^2}} \right) = Q\left(\sqrt{\frac{\eta}{\rho_{kk}^{(p)} + \eta \sum_{\substack{i=1 \\ i \neq k}}^{K_\mu} (\rho_{ik}^{(p)})^2}} \right) \tag{2.23}$$

As can be seen, projection stage enables single-user detection with operable error probabilities.

2.4.4 Projection Decorrelator (PD)

The output the projection stage can be input into decorrelator, as shown in Figure 2.7.

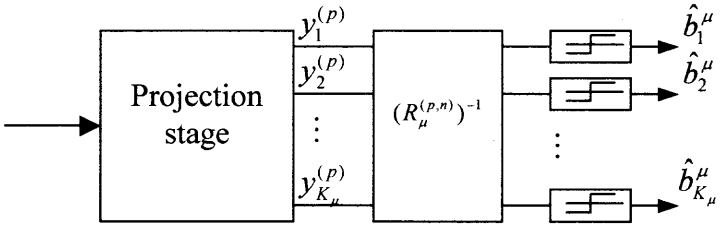

Figure 2.7 Projection decorrelator (PD).

This structure is denoted as projection decorrelator. The detected bit-vector is:

$$\underline{\hat{b}}_\mu = \mathrm{sgn}((R_\mu^{(p)})^{-1}\underline{y}^{(p)}) = \mathrm{sgn}(A_\mu^{(p,n)}\underline{b}_\mu + (R_\mu^{(p,n)})^{-1}\underline{n}^{(p,n)}) \tag{2.24}$$

The error probability for a microcell user is given by:

$$P_e^k = Q\left(\frac{a_k^{(p,n)}}{\sigma\sqrt{(R_\mu^{(p,n)})_{kk}^+}}\right) = Q\left(\sqrt{\frac{\eta\rho_{kk}^{(p)}}{(R_\mu^{(p,n)})_{kk}^+}}\right) \tag{2.25}$$

Proposition 2.3 Error probabilities (2.25) and (2.8) are equal.

Proposition 2.3 entails that the performance of the PD is equivalent to the conventional decorrelator. Indeed, conventional decorrelator projectes the signal of the desired user onto the space orthogonal to the space spanned by the interfering users. PD does the same, only in two steps: it first projects signals of microcell users onto the orthogonal macrocell space; second, it projects the signal of the desired microcell user onto the space orthogonal to the space spanned by projected signals of interfering microcell users. The two procedures are therefore equivalent.

The fundamental advantage of PD over conventional decorrelator is computational efficiency and distribution of computational burden between tiers. Note that R is a $(K_\mu+K_M)$x$(K_\mu+K_M)$ matrix, while $R_\mu^{(p,n)}$ is K_μx K_μ matrix, which makes computing the inverse of $R_\mu^{(p,n)}$ significantly faster than computing R^{-1}. Also, $(R_\mu^{(p,n)})^{-1}$ needs to be re-computed when the set of interfering microcell users changes, while the conventional decorrelator needs to re-compute R^{-1} upon a change in either set of microcell or macrocell interferers. In addition, microcell BS does not need to know signature sequences of macrocell users, but only the projection matrix P. Therefore, the projection matrix P can be computed by macrocell BS and distributed to all microcell BSs every time the set of interfering macrocell users changes. This method decreases the signaling load generated by the exchange of information about signature sequences of active users between macrocell and microcell tiers. It also entails more uniform distribution of computational effort between microcell and macrocell tier. Note that in conventional decorrelator, all computational burden is on the microcell tier.

2.4.5 Decorrelating Decision-Feedback Projection Detector (DFPD)

The DFPD (Figure 2.8) can be defined by the following decision criterion:

$$\hat{\underline{b}}_\mu = \mathrm{sgn}\{F_\mu^{(p,n)} A_\mu^{(p,n)} \underline{b} - [F_\mu^{(p,n)} - diag(F_\mu^{(p,n)})] A_\mu^{(p,n)} (\underline{b} - \hat{\underline{b}}) + \underline{n}\} \tag{2.26}$$

where $F_\mu^{(p,n)}$ is the Cholesky factorization of $R_\mu^{(p,n)}$, i.e. $R_\mu^{(p,n)} = (F_\mu^{(p,n)})^{\mathrm{T}} F_\mu^{(p,n)}$, and $\underline{n}$ is Gaussian vector with covariance matrix $\sigma^2 I$. It is straightforward to verify that $\mathrm{F}_\mu^{(p,n)} = D \cdot (\mathrm{F}_\mu^{(p)})^T$.

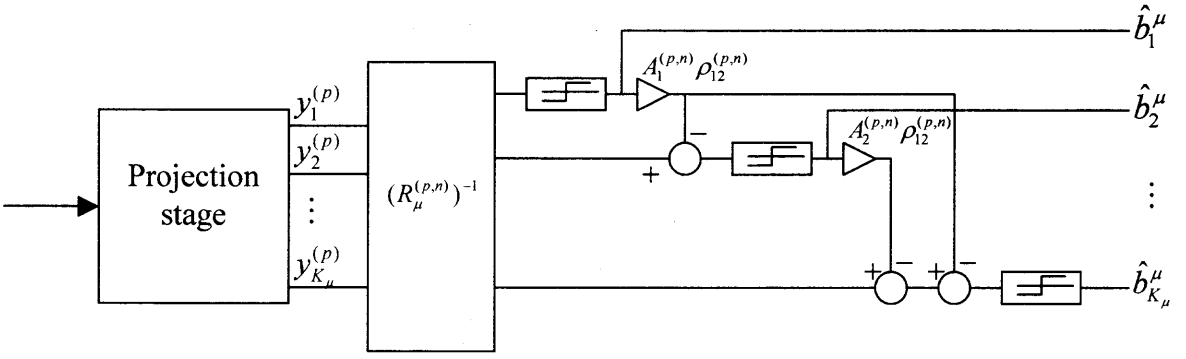

Figure 2.8 Decorrelating decision-feedback projection detector (DFPD).

Essentially, DFPD for user k first projects the signal $y^{(p)}$ onto the subspace orthogonal to the subspace spanned by users k+1, …, K_μ and then uses the previous decisions for users 1…k-1 to subtract their estimated interference. This procedure produces independent white Gaussian output noise. Like PD, DFDP is more computationally efficient than conventional decorrelating decision feedback detector, as it requires computation of K_μx K_μ-dimensional $(F_\mu^{(p,n)})^{-T}$, rather than $(K_\mu + K_M)$ x $(K_\mu + K_M)$-dimensional F^T. On the other hand, unlike PD, DFDP is sensitive to the amplitudes of the microcell interferers. In addition, the order in which the feedback is performed affects the error probability. The decreasing normalized amplitude order is the optimal way to perform feedback [46]. The error probability of the DFPD was derived in [46] and [38]. It is modified here, so to account for modified correlation matrix and amplitude distortion of projected signals.

$$P_e^k = 2^{1-k} \sum_{(b_1,\ldots,b_{K_\mu-1})\in\{-1,1\}^{k-1}} \sum_{(\hat{b}_1,\ldots,\hat{b}_{K_\mu-1})\in\{-1,1\}^{k-1}} Q\left((F_\mu^{(p,n)})_{kk} \frac{A_k^{(p,n)}}{\sigma} + \sum_{i=1}^{k-1} (F_\mu^{(p,n)})_{ki} \frac{A_i^{(p,n)}}{\sigma} (b_i - \hat{b}_i) \right) \times$$
$$\prod_{j=1}^{k-1} \left[\delta_{b_j=\hat{b}_j} + (1-2\delta_{b_j=\hat{b}_j}) \times Q\left((F_\mu^{(p,n)})_{jj} \frac{A_j^{(p,n)}}{\sigma} + \sum_{i=1}^{j-1} (F_\mu^{(p,n)})_{ji} \frac{A_i^{(p,n)}}{\sigma} (b_i - \hat{b}_i) \right) \right]$$
$$= 2^{1-k} \sum_{(b_1,\ldots,b_{K_\mu-1})\in\{-1,1\}^{k-1}} \sum_{(\hat{b}_1,\ldots,\hat{b}_{K_\mu-1})\in\{-1,1\}^{k-1}} Q\left((F_\mu^{(p,n)})_{kk} \sqrt{\eta\rho_{kk}^{(p)}} + \sum_{i=1}^{k-1} (F_\mu^{(p,n)})_{ki} \sqrt{\eta\rho_{ii}^{(p)}} (b_i - \hat{b}_i) \right) \times$$
$$\prod_{j=1}^{k-1} \left[\delta_{b_j=\hat{b}_j} + (1-2\delta_{b_j=\hat{b}_j}) \times Q\left((F_\mu^{(p,n)})_{jj} \sqrt{\eta\rho_{jj}^{(p)}} + \sum_{i=1}^{j-1} (F_\mu^{(p,n)})_{ji} \sqrt{\eta\rho_{ii}^{(p)}} (b_i - \hat{b}_i) \right) \right] \tag{2.27}$$

2.4.6 Successive Interference Cancellation Projection Detector (SCPD)

SCPD (Figure 2.9) uses the decisions for projected signals of users 1…k-1, obtained by the matched filter bank, to subtract the estimated interference from the projected signal of user k:

$$\hat{b}_k = \operatorname{sgn}\left(y_k^{(p)} - \sum_{j=1}^{k-1} a_j^{(p,n)} \rho_{jk}^{(p,n)} \hat{b}_j \right) = \operatorname{sgn}\left(y_k^{(p)} - a \sum_{j=1}^{k-1} \frac{\rho_{jk}^{(p)}}{\sqrt{\rho_{kk}^{(p)}}} \hat{b}_j \right) \tag{2.28}$$

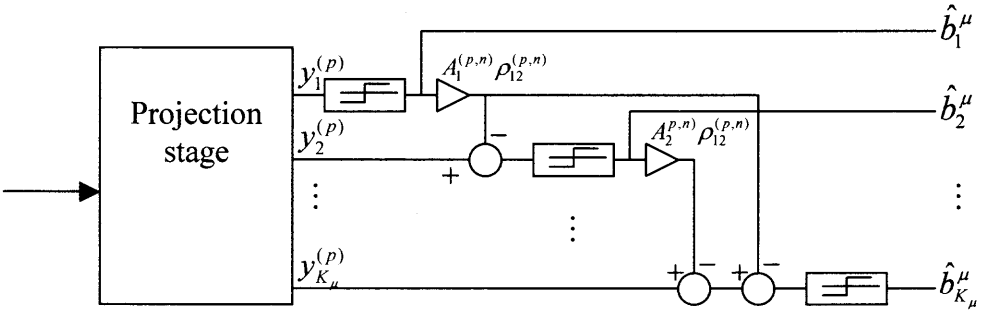

Figure 2.9 Successive interference cancellation projection detector (SCPD).

Like in DFPD, users are detected in descending order of their amplitudes, starting with the strongest users. Again, the approximate expression for error probability of

successive cancellation detector [38] are modified in order to account for modified correlation matrix and the amplitude distortion:

$$P_e^k = Q\left(\frac{a_k^{(p,n)}}{\sqrt{\sigma^2 + \sum_{j=k+1}^{K_\mu}(A^{(p,n)})^2(\rho_{jk}^{(p,n)})^2 + 4\sum_{j=1}^{k-1}(A^{(p,n)})^2(\rho_{jk}^{(p,n)})^2 P_e^{k-1}}}\right) \tag{2.29}$$

$$= Q\left(\sqrt{\frac{\eta(\rho_{kk}^{(p)})^2}{\rho_{kk}^{(p)} + \eta\sum_{j=k+1}^{K_\mu}(\rho_{jk}^{(p)})^2 + 4\eta\sum_{j=1}^{k-1}(\rho_{jk}^{(p)})^2 P_e^{k-1}}}\right)$$

2.5 Numerical Results and Analysis

For numerical evaluation of error probabilities, the processing gain is set to 255. The set of 256 Gold signature sequences of length 255 is used. There are three possible values for the cross-correlation of Gold sequences [47], which in this particular case are –0.0039, -0.0067 and 0.1216.

The error probabilities are averaged over users' error probabilities, which are generally different for each user. The computation was performed for different numbers of users per microcell, whereas the number of macrocell interferers is equal to the number of microcell users. Because of the complexity of error probability computation, there was a limit of ten users for the DFPD.

Figure 2.10 shows the detection error probability as a function of the signal-to-noise ratio of the microcell user signal for PD, SUPD, DFPD and SCPD, for the fixed number of microcell and macrocell users. As the curves clearly show, each of the detectors presented here enables microcell user detection in the microcells lying on the macrocell boundary. In fact, the MPD perform equally in every microcell, regardless of its location

and the macrocell interference power. It is worth noting that once the macrocell interference is eliminated in the projection stage, single user detection yields operable bit error probabilities. On the other hand, the conventional single user detector is disabled by macrocell interference in microcells close to the macrocell boundary. It can also be seen from the graphs that the performance of DFPD and PD is less affected by the number of interfering users than SCPD and PD.

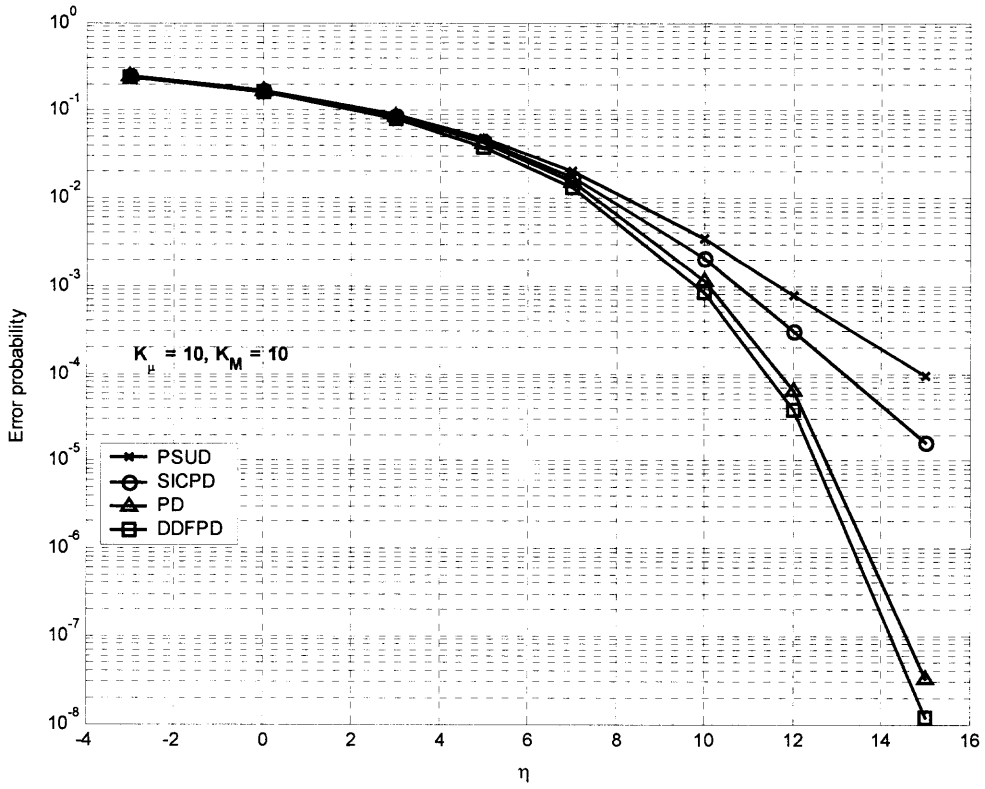

Figure 2.10 Performance comparison of multiuser projection detectors.

Clearly, the DFPD offers best performance, at the expense of computational complexity. However, if the amplitude distortion is not significant, the performance of the DFPD is close to PD. In addition, the DFPD introduces delay. The SCPD and PSUD have lower complexity but inferior performance. The SCPD is better than single user

detector. However, it also introduces delay. Finally, the PD, SCPD and SUPD have simple error probability expressions, allowing derivation of closed form expressions for system capacity for the desired error probability.

In this chapter, the techniques for receiver design for microcell/macrocell structures in CDMA were presented, which pave the way for full benefits of macrocell/microcell structuresw within single frequency band. A pre-processing stage, which projects the received signal onto the space orthogonal to the subspace spanned by the macrocell users' signature sequences, is introduced, followed by the different MUD techniques. It has been shown that this design solves the near-far problem that disables the single user detector in microcells located at the macrocell boundary. Therefore, each of the MUD techniques can be used in the detection stage of MPD. Decorrelating decision-feedback projection detector offers the best performance among the four analyzed detectors. Conventional single-user detection is shown to be feasible after the macrocell interference is eliminated in the projection stage. Interesting areas for further research are the impact of other-cell interference, and the effect of some information about macrocell user's amplitudes onto the receiver design and detection error probabilities.

CHAPTER 3

THE FUNDAMENTALS OF POWER COMBINING – DEFINITIONS, FEASIBILITY AND GAIN ANALYSIS

3.1 Introduction

In the previous chapter, the rational behind the use of transmit diversity in MANETs was established. In this section, the fundamentals of power combining for MANET are laid down, the theoretical background and the analytical results for the simulation-based analysis and results in Chapter 4 are given.

The fact that multiple nodes can transit the signal to the same destination node implies that the process of finding the minimum energy route from the source to the destination is much more involved than in the case of simple transmission. It involves the process of determining which nodes can be coupled to provide diversity transmission for all the hops along the route. Therefore, the nodes need to maintain links and exchange the routing information not only with the nodes to whom they could transmit or from whom they could receive the signal, but also with the nodes with whom they could participate in a diversity transmission to other nodes. This, on the other hand, brings into the picture the problem of maintaining network connectivity in an efficient but also distributed fashion. The issue of maintaining network connectivity will be discussed in the following chapter. The composite path loss-shadowing-fading channel model that used in this work is specified in Section 3.2. In Section 3.3, the concept of power combining triplets (PCT) is introduced. The optimal power allocation in the diversity branches is then derived and the gain in terms of the total consumed power is analytically evaluated. Finally, the graph representation and link cost computation in the network is discussed.

In Section 3.4, the generalization of the PCT concept is performed by introducing power combining chains (PCC), representing the cascade of two or more PCTs, which further reduces the total consumed power. The optimal power configuration is derived and the graph representation of PCC is introduced.

3.2 Channel Model

The channel is a composite path loss-shadowing-Rayleigh fading channel. The channel attenuation is thus given by:

$$h = d^m \cdot \gamma \cdot \beta \tag{3.1}$$

where d is the distance between the receiver and the transmitter, m is the path-loss exponent, γ is the shadowing attenuation and β is the attenuation due to Rayleigh fading. Throughout this work the typical value of m of four is used.

Field measurements have shown that the decibel representation of the shadowing attenuation has lognormal probability distribution [53], [25]:

$$f(\gamma_{dB}) = \frac{20/\ln 10}{\gamma_{dB}\sigma_{sh}\sqrt{2\pi}} \exp\left\{-\frac{(20\log_{10}\gamma_{dB} - \mu_{\gamma})^2}{2\sigma_{sh}^2}\right\} \tag{3.2}$$

Equivalently, γ_{dB} is a normal random variable with zero mean and variance σ_{sh}^2. Because of this, it is sometimes more practical to represent γ as:

$$\gamma = 10^{\frac{\gamma_{dB}}{10}} \tag{3.3}$$

This representation will be used extensively in the rest of this chapter.

The Rayleigh fading is assumed to be slow, meaning that it can be considered constant during the intervals sufficiently long to enable confident measurements of the fading attenuation at the receiver. Thus, the fading attenuation, although being random, is

assumed to be known to the receiver. Slow fading attenuation is a widely used assumption [40], since fast fading can efficiently mitigated by use of interleaving. Hence, the probability density function of the fading attenuation is given by:

$$f(\beta) = \frac{\beta}{\sigma} e^{-\frac{\beta}{\sigma}} \tag{3.4}$$

No fast-rate power control to mitigate fading is assumed. As discussed in Section 1.4.2, fast-rate (i.e. power control at fading rate, or closed-loop power control) power control in MANET environment presents several challenges, which have not been present in the cellular networks. On the other hand, the slow-rate power control (i.e. power control at shadowing rate, or open-loop power control) is being performed, as it is simple and symmetric [49]. The rate of slow-rate power control is assumed adjusted to track the changes in the path-loss and shadowing attenuations and is considered to be perfect. The rate of change of shadowing is associated with the *correlation distance*, i.e. the distance at which two samples of shadowing attenuation still show significant correlation. This distance is in the order of tens of meters, thus the rate of slow-rate power control is proportional to the rate of crossing of MT's crossing the correlation distance. For all but very fast mobile users, this rate is in the order of magnitude of Hz. Therefore, it is indeed slow and its implementation is simple. In Chapter 4, the actual random process used to generate shadowing attenuation will be described.

Based on the discussion above, because of the slow-rate power control, the receiver perceives pure Rayleigh fading channel and is able to measure the fading attenuation by averaging it over sufficiently long bit blocks. For any given modulation technique, the receiver is thus capable of computing the mean received signal power required to achieve the desired error probability, P_e. In practice, the receiver would estimate the required

mean received power by use of one of the existing techniques, such as by estimating the received signal to noise ratio or the error probability. Whichever the method, the receiver can map the incoming signal and the desired error probability into a unique value of required mean received signal power. This value is then used to perform the slow-rate power control of the transmitter by sending the adequate power control commands. The transmitter, receives the slow-rate power control commands and adjusts its transmit power accordingly. If the mean received signal power required to achieve a given desired error probability is $P^r(P_e)$, then the required mean transmit signal power will be:

$$P^t = hP^r(P_e) = d^m \gamma P^r(P_e) \tag{3.5}$$

perceives the composite path loss-shadowing-fading channel, and needs to adjust its transmit power. The actual dependence of $P^r(P_e)$ on P_e will be a function of the modulation technique used.

Having established the channel model, the idea of power combining for MANETs can be introduced now.

3.3 Power Combining Triplets

Consider a simple three-node network shown in Figure 3.1.

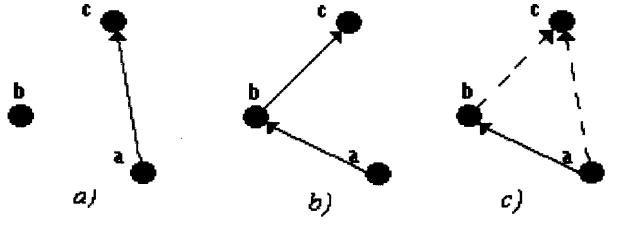

Figure 3.1 Power combining triplet.

Assume that node *a* transmits packets to node *c*. Depending on the relative location of node *b* with respect to nodes *a* and *c*, the minimum energy (power) route could either be the route $a \rightarrow c$ (Fig. 19.a) or route $a \rightarrow b \rightarrow c$ (Fig. 19.b). In either case, in order to provide transmit diversity, one can add a second transmit branch (Fig. 19.c); in the former case, the diversity can be assured by also transmitting the signal to node *b*, which then provides the second transmit branch for transmission to *c*; in the latter case, node *a* can provide the second transmit branch by also transmitting to *c*. The received signals on the two diversity branches, namely $a \rightarrow c$ and $b \rightarrow c$, will be independent provided that nodes *a* and *b* are more than few wavelengths apart, which is always true. If the average power levels of signals transmitted on the diversity branches are well adjusted, the total received power at *c* required to achieve certain error probability P_e is significantly lower with the use of transmit diversity than with a single transmitter. The total transmit power of all three nodes will in turn depend on the locations of the nodes. The transmit diversity in this context is called *power combining*, as the received powers on the two branches will be adjusted to yield minimum total transmit power. The power combining branches are marked by dashed lines.

3.3.1 Problem Statement

With respect to the discussion above, the criterion for initiating power combining needs to be defined, along with the optimal transmit power configuration, i.e. optimal transmit powers on the two diversity branches. Next, the reduction of the total transmit power achieved by power combining needs to be evaluated. Finally, the relationship between the gain and some parameters, such as the distance between nodes, desired received signal

quality (i.e. error probability) and power consumed for relaying packets, needs to be analyzed.

3.3.2 Initial Definitions

Definition 3.1 The set of nodes $\{a, b, c\}$, where the packets are transmitted from node a to node c using the transmission from node a to node c as one diversity branch, and using transmission $a \rightarrow b \rightarrow c$ as the second diversity branch, as shown in Fig. 19.c, is called *power combining triplet* and denoted by $PCT_{\{a,b,c\}}$. The transmit diversity in this context is called *power combining*. Nodes a, b and c are denoted as *primary transmitter*, *secondary transmitter* and *receiver*, respectively.

Note that the above definition does not specify the criteria for initiating $PCT_{\{a,b,c\}}$

Definition 3.2 Vector $\bar{d}_{\{a,b,c\}} = [d_{ab}, d_{bc}, d_{ac}]$ is called the *distance vector* of $PCT_{\{a,b,c\}}$.

Note that $\bar{d}_{\{a,b,c\}}$ uniquely defines $\mathrm{PCT}_{\{a,\,b,\,c\}}$ in terms of mutual positions of nodes.

Definition 3.3 Vector $\bar{\gamma}_{\{a,b,c\}} = [\gamma_{ab}, \gamma_{bc}, \gamma_{ac}]$ is called the *shadowing vector of* $PCT_{\{a,b,c\}}$.

Definition 3.4 $\Re(x) = \{\bar{r} : r_{ac} = x\}$ is the subspace spanned by the distance vector $\bar{d}_{\{a,b,c\}}$ with fixed d_{ac}, *i.e.* the set of all possible configurations of nodes a, b and c where the distance between the primary transmitter and the receiver, d_{ac}, is fixed.

Definition 3.5 *Shadowing space* $\Gamma = \{\bar{\gamma} : \gamma_{ab} \in \{-\infty, \infty), \gamma_{bc} \in \{-\infty, \infty), \gamma_{ac} \in \{-\infty, \infty)\}$ is the space spanned by $\bar{\gamma}_{\{a,b,c\}}$.

3.3.3 Optimal Transmit Power Configuration and PCT Initiation Criterion

In this section, the optimal transmit powers on the diversity branches are derived and the criteria for PCT initiation is established. The total transmit power required to achieve

desired error probability at the receiver will be derived first, for scenarios with and without power combining, respectively.

Error probability of a BPSK signal in Rayleigh fading with no diversity is [23]:

$$P_e = \frac{1}{2}\left(1 - \sqrt{\frac{P_{ac}^{r'}}{1+P_{ac}^{r'}}}\right) \tag{3.6}$$

where $P_{ac}^{r'}$ is the average signal-to-interference plus noise ratio of the signal transmitted by node a and received at node c. The prime denotes the scenario without power combining, i.e. with single transmit branch. One can assume for convenience that no other-user interference is present, and normalize the mean received power to the noise power, so that $P_{ac}^{r'}$ denotes the mean received signal power. From (3.1), one can obtain the mean received power required to achieve the desired error probability P_e:

$$P_{ac}^{r'} = \frac{(1-2P_e)^2}{4P_e(1-P_e)} \triangleq \alpha(P_e) \tag{3.7}$$

Having in mind that the minimum energy route from node a to node c can be either $a \rightarrow c$ or $a \rightarrow b \rightarrow c$, the total consumed power required to achieve the error probability P_e is

$$P'_{tot} = \min(\alpha(P_e)\gamma_{ac}d_{ac}^m + P_{rec}, \alpha(P_e)\gamma_{ab}d_{ab}^m + \alpha(P_e)\gamma_{bc}d_{bc}^m + 2P_{rec}) \tag{3.8}$$

where m is the path-loss exponent and P_{rec} is the power consumed to receive the signal.

The probability of error with power combining for BPSK modulation is the probability of error of a two-leg RAKE receiver with unequal branch powers [23]:

$$P_e = \frac{1}{2}\left\{\frac{P_{ac}^{r''}}{P_{ac}^{r''}-P_{bc}^{r''}}\left(1 - \sqrt{\frac{P_{ac}^{r''}}{1+P_{ac}^{r''}}}\right) + \frac{P_{bc}^{r''}}{P_{bc}^{r''}-P_{ac}^{r''}}\left(1 - \sqrt{\frac{P_{bc}^{r''}}{1+P_{bc}^{r''}}}\right)\right\} \tag{3.9}$$

where $P_{ac}^{r''}$ and $P_{bc}^{r''}$ are the received powers on the $a \rightarrow c$ and $b \rightarrow c$ diversity branch, respectively. The double prime denotes the scenario with power combining. The total transmit power of nodes a and b with power combining is then

$$P''_{tot} = \alpha(P_e)\gamma_{ab}d_{ab}^m + P_{ac}^{r''}\gamma_{ac}d_{ac}^m + P_{bc}^{r''}\gamma_{bc}d_{bc}^m + 2P_{rec} \tag{3.10}$$

In order to minimize P_{tot}'', the optimal values for $P_{ac}^{r''}$ and $P_{bc}^{r''}$, denoted as $(P_{ac}^{r''})_{opt}$ and $(P_{bc}^{r''})_{opt}$, need to be computed. That can be accomplished by finding the zero of the derivative of (3.5) with respect to $P_{ac}^{r''}$ or $P_{bc}^{r''}$, i.e. by solving

$$\frac{\partial(\alpha(P_e)\gamma_{ab}d_{ab}^m + P_{ac}^{r''}\gamma_{ac}d_{ac}^m + P_{bc}^{r''}\gamma_{bc}d_{bc}^m + 2P_{rec})}{\partial P_{ac}^{r''}} = 0 \tag{3.11}$$

or the equivalent derivative with respect to $P_{bc}^{r''}$, where the initial condition is given by (3.4). Clearly, this amounts to solving:

$$\frac{dP_{bc}^{r''}}{dP_{ac}^{r''}} = -\frac{\gamma_{ac}d_{ac}^m}{\gamma_{bc}d_{bc}^m} \tag{3.12}$$

where again the initial condition is given by (3.4). Unfortunately, the analytical solution is not tractable, even using software tools with symbolic mathematics capabilities, such as Matlab or Mathematica. This problem can be circumvented by resorting to numerical methods. This approach is facilitated by the fact that the solution will depend only on the ratio of the composite channel attenuations on the two diversity branches, given on the right-hand side of (3.7). Thus, one can numerically compute and tabulate the optimal received powers $(P_{ac}^{r''})_{opt}$ and $(P_{bc}^{r''})_{opt}$ for wide range of values of the ratio of the composite channel attenuations and P_e. The curves $(P_{ac}^{r''})_{opt}$ and $(P_{bc}^{r''})_{opt}$ vs. the ratio of the composite channel attenuations for different P_e, computed using this method, are given in Appendix 2.

On the other hand, closed-form analytical solution is available for high received power levels, i.e. low P_e. In this case, Equation (3.4) simplifies to [24]:

$$P_e = \frac{3}{16}\frac{1}{P_{ac}^{r''}P_{bc}^{r''}} \tag{3.13}$$

which allows for easy solving of (3.7) and yields the optimal received powers, given by:

$$\left(P_{ac}^{r''}\right)_{opt} = \frac{\sqrt{3}}{4\sqrt{\alpha}}\sqrt{\frac{d_{bc}^{m}\gamma_{bc}}{d_{ac}^{m}\gamma_{ac}}} \tag{3.14}$$

$$\left(P_{bc}^{r''}\right)_{opt} = \frac{\sqrt{3}}{4\sqrt{\alpha}}\sqrt{\frac{d_{ac}^{m}\gamma_{ac}}{d_{bc}^{m}\gamma_{bc}}} \tag{3.15}$$

Since the benefit from using transmit diversity is negligible for low received SNR, the expressions given by equations (3.9) and (3.10) can be used confidently.

The transmit powers on the two diversity branches are:

$$\left(P_{ac}^{t''}\right)_{opt} = \left(P_{ac}^{r''}\right)\gamma_{ac}d_{ac}^{m} \tag{3.16}$$

$$\left(P_{bc}^{t''}\right)_{opt} = \left(P_{bc}^{r''}\right)\gamma_{bc}d_{bc}^{m} \tag{3.17}$$

In the simple case of (3.8), (3.9) and (3.10) expressions (3.11) and (3.12) become:

$$\left(P_{ac}^{t''}\right)_{opt} = \left(P_{bc}^{t''}\right)_{opt} = \frac{\sqrt{3}}{4\sqrt{\alpha}}\left(\sqrt{d_{ac}d_{bc}}\right)^{m}\sqrt{\gamma_{ac}\gamma_{bc}} \tag{3.18}$$

It follows from Equation (3.13) that in the optimal configuration the transmit powers on the diversity branches are equal. This property is preserved in the case of the exact formula given in Equation (3.4). This reminds of the equal gain combining, only here it is applied to the transmitted rather than received powers. An important consequence of this property is that the receiver does not need to provide separate slow-rate power control on the two diversity branches; namely, since the transmit powers on

the diversity branches need to be maintained equal, the primary and the secondary transmitter can be power-controlled using identical slow-rate power control commands.

The optimal total consumed power with power combining is:

$$(P''_{tot})_{opt} = \alpha(P_e)\gamma_{ab}d_{ab}^m + (P_{ac}^{t''})_{opt} + (P_{bc}^{t''})_{opt} + 2P_{rec} \tag{3.19}$$

which using (3.13) becomes:

$$(P''_{tot})_{opt} = \alpha(P_e)\gamma_{ab}d_{ab}^m + \frac{\sqrt{3}}{2\sqrt{P_e}}\left(\sqrt{d_{ac}d_{bc}}\right)^m\sqrt{\gamma_{ac}\gamma_{bc}} + 2P_{rec} \tag{3.20}$$

Definition 3.6 Given locations of nodes *a* and *c*, node *b* is *feasible for power combining with a for transmission to c* if:

$$(P''_{tot})_{opt} < P'_{tot} \tag{3.21}$$

The location of a feasible node is called a *feasible location.* The power combining triplet $PCT_{\{a,b,c\}}$ is called *feasible power combining triplet.*

Definition 3.7 The region consisting of all feasible locations of node *b* for given locations of nodes *a* and *c* is called *feasibility region of node a to node c*, and denoted as $F(a \rightarrow c)$.

The feasibility of *b* is adopted as the necessary and sufficient condition for the initiation of power combining between nodes *a* and *b* for transmission to node *c*.

Definition 3.8 Among all nodes feasible for power combining with *a* for transmission to *c*, assume that node *b* yields the minimum total consumed power, i.e. $PCT_{\{a,b,c\}}$ consumes less power than any other $PCT_{\{a,n,c\}}, n \notin \{a,b,c\}$. Node *b* is then called *optimal feasible node for power combining with a for transmission to c.* $PCT_{\{a,b,c\}}$ is called minimal PCT.

Proposition 3.1 If there exists $PCT_{\{a,b,c\}}$ then there also exists $PCT_{\{b,a,c\}}$ with the same optimal total consumed power, $(P''_{tot})_{opt}$, and same optimal transmit powers on the power combining branches, $(P_{ac}^{t''})_{opt}$ and $(P_{bc}^{t''})_{opt}$. Consequently, the primary transmitter of $PCT_{\{a,b,c\}}$ is the secondary transmitter of $PCT_{\{b,a,c\}}$, and vice-versa.

Corollary 3.1.1 If node *b* is the optimal feasible node for power combining with *a* for transmission to *c*, then node *a* is also the optimal feasible node for power combining with *b* for transmission to *c*. Equivalently, if $PCT_{\{a,b,c\}}$ is the minimal PCT, then $PCT_{\{b,a,c\}}$ is also minimal PCT.

3.3.4 Average PCT Gain

In this section, the practical benefits of power combining are evaluated. The first goal is to evaluate the size and the shape of the feasibility region. This has a twofold rational behind it. First, it is important to find out if the feasibility region $F(a \rightarrow c)$ is large enough to insure substantial probability of finding a node inside it to be used as the second transmitter (i.e. node *b*). Second, the size of the feasibility region may be used to determine the boundary beyond which a node should not search for feasible nodes. Also, the average gain in terms of total consumed power achieved by power combining needs to be evaluated.

Definition 3.9 *Relative transmit power gain* of $PCT_{\{a,b,c\}}$ for received signal error probability P_e is defined as:

$$G(\bar{d}_{\{a,b,c\}}, \bar{\gamma}_{\{a,b,c\}}, P_e) = \frac{P'_{tot} - (P''_{tot})_{opt}}{P'_{tot}} = 1 - \frac{\alpha(P_e)\gamma_{ab} d_{ab}^m + (P_{ac}^{r''})_{opt}\gamma_{ac} d_{ac}^m + (P_{bc}^{r''})_{opt}\gamma_{bc} d_{bc}^m + 2P_{rec}}{\min(P_{ac}^{r'}\gamma_{ac} d_{ac}^m + P_{rec}, P_{ab}^{r'}\gamma_{ab} d_{ab}^m + P_{bc}^{r'}\gamma_{bc} d_{bc}^m + 2P_{rec})} \quad (3.22)$$

An alternate definition of feasibility (Definition 3.7) is now possible.

Definition 3.10 Given locations of nodes *a* and *c*, node *b* is *feasible* for power combining with *a* for transmission to *c* if $G(\bar{d}_{\{a,b,c\}}, \bar{\gamma}_{\{a,b,c\}}, P_e) > 0$.

Since $\bar{\gamma}_{\{a,b,c\}}$ is random, an estimate of the PCT gain for a given distance vector $\bar{d}_{\{a,b,c\}}$ independent from $\bar{\gamma}_{\{a,b,c\}}$ is needed. With that aim, the following definitions are introduced:

Definition 3.11 The *feasibility probability* of $PCT_{\{a,b,c\}}$ with distance vector $\bar{d}_{\{a,b,c\}}$ for error probability P_e is defined as:

$$\begin{aligned} PF(\bar{d}_{\{a,b,c\}}, P_e) &= \int_{\Gamma,\ G(\bar{d}_{\{a,b,c\}}, \bar{\gamma}_{\{a,b,c\}}, P_e)>0} f(\bar{\gamma}^{(dB)}_{\{a,b,c\}}) d\bar{\gamma}^{(dB)}_{\{a,b,c\}} \\ &= \int_{\Gamma} u[G(\bar{d}_{\{a,b,c\}}, \bar{\gamma}_{\{a,b,c\}}, P_e)] f(\bar{\gamma}^{(dB)}_{\{a,b,c\}}) d\bar{\gamma}^{(dB)}_{\{a,b,c\}} \end{aligned} \tag{3.23}$$

where $\bar{\gamma}^{(dB)}_{\{a,b,c\}} = [\gamma^{(dB)}_{ab}, \gamma^{(dB)}_{bc}, \gamma^{(dB)}_{ac}]$ is the dB-equivalent of $\bar{\gamma}_{\{a,b,c\}}$, i.e.

$\bar{\gamma}_{\{a,b,c\}} = [10^{\frac{\gamma^{(dB)}_{ab}}{10}}, 10^{\frac{\gamma^{(dB)}_{bc}}{10}}, 10^{\frac{\gamma^{(dB)}_{ac}}{10}}]$, $u[x]$ is the unit step function, and $f(\bar{\gamma}^{(dB)}_{\{a,b,c\}})$ is the p.d.f of $\bar{\gamma}^{(dB)}_{\{a,b,c\}}$, given by:

$$f(\bar{\gamma}^{(dB)}_{\{a,b,c\}}) = \frac{1}{(2\pi)^{3/2}\sigma^3_{sh}} e^{-\frac{[(\gamma^{(dB)}_{ab})^2 + (\gamma^{(dB)}_{bc})^2 + (\gamma^{(dB)}_{ac})^2]}{2\sigma^2_{sh}}} \tag{3.24}$$

Definition 3.12 *Average transmit power gain* achieved by $PCT_{\{a,b,c\}}$ for error probability P_e is defined as:

$$\begin{aligned} G(\bar{d}_{\{a,b,c\}}, P_e) &= \int_{\Gamma,\ G_R(\bar{d}_{\{a,b,c\}}, \bar{\gamma}_{\{a,b,c\}}, P_e)>0} G(\bar{d}_{\{a,b,c\}}, \bar{\gamma}_{\{a,b,c\}}, P_e) f(\bar{\gamma}^{(dB)}_{\{a,b,c\}}) d\bar{\gamma}^{(dB)}_{\{a,b,c\}} \\ &= \int_{\Gamma} G(\bar{d}_{\{a,b,c\}}, \bar{\gamma}_{\{a,b,c\}}, P_e) u[G(\bar{d}_{\{a,b,c\}}, \bar{\gamma}_{\{a,b,c\}}, P_e)] f(\bar{\gamma}^{(dB)}_{\{a,b,c\}}) d\bar{\gamma}^{(dB)}_{\{a,b,c\}} \end{aligned} \tag{3.25}$$

Integrals given in (3.18) and (3.20) can be computed numerically for a given distance vector $\bar{d}_{\{a,b,c\}}$ and error probability P_e. They depend on P_{rec}, as is clear form (3.17). In the special case when P_{rec} can be neglected, the following proposition provides useful result:

Proposition 3.3 If $P_{rec} = 0$, then

$$G(\bar{d}_{\{a,b,c\}}, \bar{\gamma}_{\{a,b,c\}}, P_e) = G(k \cdot \bar{d}_{\{a,b,c\}}, \bar{\gamma}_{\{a,b,c\}}, P_e) = G(\bar{d}^{(N)}_{\{a,b,c\}}, \bar{\gamma}_{\{a,b,c\}}, P_e) \tag{3.26}$$

where k is a constant and

$$\bar{d}^{(N)}_{\{a,b,c\}} = [\frac{d_{ab}}{d_{ac}}, \frac{d_{bc}}{d_{ac}}, 1] \tag{3.27}$$

Proof: Follows from (3.17), putting $P_{rec} = 0$

Corollary 3.3.1 If $P_{rec} = 0$, then

$$PF(\bar{d}_{\{a,b,c\}}, P_e) = PF(\bar{d}^{(N)}_{\{a,b,c\}}, P_e) \tag{3.28}$$

Corollary 3.3.2 If $P_{rec} = 0$, then

$$G(\bar{d}_{\{a,b,c\}}, P_e) = G(\bar{d}^{(N)}_{\{a,b,c\}}, P_e) \tag{3.29}$$

The idea behind the Proposition 3.3 is that when $P_{rec} = 0$, the triangle $\{a, b, c\}$ can be scaled by any factor, and its properties defined by Definitions 3.9 through 3.12 do not change. This allows tracking of the individual effect of other parameters, such as P_e and σ_{sh}, onto these properties, and visualization of feasibility regions independently from d_{ac}.

Figures 3.2.a through 3.2.d show the feasibility probability for $P_e = 10^{-1}$, $P_e = 10^{-2}$, $P_e = 10^{-3}$ and $P_e = 10^{-4}$, respectively, as a function of the location of node b, for $P_{rec} = 0$. By virtue of Corollary 3.3.1, the figures are scalable to any value of d_{ac}.

Figures 3.3.a through 3.3.d show the average transmit power gain for $P_e = 10^{-1}$, $P_e = 10^{-2}$, $P_e = 10^{-3}$ and $P_e = 10^{-4}$, respectively, as a function of the location of node b, for $P_{rec} = 0$. By virtue of Corollary 3.3.2, the figures are scalable to any value of d_{ac}.

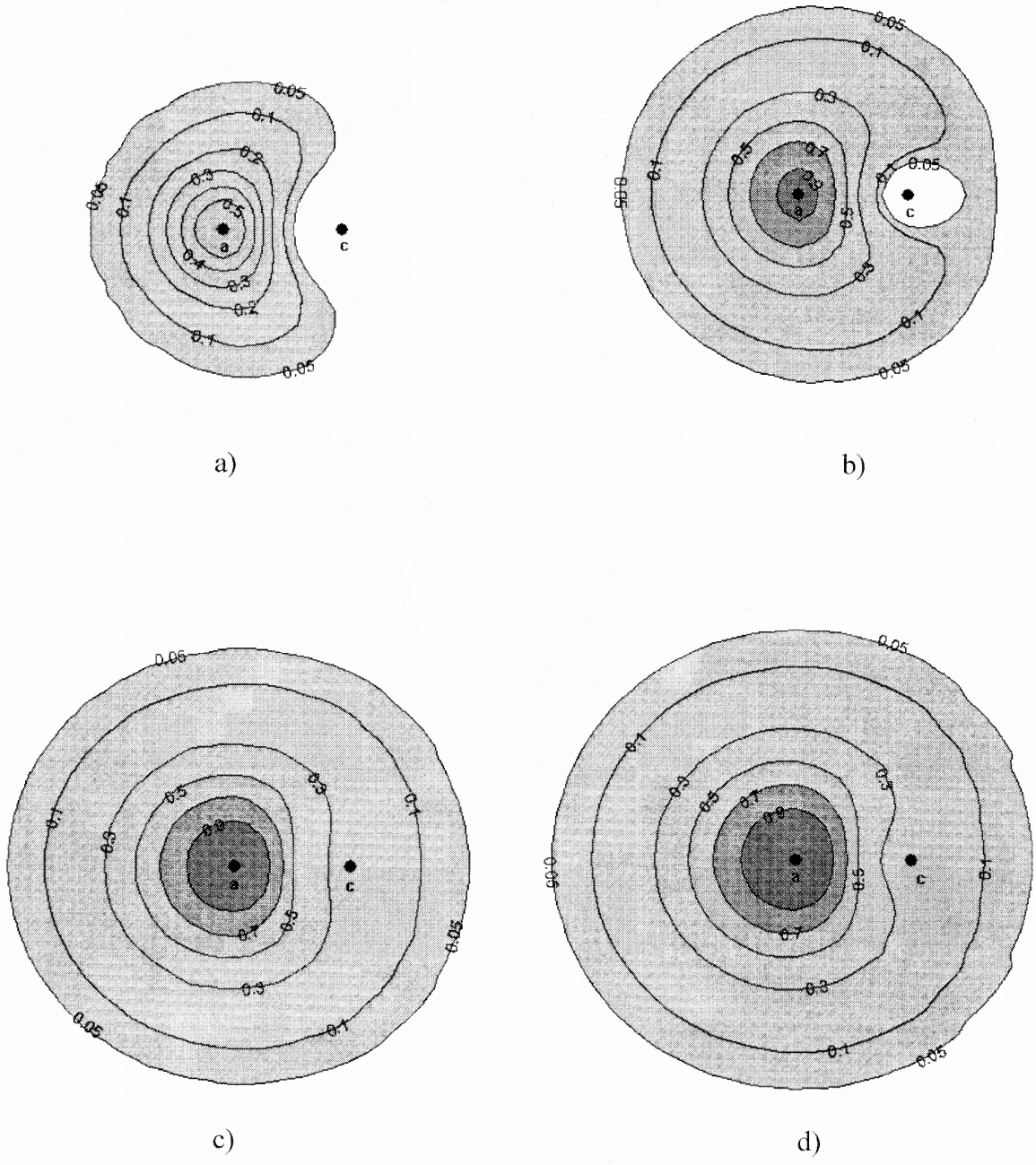

Figure 3.2 Feasibility probability regions for $d_{ac} = 1$, $P_{rec} = 0$ and $P_e = 10^{-1}$ (a), $P_e = 10^{-2}$ (b), $P_e = 10^{-3}$ (c) and $P_e = 10^{-4}$ (d).

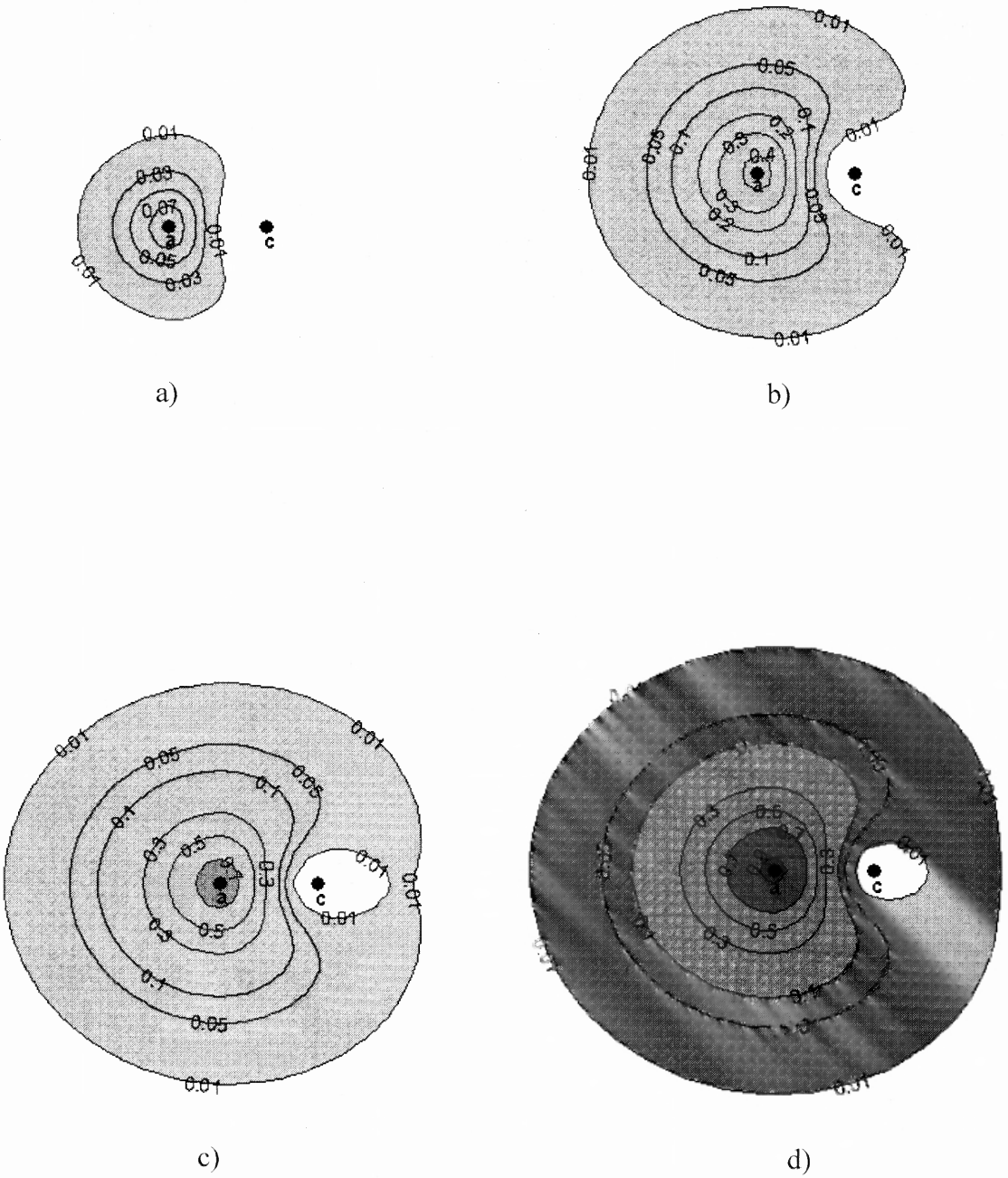

Figure 3.3 Average relative power gain regions for $d_{ac} = 1$, $P_{rec} = 0$ and $P_e = 10^{-1}$ (a), $P_e = 10^{-2}$ (b), $P_e = 10^{-3}$ (c) and $P_e = 10^{-4}$ (d).

Next, the following question needs to be answered: "Given nodes a and c, what is the average transmit power gain achievable by a $PCT_{\{a,b,c\}}$, averaged over all feasible locations of node b?" The following definition provides the way to answer the above question.

Definition 3.13 *Power combining potential* of two nodes at distance d_{ac} for error probability P_e, denoted as $PCP(d_{ac}, P_e)$, is defined as:

$$PCP(d_{ac}, P_e) = \frac{\int_{\Re(d_{ac})} G(\bar{d}_{\{a,b,c\}}, P_e) d(\bar{d}_{\{a,b,c\}})}{\int_{\Re(d_{ac})} FP(\bar{d}_{\{a,b,c\}}, P_e) d(\bar{d}_{\{a,b,c\}})} \tag{3.30}$$

Note that the denominator represents a normalizing constant.

Power combining potential of two nodes is thus the average transmit power gain of any PCT in which one node serves as the primary transmitter and the other as the receiver, averaged over all feasible locations of the second transmitter.

Proposition 3.4 If $P_{rec} = 0$, then

$$PCP(d_{ac}, P_e) = PCP(k \cdot d_{ac}, P_e) = PCP(1, P_e) \equiv PCP_N(P_e) \tag{3.31}$$

Therefore, when $P_{rec} = 0$ the power combining potential is independent from the distance d_{ac}. Table 3 shows $PCP_N(P_e)$ as a function of P_e, computed numerically from (3.25).

Table 3.1 Power Combining Potential vs. P_e

P_e	10^{-1}	10^{-2}	10^{-3}	10^{-4}
$PCP_N(P_e)$	0.041	0.295	0.460	0.525

When $P_{rec} > 0$, the power combining potential will clearly be smaller then the values given in Table 3. These values thus represent a tight upper bound on the power combining potential. Indeed, it is not reasonable to assume that P_{rec} is zero. Every receiver consumes power for receiving the signal. When P_{rec} is not neglected, it increases the cost of power combining and thus reduces the feasibility region. In this case, G becomes dependent on P_{rec} as well as on d_{ac}. Therefore, the relative benefit of power combining also depends on d_{ac}. This is expected, as larger distance between nodes a and c will open the way for more savings in transmitted power and thus alleviate the effect of the increased cost of power combining. In this case (3.25) needs to be evaluated numerically for different values of d_{ac}, α and P_{rec}. Figure 3.4 shows $PCP(d_{ac}, P_e)$ as a function of d_{ac}, P_{rec} and P_e, computed numerically from (3.25).

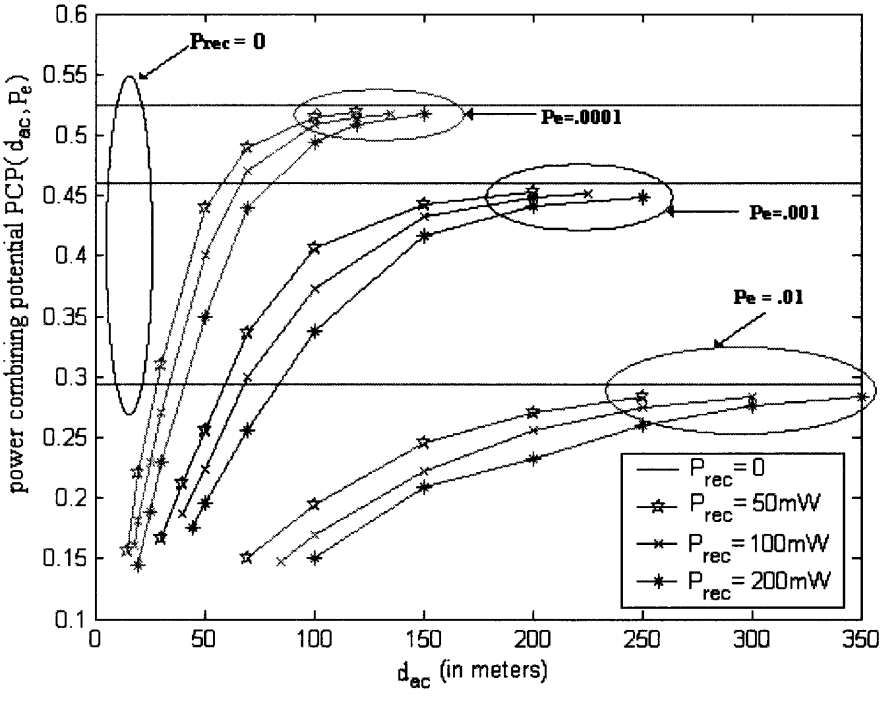

Figure 3.4 Power combining potential vs. d_{ac} for different values of P_{rec} and P_e .

The straight horizontal lines in Figure 3.4 are the values from Table 3.1 corresponding to the case when P_{rec} is neglected.

As can be seen in the Figure 3.4, for each pair (P_e, P_{rec}) there exists a value of d_{ac} below which power combining provides no substantial benefit. On the other hand, the distances for which power combining provides benefit are very realistic, especially for low P_e. Also, it can be seen that P_{rec} significantly affects the transmit power gain achievable by power combining.

Few remarks are worth making at this point. First, the receivers need not be modified to accommodate diversity reception: from the receiver's perspective the two signals coming from two transmitters are equivalent to a multipath signal coming from one transmitter. Second, the delay between the two transmit signals must be sufficient so that the receiver can resolve them. If the distances between the nodes are not large enough to insure sufficient propagation delay, node *b* could easily insert delay to provide resolvable paths at the receiver. Finally, when fading is not present, power combining simplifies to single transmission using the better of the two routes, namely $a \rightarrow c$ or $a \rightarrow b \rightarrow c$.

3.3.5 Link Costs and Graph Representation of PCT

In this section, the link costs and graph representation of a network employing PCTs are discussed. Consider again the three-node network from Figure 3.5.

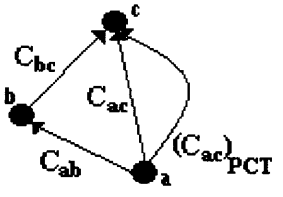

Figure 3.5 Graph representation of PCT.

In the minimum energy routing, the intent is to minimize the total transmit power required to route a packet form the source to the destination. With that goal in mind, the link costs must represent the power consumed to provide successful transmission. Therefore, in the case without power combining, i.e. when $PCT_{\{a,b,c\}}$ is not feasible:

$$C_{ab} = \alpha(P_e)\gamma_{ab} r_{ab}^m + P_{rec} \tag{3.32}$$

$$C_{bc} = \alpha(P_e)\gamma_{bc} r_{bc}^m + P_{rec} \tag{3.33}$$

$$C_{ac} = \alpha(P_e)\gamma_{ac} r_{ac}^m + P_{rec} \tag{3.34}$$

Based on the analysis from the previous section, it is known that if $PCT_{\{a,b,c\}}$ was feasible, the total transmit power with respect to the case without PCT would be less, given by (see eq. (3.11)):

$$(C_{ac})_{PCT} = \alpha(P_e)\gamma_{ab} d_{ab}^m + (P_{ac}^{t''})_{opt} + (P_{bc}^{t''})_{opt} + 2P_{rec} \tag{3.35}$$

where:

$$(C_{ac})_{PCT} \leq \min(C_{ac}, C_{ab} + C_{bc}) \tag{3.36}$$

Therefore, an additional link in the graph is needed to represent the cost of $PCT_{\{a,b,c\}}$, as shown in Figure 3.5.

3.4 Power Combining Chains

In this section, the concept of Power Combining Chains (PCC) is introduced and the additional transmit power gain they provide is discussed. Consider the network in Figure 3.6.a., in which node *a* sends the packets to node *d*.

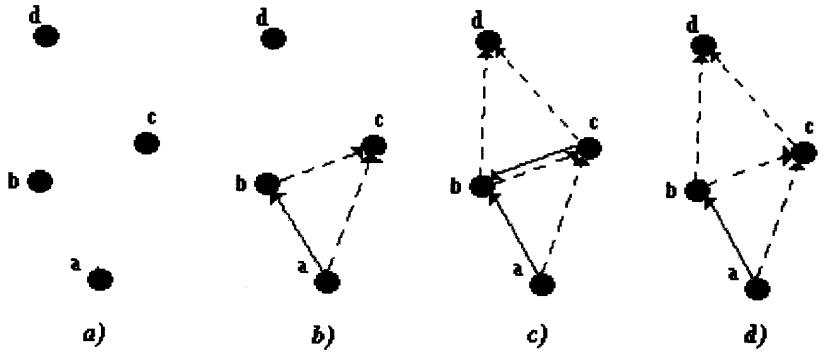

Figure 3.6 Power combining chains.

Assume that the first hop on the minimum energy route from *a* to *d* is node *c*, and that node *b* is a feasible node, i.e that $PCT_{\{a,b,c\}}$ is feasible, as shown in Figure 3.6.b. In addition, suppose that $PCT_{\{c,b,d\}}$ is also feasible. Thus, the transmission mesh of the route from node *a* to node *c* will be as shown in Figure 3.6.c. One can clearly observe that the transmission from node *b* to node *c* in the second hop is redundant, since node *b* has already received the signal from node *a* in the first hop in his role as the second transmitter in the $PCT_{\{a,b,c\}}$. Therefore, node *b* can re-transmit the signal received from node *a* in the next time slot, this time the destination node being node *d*. As a result, the link $b \rightarrow c$ can be suppressed, and additional energy can be saved (Figure 3.6.d). The set of nodes $\{a, b, c, d\}$, allowing the suppression of redundant link according to the

discussion above, is called *power combining chain* (PCC). In this section, the criteria for their initiation are discussed and the transmit power gain they provide is evaluated.

3.4.1 Definitions

As is clear from the discussion in the previous section, PCC can only occur if a node, in this case node *b*, takes part in both $PCT_{\{a,b,c\}}$ and $PCT_{\{c,b,d\}}$. Furthermore, node *b* has to be the second transmitter in both PCTs.

Definition 3.14 If two PCTs, say $PCT_{\{a,b,c\}}$ and $PCT_{\{c,b,d\}}$, share the same second transmitter, then the set of nodes $\{a, b, c, d\}$ is called *power combining chain*, denoted as $PCC_{\{a,b,c,d\}}$. The transmission graph of $PCC_{\{a,b,c,d\}}$ is shown in Figure 3.6.d.

The $PCC_{\{a,b,c,d\}}$ is called a *cascade* of $PCT_{\{a,b,c\}}$ and $PCT_{\{c,b,d\}}$.

A PCC can consist of more than two PCTs. Consequently, a more general definition of PCC needs to be established.

Definition 3.15

i) Power combining chain of three nodes, $PCC_{\{n_1,n_2,n_3\}}$ is equivalent to $PCT_{\{n_1,n_2,n_3\}}$.

ii) Power combining chain of nodes $\{n_1,n_2,\ldots,n_{m-1},n_m\}$, denoted as $PCC_{\{n_1,n_2,\ldots,n_{m-1},n_m\}}$, is a cascade of $PCC_{\{n_1,n_2,\ldots,n_{m-2},n_{m-1}\}}$ of length *m*-1 and $PCT_{\{n_{m-1},n_{m-2},n_m\}}$.

iii) Node n_1 is called the *primary transmitter of* $PCC_{\{n_1,n_2,\ldots,n_{m-1},n_m\}}$

iv) Node n_2 is called the *first secondary transmitter of* $PCC_{\{n_1,n_2,\ldots,n_{m-1},n_m\}}$

v) Node n_{m-1} is called the *last secondary transmitter of* $PCC_{\{n_1,n_2,\ldots,n_{m-1},n_m\}}$

vi) Node n_m is called the *receiver of* $PCC_{\{n_1,n_2,\ldots,n_{m-1},n_m\}}$

Note that Definition 3.15 defines PCT as a trivial version of a PCC.

It is important to note that the optimal transmit powers on the diversity branches do not change with the pruning of the redundant link. Thus, the optimal powers will be the optimal transmit powers on the diversity branches of the PCT, discussed in Section 3.3.2. Along that line of these conclusions, the following proposition is the generalization of Proposition 3.1:

Proposition 3.5 If there exists $PCC_{\{n_1,n_2,\ldots,n_{m-1},n_m\}}$ then there also exists $PCC_{\{n_2,n_1,\ldots,n_{m-1},n_m\}}$ Consequently, the primary transmitter of $PCT_{\{a,b,c\}}$ is the first secondary transmitter of $PCT_{\{b,a,c\}}$, and vice-versa. Also, the optimal total consumed power and the optimal transmit powers on the power combining branches of $PCC_{\{n_1,n_2,\ldots,n_{m-1},n_m\}}$ and $PCC_{\{n_2,n_1,\ldots,n_{m-1},n_m\}}$ are the same.

In the sense of feasibility defined by Definition 3.6, it is clear that if all the PCTs merged into a PCC are feasible the PCC is also feasible, since by pruning the redundant links one can further reduce the total transmit power. The reverse may not be true; that is, the merger of unfeasible PCTs may in fact yield a feasible PCC, because of the pruning of redundant links. In this case, however, the determination of the feasibility of PCCs would be complicated because the feasibility could not be tested until the total cost transmit power of a PCC is determined, by adding the transmit power for all the branches in the PCCs. This could only be performed by the last receiver node, which would then need to forward the feasibility information to all nodes in the PCC for PCC initiation. This centralized procedure is not suitable for distributed architecture of ad-hoc networks and would generate too much signaling between nodes.

On the other hand, if the feasibility of all PCTs merged into a PCC is adopted as the feasibility condition, than the feasibility is automatic. Therefore, the following definition of feasibility of a PCC is adopted:

Definition 3.16

i) $PCC_{\{n_1,n_2,n_3,n_4\}}$ is feasible if $PCT_{\{n_1,n_2,n_3\}}$ and $PCT_{\{n_3,n_2,n_4\}}$ are both feasible

ii) $PCC_{\{n_1,n_2,\ldots,n_{m-1},n_m\}}$ is feasible if $PCC_{\{n_1,n_2,\ldots,n_{m-2},n_{m-1}\}}$ and $PCT_{\{n_{m-1},n_{m-2},n_m\}}$ are both feasible

Based on Definition 3.14 and Definition 3.16.i, it is clear that the condition for the merger of two PCTs is the existence of the common second transmitter, as illustrated in Figure 3.6. One can now consider the criteria for the merger of a PCT and a PCC. Consider Figure 3.7.a.

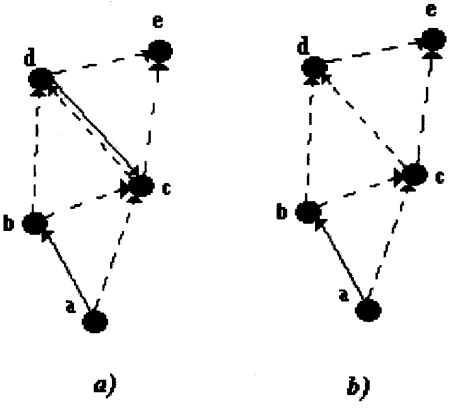

Figure 3.7 – Cascade of two PCCs.

Assume that $PCC_{\{a,b,c,d\}}$ and $PCT_{\{d,c,e\}}$ are feasible. As in the case of cascading two PCTs, the link $d \rightarrow e$ is redundant, since node c already receives the signal destined to e. In order for this to happen, the last secondary transmitter of $PCC_{\{a,b,c,d\}}$, i.e. node c, must

at the same time be the secondary transmitter of $PCT_{\{d,c,e\}}$. Hence, this is adopted as the condition for merger of a PCC and a PCT.

It is of interest to get an insight into the probability of occurrence of PCC. Unfortunately, because of the large number of nodes involved, this analysis is intractable for general case. However, if the focus is only on PCC of length 4, the probability of occurrence of PCC amounts to the probability of two PCTs having the same secondary transmitter. Let us fix the transmitter and receiver nodes for both PCTs in question, namely let node a be the primary transmitter of the first PCT, let node c be the receiver of the first PCT and the transmitter of the second PCT, and let node d be the receiver of the second PCT. For a given node b, $PCC_{\{a,b,c,d\}}$ will be feasible if both $PCT_{\{a,b,c\}}$ and $PCT_{\{d,c,e\}}$ are feasible; that is if feasibility regions $F(a \rightarrow c)$ and $F(c \rightarrow d)$ overlap and node b is located inside the overlap region. Therefore, the size of the overlap region of $F(a \rightarrow c)$ a $F(c \rightarrow d)$ will be proportional to the probability of feasibility of $PCC_{\{a,b,c,d\}}$. In order to visualize this probability of overlap, one can align nodes a, c and d, and set $d_{ac} = d_{cd} = 1$ and $P_{rec} = 0$. Figure 3.8 shows the probability of overlap of $F(a \rightarrow c)$ and $F(c \rightarrow d)$ for this case for different values of P_e.

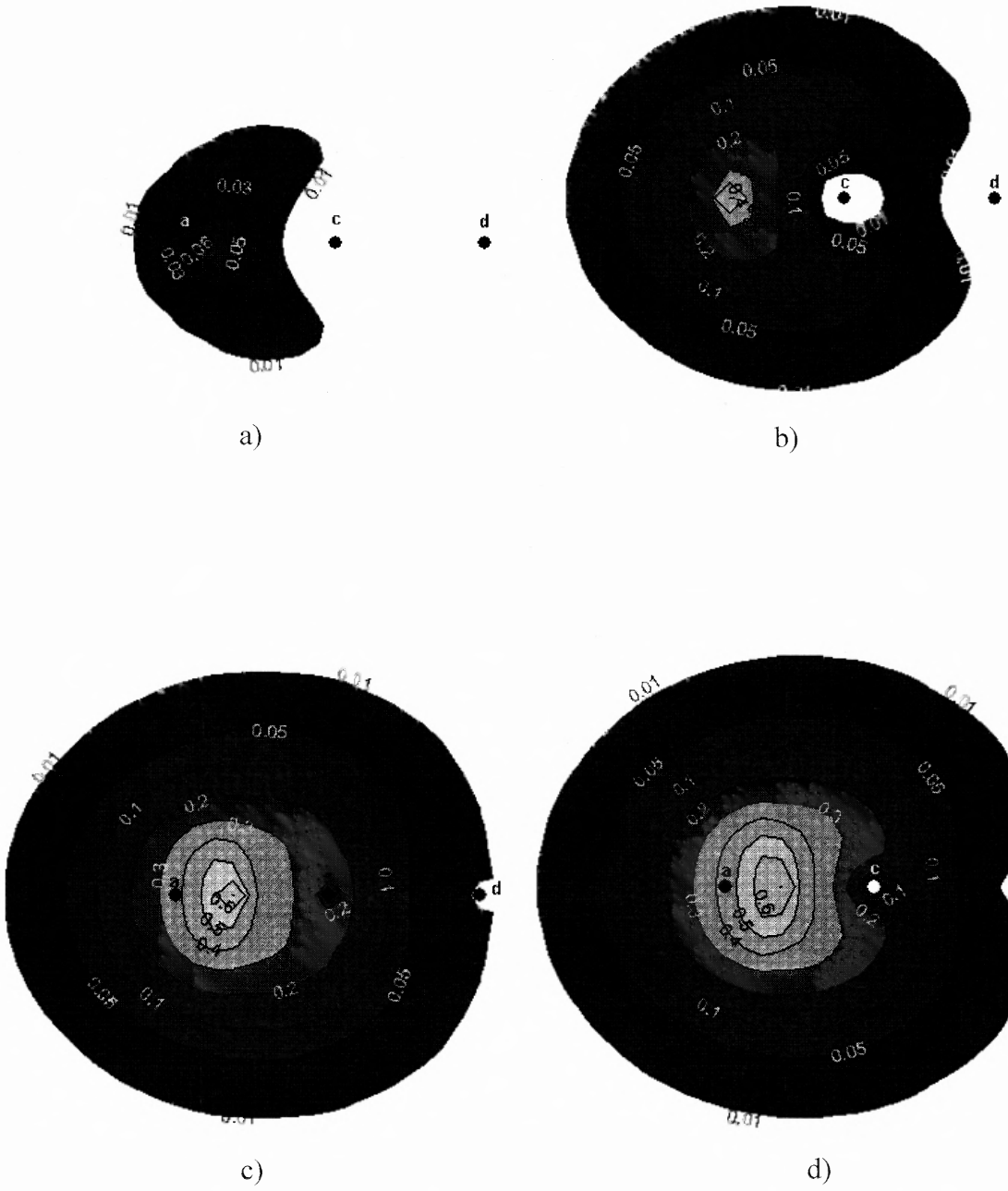

Figure 3.8 Feasibility probability regions for $d_{ac} = 1$, $P_{rec} = 0$ and $P_e = 10^{-1}$ (a), $P_e = 10^{-2}$ (b), $P_e = 10^{-3}$ (c) and $P_e = 10^{-4}$ (d).

3.4.2 Optimal Total Consumed Power

In this section, the optimal consumed power of a PCC is derived and the equivalent of Definitions 3.9 through 3.12 for the case of PCCs are provided.

Consider the simplest case of $PCC_{\{a,b,c,d\}}$ shown in Figure 3.6. The total consumed power of required to send the signal from node *a* to node *d* without power combining is:

$$\begin{aligned}(P'_{tot})_{a\to d} &= (P'_{tot})_{a\to c} + (P'_{tot})_{c\to d} = \\ &= \min(\alpha(P_e)\gamma_{ac}d_{ac}^m + P_{rec}, \alpha(P_e)\gamma_{ab}d_{ab}^m + \alpha(P_e)\gamma_{bc}d_{bc}^m + 2P_{rec}) \\ &\quad + \min(\alpha(P_e)\gamma_{bc}d_{bc}^m + P_{rec}, \alpha(P_e)\gamma_{bc}d_{bc}^m + \alpha(P_e)\gamma_{bd}d_{bd}^m + 2P_{rec})\end{aligned} \tag{3.37}$$

where the last equality has been written according to eq. (3.3). According to the discussion form the previous section, the total consumed power using $PCC_{\{a,b,c,d\}}$ will be:

$$(P''_{tot})_{\{a,b,c,d\}} = (P''_{tot})_{\{a,b,c\}} + (P''_{tot})_{\{c,b,d\}} - \alpha(P_e)\gamma_{bc}d_{bc}^m - P_{rec} \tag{3.38}$$

The last two terms correspond to the pruned redundant link. According to eq. (3.14), (3.2) becomes:

$$(P''_{tot})_{\{a,b,c,d\}} = \alpha(P_e)\gamma_{ab}d_{ab}^m + (P_{ac}^{t''})_{opt} + (P_{bc}^{t''})_{opt} + (P_{cd}^{t''})_{opt} + (P_{bd}^{t''})_{opt} + 3P_{rec} \tag{3.39}$$

Now, one can write the expression for the total consumed power of a PCC of arbitrary length:

$$(P''_{tot})_{\{n_1,n_2,\ldots,n_m\}} = \alpha(P_e)\gamma_{n_1n_2}d_{n_1n_2}^m + \sum_{i=3}^{m}\left[(P_{n_{i-2}n_i}^{t''})_{opt} + (P_{n_{i-1}n_i}^{t''})_{opt}\right] + (m-1)P_{rec} \tag{3.40}$$

In the case of simplified formula (3.15), the last expression becomes:

$$(P''_{tot})_{\{n_1,n_2,\ldots,n_m\}} = \alpha(P_e)\gamma_{n_1n_2}d_{n_1n_2}^m + \frac{\sqrt{3}}{2\sqrt{P_e}}\sum_{i=3}^{m}\left[\left(\sqrt{d_{n_{i-2}n_i}d_{n_{i-1}n_i}}\right)^m\sqrt{\gamma_{n_{i-2}n_i}\gamma_{n_{i-1}n_i}}\right] + (m-1)P_{rec} \tag{3.41}$$

Having defined the total consumed power of PCC with and without power combining, one can define the transmit power gain and average transmit power gain in the same fashion as in the case of PCTs in Definitions 3.9 and 3.12. However, computing their values becomes computationally intractable, as one has to deal with integrations over (m+1)-tiple integrations over shadowing attenuations for a PCC of length m.

3.4.3 Link Cost and Graph Representation of PCCs

In this section, the link costs and graph representation of a network employing PCCs are discussed. As discussed in Section 3.4, the total consumed power for a successful transmission is adopted as the link cost metrics. Therefore, the link cost between two nodes n_1 and n_m with a feasible $PCC_{\{n_1,n_2,\ldots,n_{m-1},n_m\}}$ will be given by (see eq. (3.13):

$$(C_{n_1n_m})_{PCC} = \alpha(P_e)\gamma_{n_1n_2} d^m_{n_1n_2} + \sum_{i=3}^{m}\left[(P^{t''}_{n_{i-2}n_i})_{opt} + (P^{t''}_{n_{i-1}n_i})_{opt}\right] + (m-1)P_{rec} \tag{3.42}$$

The total consumed power of a PCC is smaller than the total consumed power of PCTs involved in the PCC. This will require establishing direct connection between the end nodes of the PCC in the network graph, reflecting the cost of the PCC. For example, for $PCC_{\{a,b,c,d\}}$ from Figure 24:

$$(C_{ad})_{PCT} < (C_{ac})_{PCT} + (C_{cd})_{PCT} \tag{3.43}$$

The network graph corresponding to $PCC_{\{a,b,c,d\}}$ from Figure 3.6 is shown in Figure 3.9 below.

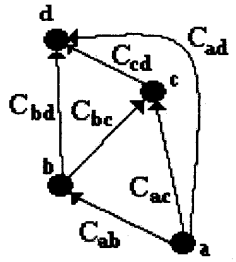

Figure 3.9 Graph representation of PCC.

3.5 Conclusion

In this section, the theoretical framework for feasibility analysis, transmit power gain evaluation and the evaluation of the effect of some system model parameters onto the performance of power combining for MER in MANETs was established. It was proved that the gains in terms of the reduction of transmit power are substantial and justify this approach. Furthermore, it was proved that the distances between MTs at which these gains can be achieved are realistic. The analytical upper bounds on the average transmit power gain as a function on the distance between the transmitter and the receiver were established.

These analytical results provide firm ground for the use of power combining for MER in MANETs. One can anticipate, based on the results of this chapter, that the gains in terms of reduction in power consumed to route a packet and in terms of network lifetime can be substantial. The performance evaluation of a MER algorithm using power combining will be pursued in the following chapter.

CHAPTER 4

MODELING AND ANALYSIS OF THE MER ALGORITHM FOR RAYLEIGH FADING CHANNELS USING POWER COMBINING

4.1 Introduction

In Chapter 1, the motivations for the development of a new minimum energy routing algorithm for MANETs for Rayleigh fading channels were presented. The minimum energy routing approach, minimizing the total consumed power of the network, was selected as the best approach, combining the benefits of extending network lifetime and reducing the total generated interference. It was also argued that transmit diversity presents efficient way to combat fading in MANET environment using inherent spatial diversity of MTs. In Chapter 3, the theoretical framework for power combining, i.e. transmit diversity in MANETs aimed at minimizing transmit power, was built. The benefits from power combining in terms of average transmit power gain were evaluated analytically. In this chapter, the new minimum energy routing algorithm for MANETs in Rayleigh fading channels using power combining is developed, and perform its performance analysis is performed. First, the assumptions in terms of network model, channel model and transceiver model are defined. Next, the new algorithm is described in details. The simulation study and the evaluation of the results in terms of their compliance with analytical results deployed in Chapter 3 and also in terms of the comparison with the existing energy efficient routing schemes available in the literature are then performed. Finally, the analysis of the messaging load generated by the algorithm is presented and the tradeoff is discussed. The results in this chapter were published in [52]

4.2 System Model

4.2.1 Network Model

Consider a MANET to be deployed in a limited geographical area with pre-defined borders. Without loss of generality, one can assume the network area to be of square shape with 1,000 m on each side. The size and the shape of the network area would affect the results in a predictable fashion. MTs are assumed to be moving in a uniform fashion with constant speed. The direction of movement is uniformly distributed from 0 to 360 degrees. The speed is a uniform random variable in the range from 0 to 22 mph. When a MT reaches the boundary of the coverage area, it reflects off of it back into the area. Initially, MTs are distributed uniformly within the network area.

4.2.2 Channel Model

The channel model described in Section 3.2, accounting for path loss, shadowing and fading, is adopted. The widely used path loss exponent of four is adopted. The standard deviation of $\sigma_\gamma = 6$ dB and correlation of $\rho = 0.5$ at the distance of $d_\rho = 20$ m are assumed as shadowing parameters. In order to accommodate spatial correlation of shadowing, it is modeled as a first-order auto-regressive (AR) process [25]:

$$\gamma(t) = \xi\gamma(t-1) + \varpi(t) \tag{4.1}$$

where ξ is a constant and $\varpi(t)$ is a zero-mean Gaussian noise with standard deviation σ_ϖ. Parameters ξ and σ_ϖ can be found from the following expressions:

$$\xi = \exp(-d_s / d_0) \tag{4.2}$$

where d_s is the step size and d_0 is the distance at which the correlation is equal to ξ, and

$$\sigma_{\varpi}^2 = \frac{1+\xi}{1-\xi}\sigma_{\gamma}^2 \tag{4.3}$$

Figure 4.1 shows an instance of the shadowing attenuation on a trajectory of 200 meters obtained from (4.1) with ξ=0.84 and σ_{ϖ} = 3.26dB.

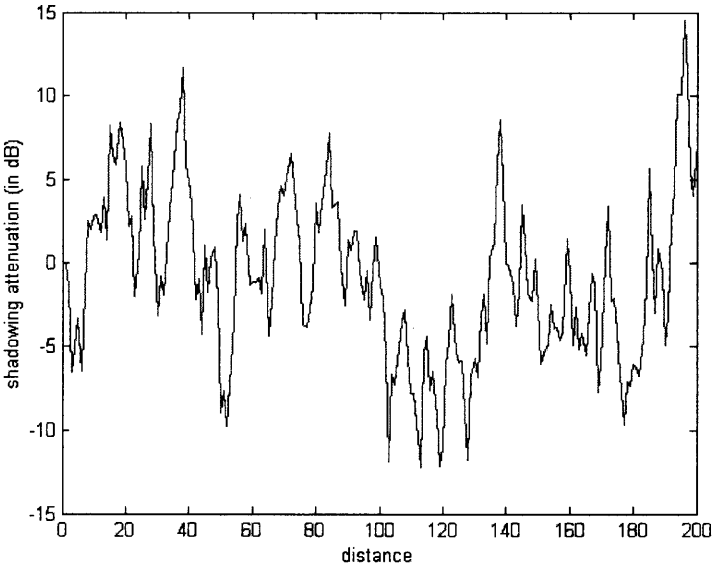

Figure 4.1 Shadowing attenuation as an AR process with correlation of ρ = 0.5 at the distance of d_{ρ} = 20 m.

Each MT updates its channel attenuations to other MTs at a pre-defined step of 5 meters. Therefore, MTs moving faster will update their channel attenuations more frequently and vice versa.

4.2.3 Transceiver Model

Consider each MT to be equipped with a full-duplex transceiver with omni-directional antennas with 0 dB gain. The carrier frequency is assumed to be 1 GHz and the transmission bandwidth is 10 KHz. The receiver has a noise figure of 10 dB, and the background noise has the power level of –160 dBm. For simplicity, the modulation is

BPSK. Each receiver is a two-tap RAKE receiver perfectly synchronized with the two multipath components coming from the two transmitters. Based on these parameters, required received power thresholds for successful detection can be computed [3] and are given in Table 4.1 below.

Table 4.1 Received Power Thresholds for Different P_e

P_e	10^{-1}	10^{-2}	10^{-3}	10^{-4}	10^{-5}
P_t (dBm)	-75	-64	-54	-44	-33

In addition, each receiver consumes a constant power of P_{rec} = 100 mW for each received signal. This is in the range of values reported in [7] and [4].

4.2.4 Power Consumption Model

In order to focus on the analysis of the effect of the algorithm onto the network lifetime, one can assume that MTs do not consume any power when they are not transmitting/receiving. Therefore, MTs consume power for transmitting/receiving signals to support the incoming connection requests. The connection requests arrive randomly according to the Poisson distribution with the mean of 2 connections per MT per minute. The source MT and the destination MT for each connection are chosen randomly among all MTs. The duration of the connection is set to 10 seconds.

Initial battery energy for each MT is set to 50 Whrs, corresponding to the battery capacity of an average laptop computer. MT is considered to have run out of energy when it has not enough energy to support a connection, i.e. to provide reception and/or transmission during the ten-second transmission interval.

4.3 New MER Scheme

The MER scheme using power combining has three principal components: PCT and PCC initiation, route computation and closed-loop slow rate power control (CLPC), as shown in Figure 4.2. PCT/PCC initiation is performed based on the feasibility of PCTs/PCCs. The role of the closed-loop slow-rate power control is to adjust the optimal transmit powers on the diversity branches in PCTs/PCCs. Based on the information about the transmit powers provided by the closed-loop slow-rate power control component, PCTs are maintained or ended, and the corresponding link costs are computed, to be used in the route computation. The route computation component computes the minimum energy routes using the Djikstra's shortest path algorithm.

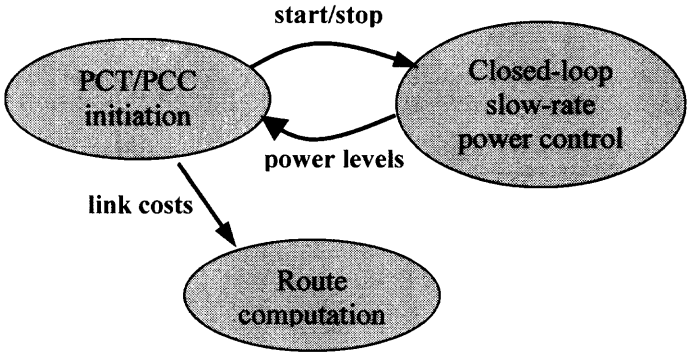

Figure 4.2 Principal components of the MER-PC scheme.

4.3.1 PCT and PCC Initiation

If there exists a $PCT_{\{a,b,c\}}$, it needs to be activated. PCT activation procedure is outlined in Figure 4.3.

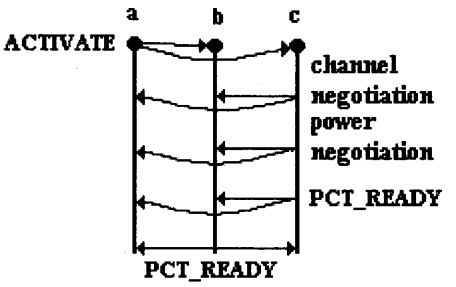

Figure 4.3 PCT initiation procedure.

Node *a* starts by sending PCT_ACTIVATE message to nodes *b* and *c*, enclosing identity of the third member of the PCT. Node *c* then starts the channel negotiation in order to find a transmit channel for power-combined transmission to *c*. It also determines the optimal received powers for signal transmitted by *a* and *b* yielding minimum total transmit power (eq.xx) and starts adjusting received power levels by slow-rate power control of *a* and *b*. Note that a burst of power control messages at a faster rate may be needed for this. However, once the power levels are adjusted, power control needed to track the shadowing can resume at the slow rate. When the process is completed, node *c* transmits PCT_READY message to two other nodes. Node *b* then also sends PCT_READY message to *a* and *c*. When each node receives two PCT_READY messages by the two other nodes, the process is completed and PCT is ready for transmission (node *b* will in fact receive one PCT_ACTIVATE and one PCT_READY message). Subsequently, when node *a* receives a data-carrying signal from the previous node in the route, it will use the $PCT_{\{a,b,c\}}$ to reach *c*. If the PCT activation procedure fails, either because of the unavailability of channels, or node *b* going out of the feasibility region, node *a* falls back onto the simple connection to *c*.

$PCC_{\{a,b,c,d\}}$ is activated by first activating $PCT_{\{a,b,c\}}$ and $PCT_{\{c,b,d\}}$, using the procedure described above. The only difference is that node a starts the activation by sending two ACTIVATE messages to node c, one PCT_ACTIVATE for $PCT_{\{a,b,c\}}$ and one PCC_ACTIVATE for $PCC_{\{a,b,c,d\}}$. Node c then starts the activation of $PCT_{\{c,b,d\}}$, and upon completion, sends the PCC_READY message to a. After the two PCTs have been activated, node a sends RELEASE message to b and c to release the redundant link l_{cb}, which completes the activation. The procedure is analogous for longer PCCs: first, the PCTs are activated, and then the redundant links are released. Note that if all the PCTs contained in a PCC are successfully activated, the PCC activation will be successful. If one or more PCTs fails it will be replaced by a simple link.

4.3.2 Closed-loop Slow-rate Power Control

The goal of the closed-loop slow-rate power control is to maintain optimal power levels on the diversity branches. Closed-loop slow-rate power control is performed by the receiver node by sending power control commands to the primary and secondary transmitter. The rate of the power control commands is adjusted to efficiently track the variations in the composite shadowing-plus-path loss attenuation. Per eq. (3.18), the optimal mean transmit power on the diversity branches are equal. Therefore, the closed-loop slow-rate power control need to maintain the mean transmit powers at the optimal level and equal. As a consequence, the same power control commands can be sent to both the primary and the secondary transmitter, which reduces the messaging load generated by the power control commands by a factor of two.

4.3.3 Route Computation and Activation

The route activation begins from the source node. The source node activates the link to the following node in the route, which follows the process to the destination node. Therefore, a generic route set up procedure applicable to any node along the route, denoted as *a*, will be described here.

Node *a* looks up in its routing table to determine the type of the connection to the next hop node, say *c*. If the link to *c*, is simple (i.e. not a PCT or a PCC), nodes *a* and *c* simply negotiate a channel for the connection.

When all the nodes from the source to the destination successfully initiate their connections, the destination node sends ROUTE_READY message to the source, acknowledging the route. The transmission can then start.

Each node keeps the table of active PCTs and PCCs in which it participates. At any change in the table (e.g. if an existing PCT becomes unfeasible and is thus deactivated or if a new PCT is initiated) a message containing the changes is broadcasted to the network.

4.4 Simulation Results

4.4.1 Network Lifetime

Figure 4.4 shows the network lifetime obtained from simulation, based on the system model described in section 4.2, for a conventional minimum energy algorithm (MER) and the minimum energy routing algorithm with power combining (MER-PC).

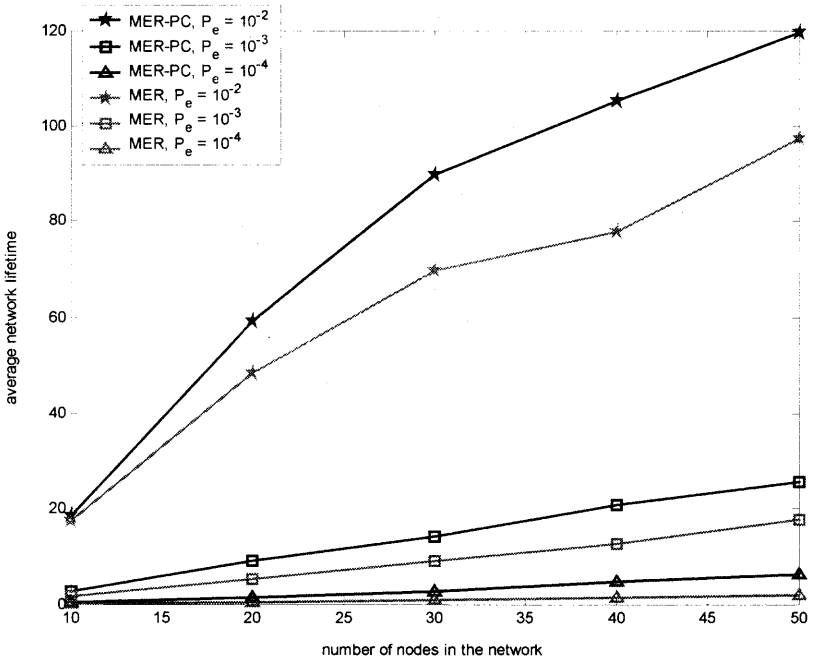

Figure 4.4 Network lifetime.

As is clearly seen on the graph, power combining significantly increases the network lifetime. The amount of increase depends greatly on the desired signal quality, represented by the received signal error probability P_e. The relative increase is bigger for lower P_e, reflecting the fact that the benefits of transmit diversity increases as P_e decreases. The increase goes from around 30% for $P_e = 10^{-2}$ to more than 100% for $P_e = 10^{-4}$.

4.4.2 Standard Deviation of Network Lifetime

Figure 4.5 shows the standard deviation of network lifetime normalized to the mean, obtained from 10 instances of the simulation. Due to very long simulation running time, only a limited number of simulation instances could be performed. However, the margin in the results is such that the conclusions can be drawn with high confidence.

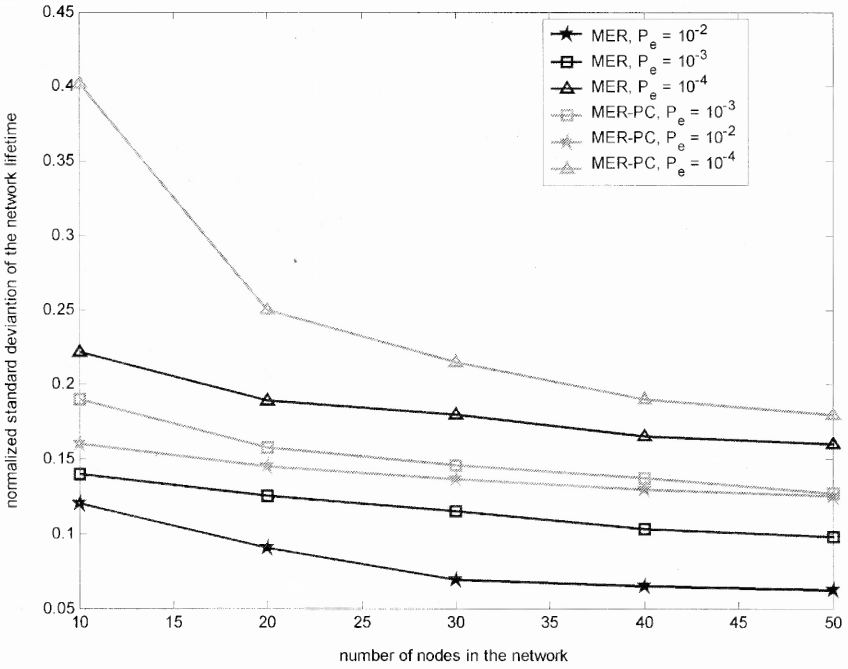

Figure 4.5 Standard deviation of network lifetime.

It can be inferred from the graph that power combining helps reduce the standard deviation of the network lifetime by approximately a factor of two. This in fact means that the network lifetime is more predictable when power combining is employed.

4.4.3 Average Power Gain per Route

Table 4.2 shows the average power consumed to route a packet per route in Watts for MER algorithm without power combining, as a function of the number of nodes in the network and the error probability P_e. Table 4.3 shows the same results for MER with power combining. The results were obtained using 10,000 routes randomly selected from the set of all possible routes in the network.

Table 4.2 Average Powers per Routed Packet Without Power Combining

Number of nodes		10	20	30	40	50
Power per route (in Watts),	$P_e = 10^{-1}$	0.77	0.52	0.41	0.36	0.31
"	$P_e = 10^{-2}$	6.74	2.92	1.58	1.36	1.18
"	$P_e = 10^{-3}$	62.73	21.2	10.3	6.5	4.22

Table 4.3 Average Powers per Routed Packet With Power Combining

Number of nodes		10	20	30	40	50
Power per route (in Watts),	$P_e = 10^{-1}$	0.76	0.50	0.39	0.34	0.30
"	$P_e = 10^{-2}$	5.81	2.46	1.37	1.18	1.05
"	$P_e = 10^{-3}$	38.35	13.13	6.34	4.47	2.93

The results in the tables indicate that the power gain per routed packet is 1-2% for $P_e = 10^{-1}$, around 20% for $P_e = 10^{-2}$ and goes up to 60% for $P_e = 10^{-3}$. These results are very similar to the average PCT power gains, computed analytically in section 3.3.4. Therefore, the simulation results lead to conclusions that go along the lines of the conclusions of section 3.3.4, i.e. that power combining yields significant gains in terms of transmit power reduction for all but very low error probabilities, i.e. SNRs.

4.4.4 Average Power Consumption of a MT

Table 4.4 shows the average power consumption of a MT in Watts for MER algorithm without power combining, as a function of the number of nodes in the network and the error probability P_e. Table 4.5 shows the same results for MER with power combining. The results were computed over the span of the network lifetime.

Table 4.4 Average Power Consumption of a MT Without Power Combining

Number of nodes	10	20	30	40	50
Power per route (in Watts), $P_e = 10^{-1}$	0.28	0.09	0.06	0.04	0.03
" $P_e = 10^{-2}$	2.78	0.89	0.64	0.51	0.43
" $P_e = 10^{-3}$	25.67	7.65	4.12	2.62	2.01

Table 4.5 Average Power Consumption of a MT With Power Combining

Number of nodes	10	20	30	40	50
Power per route (in Watts), $P_e = 10^{-1}$	0.27	0.084	0.057	0.038	0.029
" $P_e = 10^{-2}$	2.38	0.81	0.55	0.44	0.37
" $P_e = 10^{-3}$	15.6	4.53	2.55	1.81	1.41

The same discussion of the results as in the previous section applies here. The consequence of these results is that when power combining is used, a MT consumes less power and hence generates less interference. This justifies the claim that MER with power combining reduces the generated interference power.

4.4.5 Residual Battery Capacity

In this section, the effect of power combining on the residual battery capacity after the first node depletes its battery is presented. Figures 4.6 through 4.8 show the histograms of the residual battery capacity for a MER without power combining for $P_e = 10^{-2}$, $P_e = 10^{-3}$ and $P_e = 10^{-4}$, respectively. Figures 4.9 through 4.11 show the histograms of the residual battery capacity for a MER with power combining for $P_e = 10^{-2}$, $P_e = 10^{-3}$ and $P_e = 10^{-4}$, respectively.

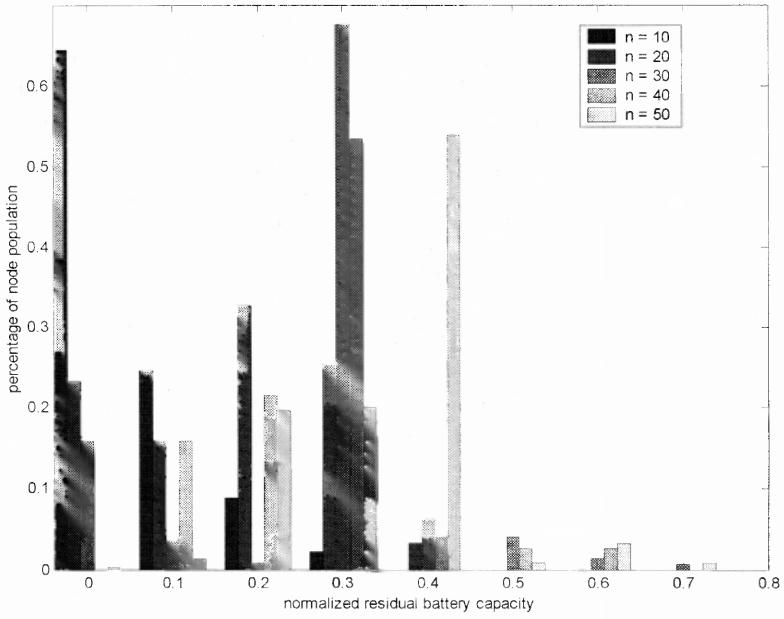

Figure 4.6 Residual battery capacity for MER without power combining for $P_e = 10^{-2}$.

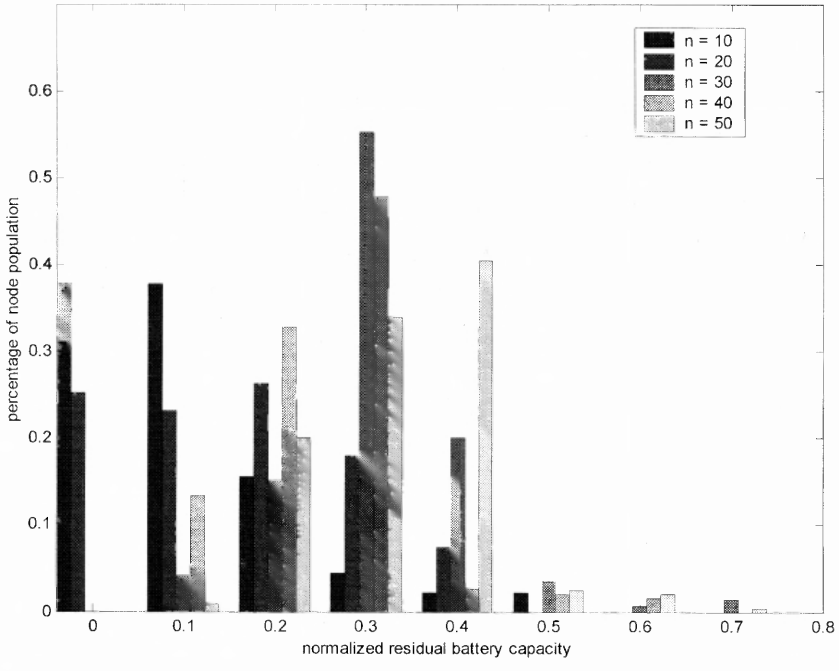

Figure 4.7 Residual battery capacity for MER without power combining for $P_e = 10^{-3}$.

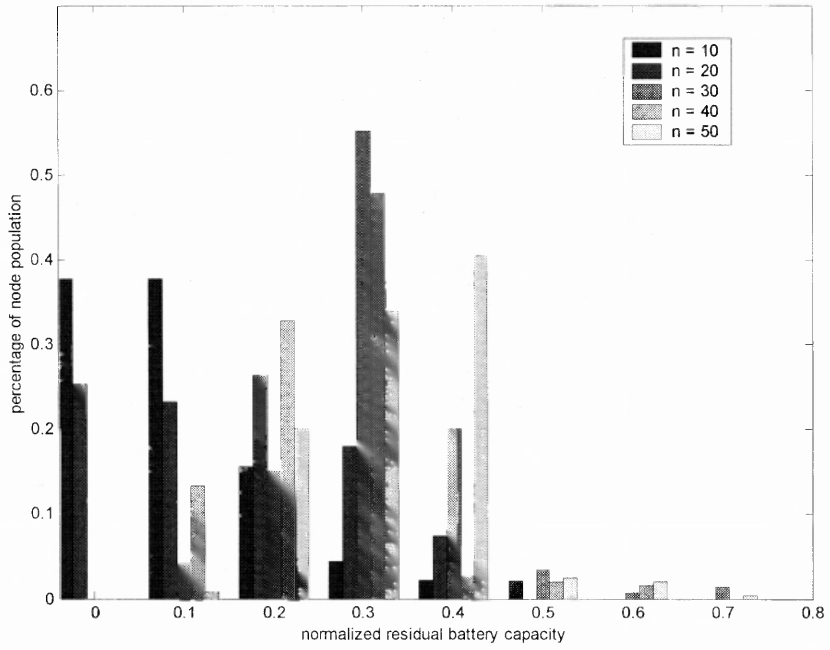

Figure 4.8 Residual battery capacity for MER without power combining for $P_e = 10^{-4}$.

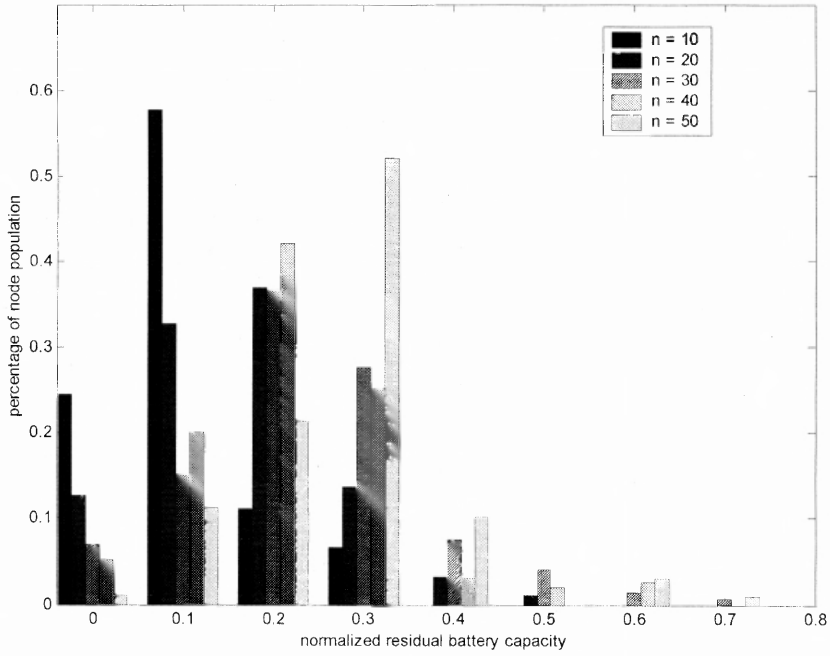

Figure 4.9 Residual battery capacity for MER with power combining for $P_e = 10^{-2}$.

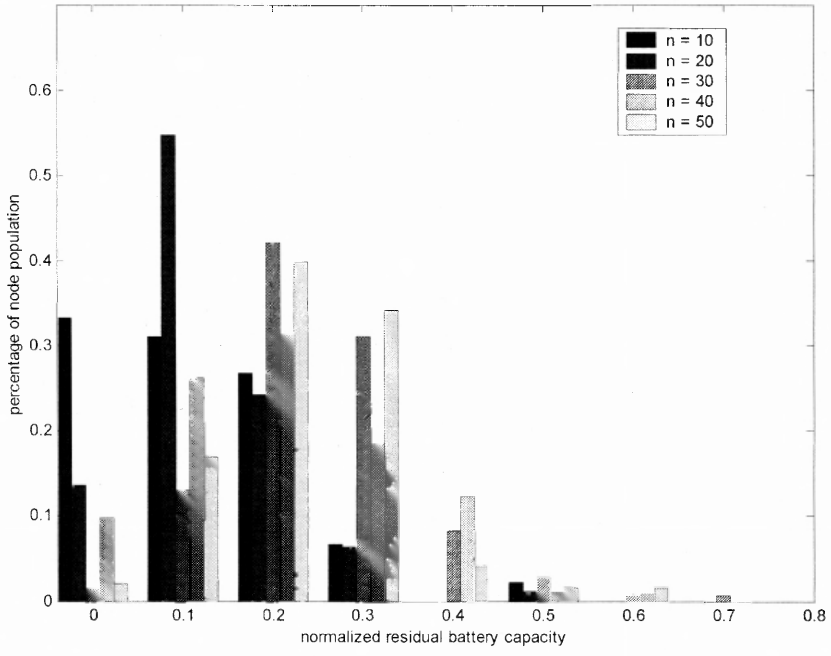

Figure 4.10 Residual battery capacity for MER with power combining for $P_e = 10^{-3}$.

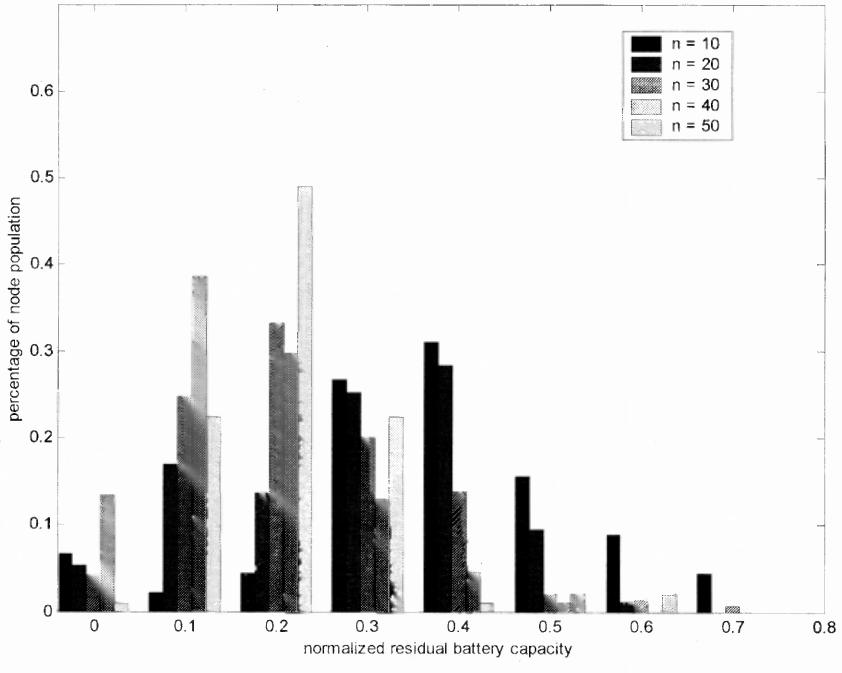

Figure 4.11 – Residual battery capacity for MER with power combining for $P_e = 10^{-4}$.

Comparing the histograms on Figures 33 through 35 with those on Figures 36 through 38 respectively, one can conclude that power combining yields more even distribution of power consumption among MTs. This is reflected through the fact that the histogram with power combining is centered more to the left, meaning that fewer MTs remain with large portion of their battery capacity preserved. Implicitly, this fact is also reflected through the longer network lifetime achieved by use of power combining.

4.4.6 Messaging Load

The cost of power combining scheme is in the messaging load required to initiate, update and release PCTs in the network. In this section, the messaging load of MER with power combining is compared with the messaging load without power combining. The ways to optimize this load are also discussed.

4.4.6.1 Messaging Load Without Power Combining. Without power combining, the messaging is required to exchange the link (i.e. channel attenuation) information among MTs. One can ssume that MTs broadcast a pilot signal whenever it crosses the distance of 5 meters. This distance has been selected with respect to a shadowing model, having correlation of 0.5 at 20 meters. This pilot is picked up by other MTs, which use it to compute channel attenuations between them. Each MT then broadcasts its channel attenuations to all other MTs in a single message.

4.4.6.2 Messaging Load with Power Combining. With power combining, there is additional messaging required to initiate and release PCTs and PCCs, and exchange the related information among MTs. In additional, closed-loop slow-rate power control also generates messages, required to maintain optimal power levels on the diversity branches

in PCTs and PCCs. The messaging related to PCT initiation, release and closed-loop slow rate power control was discussed in sections 4.3.1 and 4.3.2, respectively. Figure 4.12 shows the messaging load in terms of number of messages per MT per minute vs. number of nodes in the network.

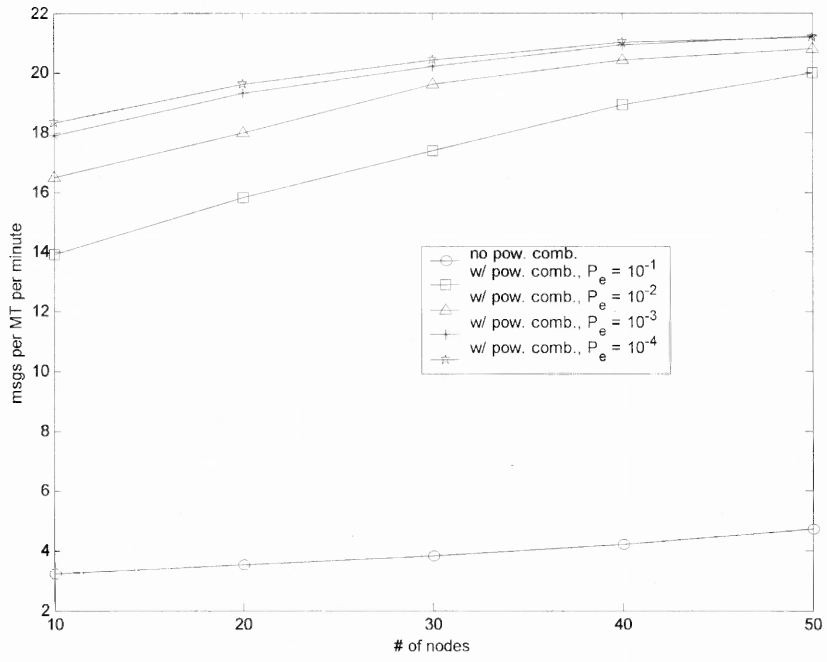

Figure 4.12 Messaging load with and without power combining.

The graphs indicate that power combining generates significant messaging load with respect to the case without power combining. However, this load is only *relatively* large. In absolute sense, the amount of load ranges from 10 to 15 messages per MT per minute. This is indeed not a large load. On the other hand, this messaging scheme is not optimized. Namely, in the model, MTs initiate, maintain and release every PCT that is feasible, and they exchange the information pertaining to these processes among themselves. However, based on the idea presented in [7], it is possible for a MT to reduce

the number of PCTs they actually initiate or maintain. In such case, the messaging load would also be reduced. Consequently, the graphs in Figure 39 represent the *upper bound* on the messaging load generated by power combining.

4.4.7 Typical Route Examples

Figure 4.13 shows the example of the routes for a network with 10 nodes, obtained using MER without power combining for different error probabilities. The MT node is denoted as 1 and the destination MT is denoted as 2. The solid lines represent simple links and the dashed lines represent PCT diversity branches. Figure 4.14 shows the example of the routes obtained using MER with power combining for the same error probabilities and source and destination MTs. Figures 4.15 and 4.16 show the same as 4.13 and 4.14 for a network with 30 nodes.

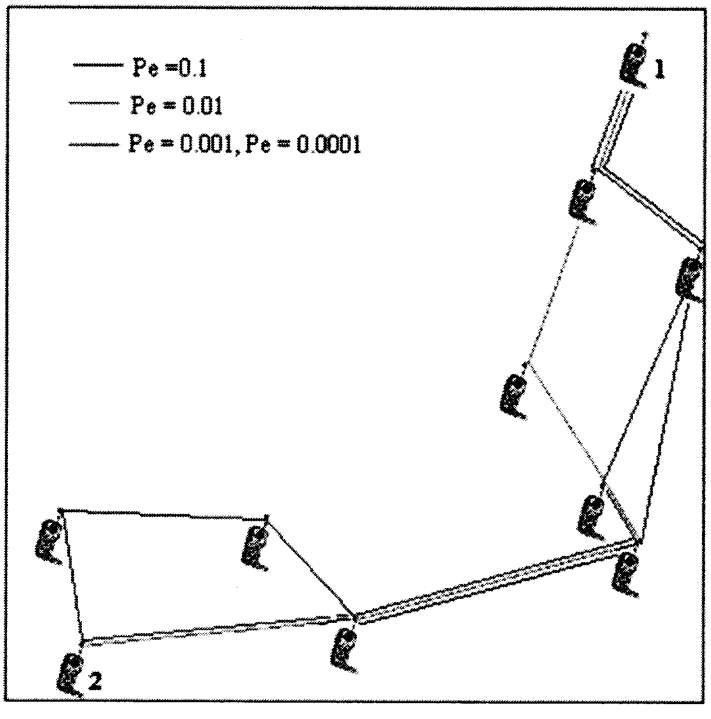

Figure 4.13 Example of the MER without power combining for a network with 10 nodes.

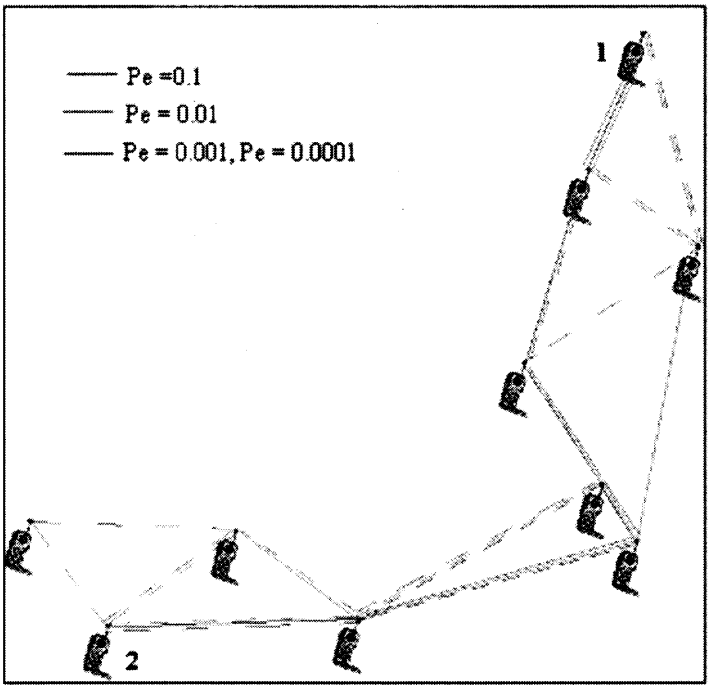

Figure 4.14 Example of the MER with power combining for a network with 10 nodes.

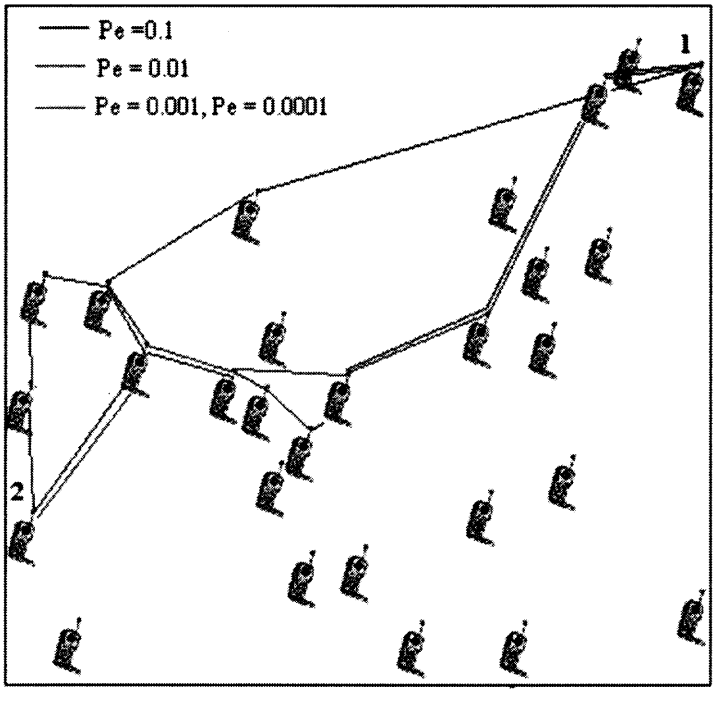

Figure 4.15 Example of the MER without power combining for a network with 30 nodes

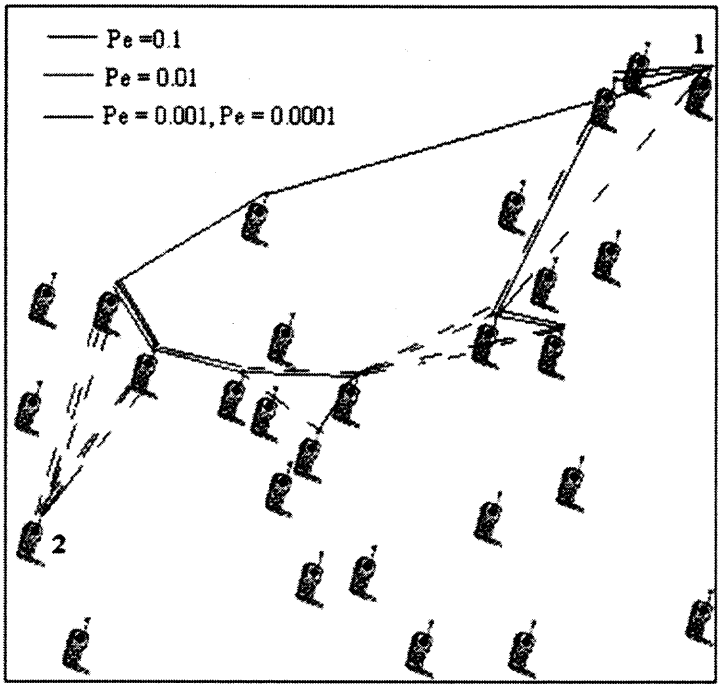

Figure 4.16 Example of the MER with power combining for a network with 30 nodes.

4.5 Discussion and Conclusion

In this chapter, the MER scheme using power combining as a method to reduce total transmit power, combat fading and extend network lifetime, was presented. This is the first research effort in the area of energy efficient routing in which realistic channel model, including shadowing and fading, is used, and in which transmit diversity is used to combat fading and reduced the total transmit power.

The extension of the network lifetime achieved by MER-PC scheme ranges from 15% to 90%, depending on the desired error probability, higher error probabilities being less susceptible to benefits from power combining. Therefore, although not directly addressing the problem of maximizing network lifetime, power combining implicitly extends network lifetime. On the other hand, the average power consumed to route a packet from the source to the destination is reduced by 5% to 95%, again depending in

the same fashion on the error probability as the network lifetime. This reduction in the average consumed power per routed packet has two implications: one is the extended network lifetime, as discussed above; the other is reduced average total transmit power of the network and hence reduced interference generated to the environment. This is indeed important goal to achieve, as most of the next generation wireless systems will operate in the unlicensed spectrum, and will therefore be interference sensitive.

It is important to mention that average gains in terms of network lifetime and average power consumption obtained in chapter 4 well fit the analytically computed average relative gains achieved by PCTs in chapter 3. This may be explained by very large areas of PCT feasibility regions. Therefore, the probability of the existence of a feasible PCT for any pair of transmitter and receiver is very large. Thus, in average, the gain over the route equals the gain on one hop, which is in fact the average gain of a PCT. Hence, the analytical estimates of the transmit power gains achieved by power combining can be used as a good approximation for actual gains over the routes in the network.

The MER-PC approach adds no complexity to the receiver design. Namely, the receiver is a typical RAKE receiver. In fact, the receiver does not have to know if the signal is coming from one or two separate MTs. This information is irrelevant to the signal detection process. In some presentations of this work in the research communities it has been argued that this approach would not bring as much benefit if a multipath channel model was considered. Indeed, the benefit from transmit diversity is the greatest when one compares a signal received with no diversity with the signal received from two different transmitters. The comparative benefit from including a third transmitter, or a

third multipath component is smaller than in the first case, and it decreases differentially with the number of transmitters/multipath components. However, the field measurements of the delay spread of the mobile-to-mobile channel have shown that the delay spread is well below the resolvability capabilities of RAKE receivers operating at chip rates prescribed by 2G and 3G standards. Namely, the delay spread of the delay spread of the mobile-to-mobile channel is less than 100 ns, while the RAKE receiver operating at a 3G rate of cca. 5 Mchips per second has the resolvability resolution of 220 ns.

The minimum energy routes returned by the MER scheme are generally different from the routes returned by conventional MER algorithms. This proves the earlier claims that simplifications of the channel model lead to non-optimal routes. This argument adds up to another argument against simplistic channel models, namely that the practicability of fast rate power control schemes in MANETs is questionable.

The complexity that MER-PC approach adds into the system consists in messaging load required to initiate, maintain and release PCTs (PCCs), and to perform slow-rate power control. Slow-rate power control is necessary to maintain the optimal average transmit power levels on the diversity branches in PCTs. It cannot be performed in the open-loop fashion as traditional power control schemes in cellular systems aiming at adjusting the average power of the received signal. Hence, the receiver needs to explicitly adjust the transmit power levels of the two transmitters to their optimal values, which were proved to be mutually equal.

The generated messaging load is relatively much higher than the messaging load not involved with power combining, i.e. related to the exchange of the link information in the network. However, this increase is only relative. One can argue that in the absolute

sense it is acceptable. Namely, 15-20 messages per MT per minute may be very acceptable price to pay for significant gains in terms of extended network lifetime and reduced interference. In addition to this, the messaging load is subject to further optimization.

MER-PC scheme has lot of potential of improvement and for performance analysis outside the borders of the system model assumptions, which had to be assumed in order to keep the analysis tractable. Different modulation schemes will yield different relative power gains. Also, addition of the third transmitter is something that deserves attention, although intuitively one may infer that there is a limit to the number of transmitters with respect to the messaging overload that additional transmitters would bring about. The evaluation of this limit has significant importance. Applicability and potential gains of the new scheme to the routing problems with multicast nature is a very interesting question. It seems evident that power combining is very suitable for scenarios with multiple destinations.

APPENDIX A

PROOF OF PROPOSITIONS

In this appendix, the proofs for Proposition 2.1 and Proposition 2.3 are derived.

Proof of Proposition 2.1

If $\rho_{ij} = \rho$ for $i \neq j$, we have the KxK crosscorrelation matrix $R_{KxK} = \begin{bmatrix} 1 & \rho & \cdots & \rho \\ \rho & 1 & \cdots & \\ \vdots & & \ddots & \rho \\ \rho & \cdots & \rho & 1 \end{bmatrix}$.

Therefore,

$$R^{+}_{kk,} = R^{+}_{11} = \frac{\det R_{(K-1)x(K-1)}}{\det R_{KxK}} \tag{A.1}$$

Adding columns 2,3, ...K to column 1, and then subtracting row 1 from rows 2,3,...K, yields

$$\det(R_{KxK}) = \begin{bmatrix} 1+(K-1)\rho & 0 & \ldots & 0 \\ 0 & 1-\rho & \ldots & \\ . & & \ldots & 0 \\ 0 & \ldots & 0 & 1-\rho \end{bmatrix} = [1+(K-1)\rho](1-\rho)^{K-1} \tag{A.2}$$

From (A.1) and (A.2) one can compute

$$R^{+}_{kk} = \frac{1+(K-2)\rho}{[1+(K-1)\rho](1-\rho)} \tag{A.3}$$

Now, using Equation (2.8) and (A.3), one can obtain (2.9)

Proof of Proposition2.3

Lemma1 $R_{\mu}^{(p)}$ is the Schur component of R_{μ} in R.

Proof of Lemma1:

The crosscorrelation matrix R can be written as a partitioned matrix

$$R = S^T S = [S_\mu | S_M]^T [S_\mu | S_M] = \begin{bmatrix} S_\mu^T \\ S_M^T \end{bmatrix} [S_\mu | S_M] = \begin{bmatrix} S_\mu^T S_\mu & S_\mu^T S_M \\ S_M^T S_\mu & S_M^T S_M \end{bmatrix} = \begin{bmatrix} R_\mu & R_{\mu M} \\ R_{M\mu} & R_M \end{bmatrix} \quad \text{(A.4)}$$

On the other hand:

$$\begin{aligned} R_\mu^{(p)} &= (S_\mu^{(p)})^T S_\mu^{(p)} \\ &= (PS_\mu)^T (PS_\mu) \\ &= S_\mu^T P S_\mu \\ &= S_\mu^T (I - S_M S_M^+) S_\mu \\ &= R_\mu - S_\mu^T S_M S_M^+ S_\mu \\ &= R_\mu - S_\mu^T S_M [(S_M^T S_M)^{-1} S_M^T] S_\mu \\ &= R_\mu - R_{\mu M} R_M^{-1} R_{M\mu} \end{aligned} \quad \text{(A.5)}$$

Therefore, $R_\mu^{(p)}$ is indeed the Schur component of R_μ in R. □

Now, using equations (2.14), (2.25) can be written as:

$$P_e^k = Q\left(\sqrt{\frac{\eta}{(R_\mu^{(p)})_{kk}^+}}\right) \quad \text{(A.6)}$$

By the formula for the inverse of a partitioned matrix E [Scharf]:

$$E = \begin{bmatrix} A & B \\ C & D \end{bmatrix}^{-1} = \begin{bmatrix} Sch(A)^{-1} & -A^{-1}BSch(D)^{-1} \\ -Sch(D)^{-1}CA^{-1} & Sch(D)^{-1} \end{bmatrix} \quad \text{(A.7)}$$

where *Sch(A)* denotes the Schur component of A in E.

From Equation (2.33), (2.36) and Lemma 1, we have

$$R_{K_\mu x K_\mu}^{-1} = (R_\mu^{(p)})^{-1} \quad \text{(A.8)}$$

Therefore, expressions (2.8) and (2.25) are indeed equivalent.

APPENDIX B

OPTIMAL POWERS ON THE DIVERSITY BRANCHES

In this appendix, the curves of the optimal received powers $(P_{ac}^{r''})_{opt}$ and $(P_{bc}^{r''})_{opt}$ are computed numerically as a function of the ratio of channel attenuations, r:

$$r = \frac{d_{bc}^{m}\gamma_{bc}}{d_{ac}^{m}\gamma_{ac}} \tag{B.1}$$

for uncoded BPSK modulation. Only the curves for $P_e = 10^{-1}$ and $P_e = 10^{-2}$ are given here. The curves for $P_e = 10^{-3}$ and $P_e = 10^{-4}$ are impractical because of the range of both x and y axis. However, the trend of increase/decrease is equivalent to the figures below.

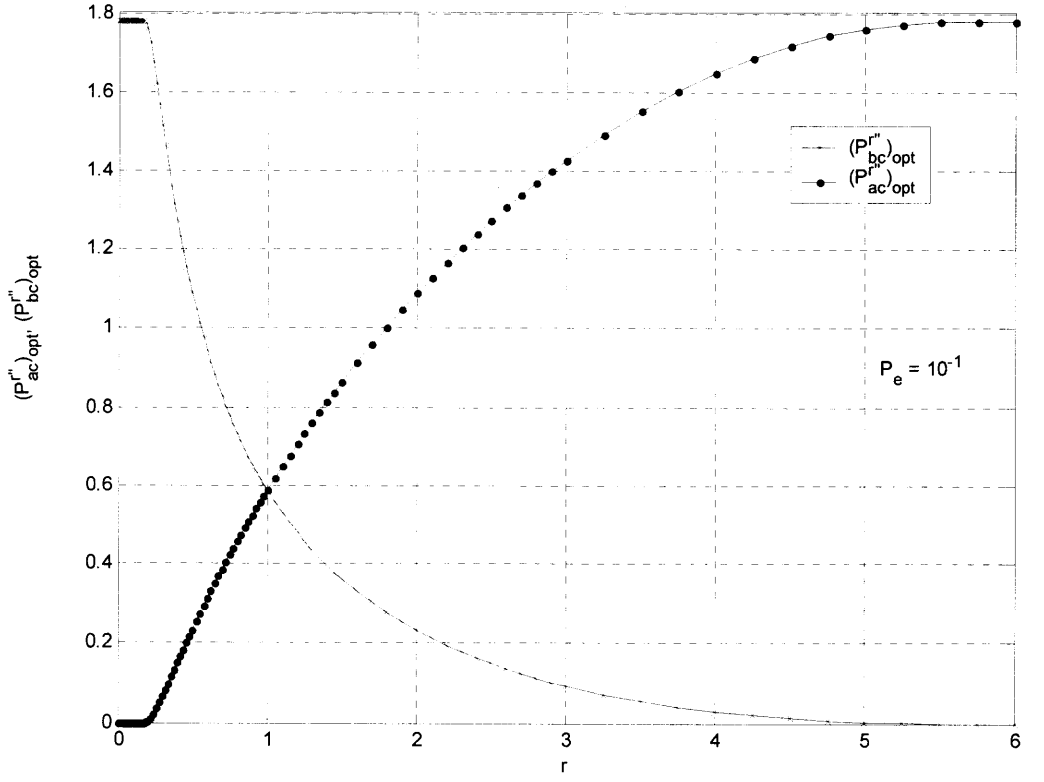

Figure B.1 Optimal received powers on the two diversity branches for a two-finger RAKE receiver for BPSK modulation and $P_e = 10^{-1}$.

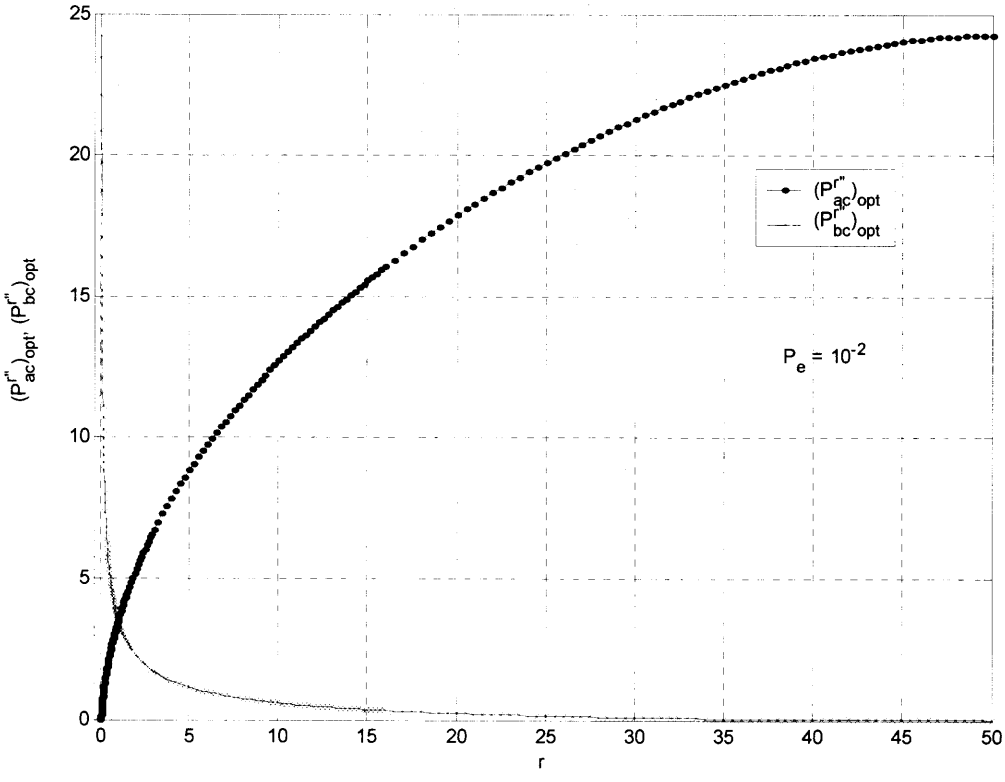

Figure B.2 Optimal received powers on the two diversity branches for a two-finger RAKE receiver for BPSK modulation and $P_e = 10^{-2}$.

REFERENCES

[1] S. Tekinay, *Wireless Network Engineering: Design, Management and Practice,* Kluwer Academic Publishers, under preparation.

[2] W. Hongyi, Q. Chunming, S. De, O. Tonguz, "Integrated cellular and ad hoc relaying systems: iCAR", IEEE Journal on Selected Areas in Communications, Vol. 19, No. 10, Oct. 2001, pp. 2105-2115.

[3] S. Mattison, "Minimizing power dissipation of cellular phones", Proc. 1997 Int. Symp. Low Power Electronics and Design, August 1998, pp. 42-45 .

[4] S. Singh, M. Woo, C.S. Raghavendra, "Power-aware routing in mobile ad hoc networks", Proceedings of Fourth Annual ACM/IEEE International Conference on Mobile Computing and Networking, Dallas, TX, Oct. 1998, pp. 181-190.

[5] C.-K. Toh, "Maximum battery life routing to support ubiquitous mobile computing in wireless ad hoc networks", IEEE Communications Magazine, Vol. 39, No. 6, June 2001, pp. 138-147.

[6] T. Rappaport, *Wireless Communications: Principle and Practice,* Prentice Hall, 2nd edition, December 2001.

[7] V. Rodoplu, T. Meng, "Minimum energy mobile wireless networks", IEEE Journal on Selected Areas in Communications, Vol. 17, No. 8, Aug. 1999, pp. 1333-1344.

[8] A. Michail, A. Ephremides, "A distributed routing algorithm for supporting connection-oriented service in wireless networks with time-varying connectivity", Proceedings of the Third IEEE Symposium on Computers and Communications, ISCC'98, Athens, Greece, June 1998, pp. 587-591.

[9] K. Scott, N. Bambos, "Routing and channel assignment for low power transmission in PCS", Proc. ICUPC Fifth Int. Conf. Universal Personal Communications, Oct. 1996, Vol. 2, pp. 498-502.

[10] C.E. Jones, K.M. Sivalingam, P. Agrawal, J.C. Chen, "A survey of energy efficient network protocols for wireless networks", Wireless Networks, Vol. 7, 2001, pp. 343-358.

[11] J.-H. Chang, L. Tassiulas, "Routing for maximum system lifetime in wireless ad hoc networks", Proceedings of 37th Annual Alerton Conference on Communication, Control and Computing, Monticello, IL, Sept. 1999.

[12] M.R. Pearlman et al., "On the impact of alternate path routing for load balancing in mobile ad hoc networks", Proceedings of the IEEE MobiHoc First Annual Workshop on Mobile Ad Hoc Networking and Computing, Aug. 11, 2000, Boston, MA.

[13] A. Nasipuri et al., "Performance of multipath routing for on-demand protocols in mobile ad hoc networks", Mobile Networks and Applications, Vol. 6, pp. 339-349.

[14] M. Bhardwaj et al., "Upper bounds on the lifetime of sensor networks", Proceedings of the ICC 2001, Vol. 3, pp. 785-790.

[15] S.-J. Lee, "A simulation study of table driven and on demand routing protocols for mobile ad hoc networks", IEEE Network, Vol. 13, No.4, July-Aug. 1999, pp. 48-54.

[16] Y. Xu et al., "Adaptive energy conserving routing for multihop ad hoc networks", Research Report 527, USC/Information Science Institute, October 2000.

[17] L. M. Feeney, "An energy consumption model for performance analysis of routing protocol for mobile ad hoc networks", Mobile Networks and Applications, Vol. 6, 2001, pp. 239-249.

[18] J. Boyer et al., "A theoretical characterization of the multihop wireless communications channel with diversity", IEEE GLOBECOM 2001, Vol. 2, pp. 841-845.

[19] M. Souryal et al., "Ad hoc, multihop CDMA networks with route diversity in a Rayleigh fading channel", IEEE Military Communications Conference MILCOM 2001, Vol. 2, pp. 1003-1007.

[20] J.H. Winters, "The diversity gain of transmit diversity in wireless systems with Rayleigh fading", IEEE Transactions on Vehicular Technology, Vol. 47, No. 1, Feb.1998, pp. 119-123.

[21] H.K. Mecklai, R.S. Blum, "Transmit antenna diversity for wireless communications", IEEE Conference on Communications ICC'95, Seattle, Vol. 3, pp. 1500-1504.

[22] S.M. Alamouti, "A simple transmit diversity technique for wireless communications", IEEE Journal on Selected Areas in Communications, Vol. 16, No. 8, Oct. 1998, pp. 1451-1458.

[23] J. Proakis, *Digital Communications,* McGraw-Hill Higher Education, 4th edition, August 2000.

[24] M.K. Simon, M. Alouini, *Digital Communications over Fading Channels*, John Wiley and Sons, New York, 2000.

[25] G.L. Stuber, *Principles of Mobile Communication,* Kluwer Academic Publishers, Norwell, MA, 1996.

[26] J. Zander, "Performance of optimum transmitter power control in cellular radio systems", IEEE Trans on Veh. Technology, Vol. 41, No. 1, Feb.1992, pp. 57-62.

[27] G.J. Foschini, Z. Miljanic, "A simple distributed autonomous power control algorithm and its convergence", IEEE Transactions on Vehicular Technology, Vol. 42, No. 4, Nov.1993, pp. 641-646.

[28] R.D. Yates, "A framework for uplink power control in cellular radio systems", IEEE Journal on Selected Areas in Communications, Vol. 13, No. 7, Sept. 1995, pp. 1341-1347.

[29] D. Goodman, N. Mandayam, "Power control for wireless data", IEEE Personal Communications, Vol. 7, No. 2, April 2000.

[30] Institute for Telecommunication Sciences, Wireless Propagation Research Outputs, http://www.its.bldrdoc.gov/tpr/2000/its_t/wireless/wireless.html.

[31] S.A. El-Dolil et al., "Teletraffic Performance of Highway Microcells with Overlay Macrocell', IEEE Journal on Selected Areas in Communications, Vol. 7, No.1, pp. 71-78, 1989.

[32] T.-S.P. Yum, W.-S. Wong, "Hot-spot Traffic Relief in Cellular Systems", IEEE Journal on Selected Areas in Communications, Vol. 11, No. 6, pp. 934 –940, 1993.

[33] A. Catovic, B. Jabbari, "Effect of Non-uniform Traffic Load on Erlang Capacity of CDMA", Proceedings of the 49th IEEE Vehicular Technology Conference, Vol. 1, pp. 816-820, Houston, Texas, USA, May 1999.

[34] L.-C. Wang et al., "Architecture Design, Frequency Planning and Performance Analysis for a Microcell/Macrocell Overlaying System", IEEE Transactions on Vehicular Technology, Vol. 46, No. 4, pp. 836-848, 1997.

[35] C.-L. I et al., "A Microcell/Macrocell Cellular Architecture for Low- and High-Mobility Wireless Users", IEEE Journal on Selected Areas in Communications, Vol. 11, No. 6, pp. 885-891, 1993.

[36] E. Dahlman et al., "UMTS/IMT-2000 Based on Wideband CDMA", IEEE Communications Magazine, Vol. 36, No. 9, pp. 70-80, 1998.

[37] A. Duel-Hallen et al., "Multiuser Detection for CDMA Systems", IEEE Personal Communications, Vol. 2, No. 2, pp. 46-57, 1995.

[38] S. Verdú, *Multiuser Detection,* Cambridge University Press, 1998.

[39] H.V. Poor, S. Verdú, "Probability of Error in MMSE Multiuser Detection", IEEE Transactions on Information Theory, Vol. 43, No. 3, pp. 858-871, 1997.

[40] A.J. Viterbi, CDMA, *Principles of Spread Spectrum Communication*, Addison-Wesley, 1995.

[41] K.S. Gilhousen et al., "On the capacity of a cellular CDMA system", IEEE Transactions on Vehicular Technology, Vol. 40, No. 2, pp. 303 –312, 1991.

[42] A.J. Viterbi et al., "Other-cell interference in cellular power-controlled CDMA", IEEE Transactions on Communications, Vol. 42, No. 2, pp. 1501 –1504, 1994.

[43] R. Lupas, S. Verdú, "Linear multiuser detectors for synchronous code-division multiple-access channels", IEEE Transactions on Information Theory, Vol. 35, No. 1, pp.123-136, 1989.

[44] M. K. Varanasi, B. Aazhang, "Near-optimum detection in synchronous CDMA systems", IEEE Transactions on Communications, Vol. 39, No. 5, pp. 725-736, 1991.

[45] M. K. Varanasi, B. Aazhang, "Multistage detection in asynchronous CDMA communications", IEEE Transactions on Communications, Vol. 38, No. 4, pp. 509-519, 1990.

[46] A. Duell-Hallen, "Decorrelating Decision-feedback multiuser detector for synchronous CDMA channel", IEEE Transactions on Communications, Vol. 41, No. 2, pp. 285-290, 1993.

[47] E.H. Dinan, B. Jabbari, "Spreading codes for direct sequence CDMA and wideband CDMA cellular networks", IEEE Communications Magazine, Vol. 36, No. 9, Sept. 1998, pp. 48 –54.

[48] E. Perahia et al., "Shadow fading correlation between uplink and downlink", 53rd IEEE Vehicular Technology Conference, IEEE VTC 2001 Spring, Rhodes, Greece, Vol. 1, pp. 293-297.

[49] S. Soliman et al., "CDMA reverse link with open loop power control", IEEE GLOBECOM 1992, Vol. 1, pp. 69-73.

[50] A. Catovic, S. Tekinay, "Multiuser detection techniques for hierarchical cell structures in CDMA cellular systems", International Journal of Wireless Information Networks, Vol. 9, No. 1, January 2002, pp. 23-35.

[51] A. Catovic, S. Tekinay, "Projection multiuser detectors for hierarchical cell structures in CDMA cellular systems", IEEE 53rd Vehicular technology Conference, VTC 2001 Spring, Vol. 3, pp. 1853-1857.

[52] A. Catovic, S. Tekinay, "Reducing transmit power and extending transmit power via user cooperation in next generation multihop wireless networks", Journal of Communications and Networks, Vol. 4, No. 4, December 2002, pp.1-12.